Vilnius University
Institute of Theoretical Physics and Astronomy

Oliver Scharf

On the Theory of Hyperfine Structure of Many-Electron Atoms

Doctoral Dissertation
Physical Sciences, Physics (02P)

Vilnius, 2006

The dissertation has been accomplished in 2002 – 2006 at Vilnius University Institute of Theoretical Physics and Astronomy, Vilnius, Lithuania.
The Institute is entitled to give a doctorate with Vilnius University, following resolution No. 457 adopted by the Government of the Republic of Lithuania, April 14, 1998.

Scientific supervisor

Zenonas Rudzikas, prof. habil. dr. (Vilnius University Institute of Theoretical Physics and Astronomy, Physical sciences, Physics, 02P)

Consultant

Gediminas Gaigalas, prof. habil. dr. (Vilnius University Institute of Theoretical Physics and Astronomy, Physical sciences, Physics, 02P)

The Doctorate Committee

Chairman

Bronislovas Kaulakys, prof. habil. dr. (Vilnius University Institute of Theoretical Physics and Astronomy, Physical sciences, Physics, 02P)

Members

Romualdas Karazija, prof. habil. dr. (Vilnius University Institute of Theoretical Physics and Astronomy, Physical sciences, Physics, 02P)

Gintautas Kamuntavičius, prof. habil. dr. (Vytautas Magnus University, Physical sciences, Physics, 02P)

Algirdas Audzijonis, prof. habil. dr. (Vilnius Pedagogical University, Physical sciences, Physics, 02P)

Kazimieras Glemža, dr. (Vilnius University, Physical sciences, Physics, 02P)

Opponents

Pavelas Bogdanovičius, prof. habil. dr. (Vilnius University Institute of Theoretical Physics and Astronomy, Physical sciences, Physics, 02P)

Dalis Baltrūnas, habil. dr. (Institute of Physics, Physical sciences, Physics, 02P)

This thesis is scheduled to be maintained at on March 17th, 2006 at Vilnius University Institute of Theoretical Physics and Astronomy.

Address: A. Goštauto 12, 01108 Vilnius, Lithuania.

The thesis summary was posted on February, 2006.

The copies of the entire thesis are exposed at the library of Vilnius University Institute of Theoretical Physics and Astronomy.

Vilniaus universitetas
Teorinės fizikos ir astronomijos institutas

Oliver Scharf

Hipersmulkiųjų saveikų daugiaelektroniuose atomuose teorijos plėtojimas

Daktaro disertacijos santrauka
Fiziniai mokslai, fizika (02P)

Vilnius, 2006

Disertacija rengta 2002–2006 Vilniaus universiteto Teorinės fizikos ir astronomijos institute.
Doktorantūros teisė suteikta su Vilniaus universitetu, 1998 04 14 Lietuvos Respublikos Vyriausybės nutarimas Nr. 457.

Mokslinis vadovas

Zenonas Rudzikas, prof. habil. dr. (Vilniaus universiteto Teorinės fizikos ir astronomijos institutas, fiziniai mokslai, fizika, 02P)

Konsultantas

Gediminas Gaigalas, prof. habil. dr. (Vilniaus universiteto Teorinės fizikos ir astronomijos institutas, fiziniai mokslai, fizika, 02P)

Doktorantūros komitetas

Pirmininkas

Bronislovas Kaulakys, prof. habil. dr. (Vilniaus universiteto Teorinės fizikos ir astronomijos institutas, fiziniai mokslai, fizika, 02P)

Nariai

Romualdas Karazija, prof. habil. dr. (Vilniaus universiteto Teorinės fizikos ir astronomijos institutas, fiziniai mokslai, fizika, 02P)

Gintautas Kamuntavičius, prof. habil. dr. (Vytauto Didžiojo universitetas, fiziniai mokslai, fizika, 02P)

Algirdas Audzijonis, prof. habil. dr. (Vilniaus pedagoginis universitetas, fiziniai mokslai, fizika, 02P)

Kazimieras Glemža, doc. (Vilniaus universitetasi, fiziniai mokslai, fizika, 02P)

Oponentai

Pavelas Bogdanovičius, prof. habil. dr. (Vilniaus universiteto Teorinės fizikos ir astronomijos institutas, fiziniai mokslai, fizika, 02P)

Dalis Baltrūnas, habil. dr. (Fizikos institutas, fiziniai mokslai, fizika, 02P)

Disertacija bus ginama viešame doktorantūros posėdyje, kuris vyks 2006 m. kovo 17 d. val.

Vilniaus universiteto Teorinės fizikos ir astronomijos instituto salėje.

Adresas: A. Goštauto g. 12, 01108 Vilnius, Lietuva. Tel. 2620939, faks. 2125361

Disertacijos santrauka išsiųsta 2006 m. vasario d.

Su disertacija galima susipažinti Vilniaus universiteto Teorinės fizikos ir astronomijos instituto bibliotekoje.

Contents

Introduction

With the advent of high resolution spectroscopy at the end of the last century, an additional structure became visible in many fine structure transition lines in atoms and ions, typically a hundred times smaller than the fine structure. Some of these lines arise due to the different nuclear mass and nuclear volume of the different isotopes of an element. This isotope shift alone, however, can not explain all the lines observed.

The additional hyperfine structure lines arise from the orientation energy between the static magnetic and electric fields of the nucleus and the static magnetic and electric fields of the electron core. The splitting from this interaction energy E_{hfs} is given in very good approximation by Casimir's formula [1]:

$$E_{hfs} = \frac{1}{2} C A + \frac{3}{4} \frac{C(C+1) - I(I+1)J(J+1)}{2I(2I-1)J(2J-1)} B \qquad \text{(I)}$$

with $C = F(F+1) - I(I+1) - J(J+1)$. The separation between two hyperfine lines is proportional to the A factor with some correction given by the B factor. Additional corrections are, except for special cases, even smaller and rarely resolved. The number of hyperfine lines follow from angular momentum coupling of the nuclear spin $\mathbf{I}$ with the angular momentum of the electrons $\mathbf{J}$ to the final momentum $\mathbf{F}$ and the selection rules for photon emission.

Modern experimental methods allow the measurement of this splitting for practically any atom and ion, including extreme ionization degrees. The high precision with which the hyperfine lines can be determined make them an ideal tool for calibration and frequency reference standards throughout the whole spectral range. The definition of one second, for example, is based on the splitting between the hyperfine levels with $F = 4$ and $F = 3$ of the fine structure level $^2S_{1/2}$ in Cesium (^{133}Cs). This transition is measured and defined as the frequency standard $\Delta\nu \equiv 9\,192\,631\,770\,\text{Hz}$ [2]. Another well-known hyperfine line arises from the magnetic dipole transition between the hyperfine levels $F = 1$ and $F = 0$ of the ground state of hydrogen. This is the $21\,\text{cm}^{-1}$ line whose spatial distribution in space revealed the spiral structure of our Milky Way for the first time. Since then there is constant need for accurate hyperfine structures for analyzing stellar spectra [3, 4].

For the spectroscopist, the distinct structure of the lines contributes considerably to the interpretation and analysis of high resolution spectra. Knowledge of the A and B

factors helps to interpret line forms, to identify fine structure transitions in many line spectra and to designate fine structure levels. Recent hyperfine measurements for the well-known element Niobium have revealed, for example, that false designations of its fine structure levels exist in standard tables [5].

From the theoretical point of view the A and B factors represent a bridge between properties of the nucleus and the electrons. The A factor is a product of the static nuclear magnetic moment and the magnetic field produced by the electrons (see Eq. 2.6). The nuclear magnetic moment can be measured directly (for example with atomic beam magnetic resonance techniques) without the use of hyperfine structure. The magnetic field of the electron core can then be calculated from the atomic wave function.

The B factor is a product of the nuclear quadrupole moment and the electric field gradient of the electrons (see Eq. 2.7). As no experimental technique exists to determine nuclear quadrupole moments in a direct way, most information about the nuclear quadrupole moment is obtained from hyperfine structure calculations.

Comparison of the experimental splitting with the theoretically calculated one allows for a test of correlation and relativistic effects and, as a result, of the atomic wave function. With the advent of nano technology, accurate wave functions are of great importance for the growing need to predict various physical properties of atomic systems. It is therefore of importance to develop reliable computational methods that can be used to supply hyperfine structure data.

During the past two decades the methods for obtaining the required wave functions and the numerical codes have been developed to a high level [6,7]. Although large-scale fully relativistic calculations are now feasible and can give fairly accurate results [8,9], the large-scale multiconfiguration calculations are still very expensive computationally. Recent progress in large scale multiconfiguration and configuration interaction calculations, together with today's powerful computers, has made it possible to calculate hyperfine structure in light atoms to very high accuracy [10, 11]. For heavy elements and atoms with many strongly correlated electrons, however, various problems are encountered and *ab initio* calculation of the hyperfine structure remains a great challenge for atomic theoreticians.

The main task in a multiconfiguration calculation is to find a method for the generation of the configuration state functions. In practical calculations, and especially for heavier elements, their number is constrained by available computer storage, convergence problems, and other hardware and software limitations. The number of configuration

state functions must be kept to a manageable level, and therefore restrictions have to be imposed so that the most important electron correlation effects are captured. There are many different ways of doing this, depending on the atomic property that is to be obtained. For the hyperfine structure, the most common approaches are the orbital-driven method [12] and the approach by Bieroń *et. al.* [13]. These approaches have been applied only to atoms and ions with one or two outer (valence) electrons. For more complex atoms the core correlations were neglected leading to deviation of more than 100% from the experimental results [14, 15]. Recently, most attention was payed to evaluate the B factor were core correlations are less important [16]. To apply these approaches to the A factor of more complex many-electron atoms and ions, more details about the correlations that are important for the hyperfine structure are necessary.

The aim of the thesis

The purpose of the present work is to further extend the multiconfiguration calculation of the hyperfine structure to complex many-electron atoms and ions. The thesis aims at designing a systematic method which makes it possible to obtain the important correlations and to estimate the uncertainty of the results of the hyperfine structure factors for atomic systems with many outer (valence) electrons.

The main tasks of the thesis

To achieve this aim, more time efficient programs, advanced computing facilities and a method for the detailed study of the correlations that are important for the hyperfine structure are needed. That leads to the following tasks:

1. Adapt the hyperfine structure operators to the new developments in spin-angular integration techniques. The relevant expressions for the A and B factors have to be transformed from coordinate into second quantized particle representation with additional quasispin space. Using graphical methods closed expressions for the A and B factors for any complex many-electron atom or ion with an arbitrary number of open shells is to be obtained that is based on the smallest set of standard quantities, the reduced coefficients of fractional parentage.

2. Implement the general underlying technique in the form of the symbolic programming language MAPLE [17] for the atomic application development systems RACAH

and JUCYS. Use these enhancements to program the hyperfine structure utility HFS that allows the efficient manipulation and calculation of hyperfine structure expressions.

3. Based on the experience from the symbolic HFS package, implement the spin-angular integration technique into the HSF module of the ATSP package for large scale calculations.

4. Install and test the software for obtaining multiconfiguration atomic state functions on the BENDROSIOS FIZIKOS KATEDROS cluster at Vilnius Pedagogical University.

5. Design the systematic method that observes the correlations, that estimates the convergence and that allows one to assign an error to the hyperfine structure calculation. Test the method.

The scientific innovations

1. The new expression for the magnetic dipole and electric quadrupole factor is valid for any open-shell atomic system and is based on the smallest set of standard quantities, the reduced coefficients of fractional parentage.

2. The atomic application development systems RACAH and JUCYS are extended by the vital part of one-particle spin-angular integration. Based on the new developments in programming paradigm, the symbolic programming, they are not only able to provide the standard quantities from the atomic shell theory but also to support the symbolic manipulations and the numerical computations of expressions from the atomic structure theory.

3. The calculations are performed on a five node cluster allowing for large scale calculations. Together with the new version of the hyperfine structure program a method for the detailed study of the hyperfine structure of complex many-electron atoms is feasible. Compared with existing approaches less *ad hoc* assumptions about important correlations have to be made and more detailed information about the influence and convergence of the correlations is obtained.

4. The detailed influence of correlations on the hyperfine structure of Vanadium is calculated using multiconfiguration approximations.

Statements to be defended

1. The expressions of the hyperfine structure factors are valid for any open-shell atom or ion. Compared to known expressions, less computation time is spend for their evaluation.

2. The atomic application development systems RACAH and JUCYS together with the hyperfine structure package HFS are of help for theoretical work as well as for the experimentalist. For the hyperfine structure, they allow on the fly evaluation and presentation of hyperfine structure data and expressions, both in semiempirical and *ab initio* approach. A fast adaption to similar physical problems is possible.

3. The proposed method for the multiconfiguration hyperfine structure calculations allows one to make efficient approximations on the configuration state function space, to monitor the convergence and influence of various correlations and to assign an error on the calculation.

4. Expression, programs and the method give the possibility to study hyperfine structure splitting of complex atoms and ions and using modern computing facilities to achieve fairly accurate results.

Organization of the thesis

The thesis is organized into five chapters. Chapter 1 presents a historical overview of the developments in the field of hyperfine structure calculations. The common approaches are reviewed and the theoretical background of the multiconfiguration approach as well as symmetry-adapted wave functions in quasispin space are explained in more detail. Based on this theory, new explicit expressions of the hyperfine structure matrix elements are derived in Chapter 2. The explicit expressions for a two-shell system are presented. The third chapter shows the implementation of the underlying theory, in particular the general expression for the hyperfine structure, in computer codes. In Chapter 4 the new method for hyperfine structure calculation is developed. It is applied to the ground state hyperfine structure calculation of Vanadium, in both multiconfiguration Hartree-Fock and Dirac-Fock approximations. The thesis ends with the conclusions and outlook.

Contributions made by the author

The author carried out the theoretical investigations presented in the dissertation. The extensions to the data-structures and the spin-angular integration of the JUCYS package as well as the HFS package were written by the author. He developed the method for the hyperfine structure calculations, performed the calculations and analysis and formulated conclusions.

Contributions made by the co-authors:
Prof. Z. Rudzikas: General supervision, consultant on the modern aspects of the atomic theory and the quasispin approach.
Prof. G. Gaigalas: General consultant on the spin-angular integration technique, on the multiconfiguration approach and on the calculations. He contributed much to the writing of the HFS program for the ATSP package.
The installation of the ATSP and GRASP packages were done in collaboration with C. F. Fischer, National Institute of Standards and Technology.
Further developments of the JUCYS package were done in collaboration with S. Fritzsche, Technische Universität Kassel.
Suggestions for the HFS package for experimental hyperfine structure measurements and the investigations on the hyperfine structure of Niobium were done in collaboration with S. Kröger, Technische Universität Berlin and G. Guthöhrlein, Universität der Bundeswehr Hamburg.

List of author's publications

The thesis is based on the following articles published together with co-authors:

1. S. Kröger, O. Scharf and G. Guthöhrlein. New and revised energy levels of atomic Niobium. *Europhysics Letter*, **66(3)**: pp. 344 – 349, 2004.

2. G. Gaigalas, Z. Rudzikas and O. Scharf. Hyperfine Structure Operator in the Tensorial Form of Second Quantization. *Central European Journal of Physics*, **2**: pp. 720 – 736, 2004.

3. G. Gaigalas, O. Scharf and S. Fritzsche. Maple procedures for the coupling of angular momenta. VIII. Spin-angular coefficients for single-shell configurations. *Computer Physics Communications* , **166**: pp. 141 – 169, 2005.

4. O. Scharf, G. Gaigalas, S. Fritzsche, M. Gedvilas, E. Gaidamauskas and G. Kirsanskas. Application of the Racah package for dealing with the expressions from the atomic shell model. *Nuclear Instruments and Methods in Physics Research B*, **235**: pp. 135 – 139, 2005.

5. G Gaigalas, O. Scharf and S. Fritzsche. Hyperfine structure parametrization in Maple. *Computer Physics Communications*, **174**(3): pp. 202 – 221, 2006.

6. O. Scharf and G. Gaigalas. Large scale multiconfiguration Hartree-Fock calculation of the hyperfine structure of the ground state of Vanadium. *Central European Journal of Physics*, 4: pp. 42 – 57, 2006.

The results of this thesis were presented at the following conferences (with published abstracts):

1. 35th Conference of the European Group for Atomic Spectroscopy, Bruxelles (Belgium), July 15th – 18th, 2003.

2. 8th European Conference on Atomic and Molecular Physics, Rennes (France), July 6th – 10th, 2004.

3. 12th International Conference on the Physics of Highly Charged Ions, Vilnius (Lithuania), September 6th – 11th, 2004.

4. 36th Lithuanian National Physics Conference, Vilnius (Lithuania), June 16th – 18th, 2005.

5. 37th Conference of the European Group for Atomic Systems, Dublin (Ireland), August 3rd – 6th, 2005.

1 Historical and theoretical background

Wolfgang Pauli interpreted, in 1924, the magnetic interaction part of the hyperfine structure. A nucleus has a magnetic dipole moment in the direction of its spin-angular momentum. The electron shell forms an effective magnetic field directed along the electron quantization axis. The magnetic part of the hyperfine structure therefore results from the magnetic coupling (orientational energy) between the nucleus and the electrons leading to the A factor. Significant deviations from the theoretical predictions thus far led Schüler and Schmidt to introduce quadrupole coupling into the theory in 1935. The nucleus is modeled as an equatorial symmetric charge distribution around its nuclear axis. The electrostatic potential at the electron position, due to the nucleus, leads to additional electric perturbation and defines the B factor. The hyperfine energy expressed by these factors leads to Casimir's formula, Eq. I of the introduction.

In terms of angular theory, the hyperfine interaction couples the electron core momentum $\mathbf{J}$ weakly with the nuclear momentum $\mathbf{I}$ to the final atomic momentum $\mathbf{F}$. In the multiconfiguration Hartree-Fock approximation, the fine structure splitting of the energy terms is treated as a first order perturbation. The matrix element of the operator is calculated with respect to the zero-order wave function. Consequently, the hyperfine splitting, as an even smaller perturbation, can be treated in the same approximation. The angular momentum coupling between the electron core and the nucleus is regarded as being so weak that the angular momenta $\mathbf{J}$ and $\mathbf{I}$ are independently observable as is their coupled momentum $\mathbf{F}$. The potentials of the electric and magnetic fields of the nucleus, caused by the distribution of nuclear charges and currents, are expanded into multipole momenta of rank k around $\mathbf{I}$. The hyperfine structure energy E_{hfs} can then be calculated as the decoupled product of a nuclear part $\mathbf{M}^{(k)}$ and an electronic part $\mathbf{T}^{(k)}$ by [18]:

$$\begin{aligned} E_{hfs} &= \langle\, JIF \,\|\, \mathbf{M}^{(k)} \cdot \mathbf{T}^{(k)} \,\|\, JIF \,\rangle \\ &= \sum_{k=1} (-1)^{J+I+F} \left\{ \begin{array}{ccc} J & I & F \\ I & J & k \end{array} \right\} \langle\, I \,\|\, \mathbf{M}^{(k)} \,\|\, I \,\rangle\, \langle\, J \,\|\, \mathbf{T}^{(k)} \,\|\, J \,\rangle\,. \end{aligned} \tag{1.1}$$

The explicit formulas for the nuclear multipole moments are derived in [19]. The nuclear magnetic multipole momentum of order k is given by

$$\mathbf{M_m}^{(k)} = (-1)^k \left[\nabla^{(1)} \{ r^k \mathbf{C}^{(k)} \} \cdot \left(\frac{2}{k+1} g_l \mathbf{L}^{(1)} + g_s \mathbf{S}^{(1)} \right) \right] \tag{1.2}$$

and the nuclear electric multipole momentum by

$$\mathbf{M_e}^{(k)} = r^k \mathbf{C}^{(k)} . \tag{1.3}$$

The components of the spherical tensor $\mathbf{C}^{(k)}$ are related to the spherical harmonic function Y_{kq} by

$$\mathbf{C}_q^{(k)} = \left(\frac{4\pi}{2k+1} \right)^{1/2} Y_{kq} . \tag{1.4}$$

The gradient in Eq. 1.2 only applies to the expression in the curled brackets. The gyromagnetic ratios are equal to $g_l = 1$ and $g_s = 5.58$ for protons and $g_l = 0$ and $g_s = -3.82$ for neutrons. One important observation can be made from Eq. 1.2 and Eq. 1.3. As inversion symmetry is conserved and the nucleus has (to very good approximation) well defined inversion symmetry, the magnetic multipoles have to be zero for even k and the electric multipoles have to be zero for odd k.

The first term of the magnetic multipole momentum is the magnetic dipole moment having $k = 1$. For a nucleus abbreviated by $|IM_I\rangle$, the magnetic dipole moment is defined as the matrix element with the projection $M_I = I$ of the total spin $\mathbf{I}$,

$$\mu_I \equiv \langle I M_I = I | \mathbf{M_m}^{(1)} | I M_I = I \rangle . \tag{1.5}$$

This quantity is directly observable in experiments and often known to within a few millinuclear magnetons ($\mu_N = 5.0507866(17) \cdot 10^{-27}\,\mathrm{Am}^2$). The first electric multipole moment with $k = 0$ is the usual Coulomb interaction with a point-like nucleus already included in the atomic Hamiltonian, compare Eq. 1.7. The next term with $k = 2$ defines the electric quadrupole moment,

$$Q \equiv 2 \langle I M_I = I | \mathbf{M_e}^{(2)} | I M_I = I \rangle . \tag{1.6}$$

As mentioned in the introduction, there is no direct experiment to measure this value. The electric quadrupole moments obtained by different authors often differ and are

usually only known within some millibarn ($b = 10^{-28}\,m^2$). Higher order multipole moments are barely observed[†]. This work takes the nuclear parts from experiments. Extensive tables of nuclear magnetic dipole and electric quadrupole moments of many atoms can be found in [20].

For the calculation of the hyperfine structure, sophisticated semiempirical, perturbational and multiconfiguration approaches have been developed. The Sandars-Beck effective-operator formulation of the theory of hyperfine structure [21] allows one to interpret the hyperfine structure data for complex many-electron atoms and ions. Intermediate coupled wave functions for the fine structure states of interest are calculated within the semiempirical parametric fitting approach. These wave functions are used to calculate expansion coefficients of the Sandars-Beck radial integrals that, in turn, are treated as adjustable parameters [21]. This allows one to represent many experimental data in terms of a few fundamental parameters. The inherent problem of this approach is the lack of detailed understanding of the interactions responsible for the hyperfine structure observed. For complex atoms, parameters are often ignored to avoid nonphysical conditions [22] and further theoretical modeling is necessary [23, 24]. While still providing the best quantitative reproduction of a large body of experimental information, this approach has been challenged within the past few years by the *ab initio* approaches.

The main breakthrough in this field has been the introduction of many-body perturbation theory. The techniques are similar to those introduced by Feynman in the work on quantum electrodynamics. A systematic perturbation expansion is taken to represent the wave function. Lindgren and Morrison [25] give many details of the approach in their book. The perturbation method has the great advantage that one can take a certain (small) property, like hyperfine interaction, as a perturbation and, using the many-body diagrammatic analysis, calculate only the modifications of the total wave function which contribute to the value of that property. Parts of the wave function that do not contribute are ignored. The coupled cluster theory is a new development in this field.

An alternative method, developed at the same time as the many-body approach is the multiconfiguration formalism. The Hartree-Fock method assumes that each electron

[†]For atoms in special fields (ligandenfield or crystalfield) or due to selection rules higher order multipoles can be observed.

is orbiting in an central field independently of the nucleus and the remaining electrons. The correlated consistent movements of the electrons are ignored. But these movements, causing the additional so-called correlation energy, are indispensable for many atomic properties. Correlation can be included using a multiconfiguration atomic state function. The atomic wave function is expressed as a mixture (superposition) of wave functions of different electronic configurations of the same parity. In 1952 Jucys derived the multiconfiguration Hartree-Fock equations [26]. Both the mixing coefficients and radial orbitals are obtained in a self-consistent procedure from these equations. The wave function is further used in the first-order perturbation theory for the hyperfine interaction to calculate the magnetic dipole and the electric quadrupole interaction constants for any specified state, using no adjustable parameters. The advantage of the multiconfiguration approach is its ability to work with atoms and ions having any number of open shells.

The multiconfiguration approach holds the promise of greater physical insight into the various mechanisms responsible for observed trends as well as anomalies in the hyperfine structure. This does not necessarily result in an improvement, but the case for the discrepancies between experiment and *ab initio* values might be deduced. The main ideas behind this approach are given in the following section.

The theoretical frame for studying the properties of free atoms and ions is the atomic shell theory. The concepts of angular momentum and spherical tensor operators are combined in an intricate way to make use of both the spherical symmetry of free atoms and the indistinguishability of identical particles in quantum mechanics. Since the pioneering work of Racah [27–30] in the 1940s, many people have helped to develop this powerful theory which today is used in a large number of atomic codes and case studies on the behavior of free atoms and ions.

The atomic shell structure explains the chemical properties of the elements and the periodic table. The central topic of this model concerns the efficient evaluation and computation of the many-electron matrix elements for different one- and two-particle operators. For any properly adapted many-particle basis, the matrix elements can always be decomposed into the so-called spin-angular coefficients and radial integrals. The spin-angular coefficients are expressions in $3nj$-symbols and are the building blocks for most atomic structure computations as well as for atoms and molecules within crystals.

Any computer program for atomic physics therefore necessarily needs to compute spin-angular coefficients. The practical theoretical foundation to do this in the form of Racah algebra was given by Jucys, Levinson and Vanagas in their famous work [31].

Jucys and Bandzaitis [32] developed general graphical methods and sum rules that allow one to simplify the matrices, to detect symmetries and zero elements and, for the first time, to compute the phase from the graphical rules. Based on this work, one of the first codes, NJSYM [33] was replaced by NJGRAF [34] leading to a considerable speed-up of atomic structure calculations. More complex calculations became feasible. The packages based on this approach are still used in a large number of computations [35]. However, accurate atomic structure calculations are needed for more efficient approaches as more correlation effects are required to explain the improved experimental accuracy and number of atomic data that are obtained, especially for open d- or f-shell atoms.

Another milestone was laid by Gaigalas, Kaniauskas and Rudzikas [36] by considering graphs that are based on second quantization in coupled tensorial form and an additional quasispin symmetry. Considering quasispin explicitly [37] allows one to obtain matrix elements of any one- or two-particle operator that are independent of the occupation number of the subshells. The refined graphical methods allow one to find expressions for matrix elements of any one- or two-electron operator for an arbitrary number of shells in an atomic configuration. Both diagonal and off-diagonal, with respect to the configuration, matrix elements are treated uniformly. The coefficients of fractional parentage or unit tensors form a large set of standard quantities used in traditional approaches. The approach used in this thesis uses a smaller set of standard quantities: the (in all three spaces) reduced coefficients of fractional parentage [38]. In contrast to the coefficients of fractional parentage, they are independent of the shell occupation and their phase is uniquely defined. The representation of the wave function in this approach is reviewed in the second section of this chapter.

1.1 The multiconfiguration approach

The Hamiltonian of the atomic shell model exhibits the spherical symmetry and every electron moves independently in the field of the nucleus and some average potential V due to the remaining electrons. An electron ψ_k bound to an atom of nuclear charge

Z with energy ϵ_k is described by the stationary Schrödinger equation (in atomic units [au])

$$H_k|\psi_k\rangle = [-\boldsymbol{\nabla}_k^2 - \frac{Z}{r_k} + V_k]|\psi_k\rangle = \epsilon_k|\psi_k\rangle\,, \tag{1.7}$$

where other nuclear and relativistic effects as well as external fields are ignored. The potential V_k is the averaged Coulomb repulsion energy due to all other $N-1$ electrons,

$$V_k = \sum_{j=1,j\neq k}^{N} \langle\psi_j|\frac{1}{|\mathbf{r}-\mathbf{r}_j|}|\psi_j\rangle\,. \tag{1.8}$$

The total atomic wave function of all electrons is formed by an antisymmetrized product wave function Ψ based on the single electron wave functions ψ. As this atomic wave function is a normed state of a Hilbert space, the expectation value of Eq. 1.7 defines the energy functional $E[\Psi]$,

$$\langle H\rangle = \frac{\langle\Psi|H|\Psi\rangle}{\langle\Psi\|\Psi\rangle} \equiv E[\Psi]\,. \tag{1.9}$$

If $|\Psi\rangle$ is an eigenvalue of H, than $E[\Psi]$ is stationary at Ψ. This is equivalent to [39]

$$\delta E \equiv E[\Psi+\delta\Psi]-E[\Psi]=0\,, \tag{1.10}$$

where $|\Psi+\delta\Psi\rangle$ is an infinitesimally small variation of $|\Psi\rangle$.

The spherical symmetry is best exploited if the one-electron wave function is expressed as eigenfunction of the spin and angular momentum operator using the ansatz [18]

$$|\psi_k\rangle = |nlm_l sm_s\rangle = R_{nl}(r)\,Y_{m_l}^{(l)}(\theta,\varphi)\,\sigma_{m_s}^{(s)}\,. \tag{1.11}$$

The angular momentum part is represented by the eigenfunctions of the angular momentum operator $\mathbf{l}$, the spherical harmonics $Y_{m_l}^{(l)}$ and the spin part of the wave function is given by the eigenfunction $\sigma_{m_s}^{(s)}$. Choosing the radial part of the orbitals so that the energy in Eq. 1.7 is minimized, the Hartree-Fock equation is obtained [40]. The bound state solutions for this equation are a discrete set of radial parts $R_{nl}(r)$. The wave functions (Eq. 1.11) are called single electron spin-orbitals or spectroscopic orbitals.

A more realistic model uses a linear combination of orthonormal states $|\psi_i\rangle$,

$$|\Psi\rangle = \sum_{i=1}^{N} c_i |\psi_i\rangle \,. \tag{1.12}$$

The expansion Eq. 1.12 includes so-called correlation orbitals that do not necessarily have the number n of nodes, but an arbitrary number [40]. They augment the spectroscopic orbitals and account for the correlation in the electron core. Applying the variational principle leads to the equivalent expression of Eq. 1.10,

$$\sum_{j=1}^{N} (\langle \psi_i | H | \psi_j \rangle - E\delta(i,j)) c_j = 0 \quad \text{for all } i = 1, \ldots, N \,. \tag{1.13}$$

Using the explicit expression for the Hamiltonian (Eq. 1.7), a coupled system of integro-differential equations, the so-called Hartree-Fock-Jucys equations are obtained (see [41] and references therein). The radial functions depend on the potential formed by the orbitals and on the mixing coefficients c_i. The equations can be solved self-consistently. The potentials are calculated from some initial estimates for the radial functions and mixing coefficients. The potentials are used to determine new radial wave functions and the new mixing coefficients which are used for new estimates of the potentials. This procedure is repeated until convergence is obtained.

The multiconfiguration Hartree-Fock approximation captures correlation effects. The solution can be approximated with arbitrary accuracy if enough terms in Eq. 1.12 are taken into account. This, however, is constrained by computing capacities and limitation methods for the expansion have to be used.

So far relativistic effects have been neglected. A first correction to the multiconfiguration Hartree-Fock approximation is done by adding Breit-Pauli operators to the Hamiltonian Eq. 1.7. These seven operators are obtained by expanding the relativistic many-electron equation in powers of the fine structure constant α and taking the terms until α^2 into account. A part of these operators commute only with $\mathbf{J}$, therefore the wave function is the eigenfunction of $\mathbf{J}$ and its projection J_z,

$$|JM_J\rangle = \sum_{i=1}^{N} c_i |L_i S_i J M_J\rangle \,. \tag{1.14}$$

The wave function is given in so-called intermediate coupling and configuration state functions with different LS are included. A comprehensive treatment can be found in [42] and computational aspects in [6].

The full relativistic generalization of the multiconfiguration Hartree-Fock approximation is the multiconfiguration Dirac-Fock approximation. The Hamiltonian is replaced by its relativistic analog,

$$H_k = c\boldsymbol{\alpha}\cdot\mathbf{p} + (\beta - 1)c^2 + V_N + V_k\,, \tag{1.15}$$

with $\boldsymbol{\alpha} = \left(\begin{smallmatrix} 0 & \sigma \\ \sigma & 0 \end{smallmatrix}\right)$, $\beta = \left(\begin{smallmatrix} 1 & 0 \\ 0 & -1 \end{smallmatrix}\right)$. The Pauli spin matrices are $\boldsymbol{\sigma}$ and $\mathbf{1}$ is the 2×2 unit matrix. In this work the monopole part of the electron-nucleus Coulomb interaction V_N is modeled from a two-parameter Fermi function of the nuclear density [43]

$$\rho(r) = \frac{\rho_0}{1 + e^{(r-c)/a}}\,. \tag{1.16}$$

The potential V_k is the mutual electron Coulomb repulsion, see Eq. 1.8, and $\mathbf{p}$ is the energy-momentum vector. Relativistic single electron spin-orbitals are of the form

$$|\,n\kappa j m_j\,\rangle = \frac{1}{r}\begin{pmatrix} P_{n\kappa}\,\Omega_m^{(\kappa)} \\ iQ_{n\kappa}\,\Omega_m^{(-\kappa)} \end{pmatrix}, \tag{1.17}$$

where $\Omega_m^{(\kappa)}$ denotes the two-component angular dependent spin-orbital function and P and Q are the radial components [41]. The quantum number κ is defined by

$$\kappa \equiv \pm(j + 1/2) \quad \text{for } l = j \pm 1/2\,. \tag{1.18}$$

The variational principle leads to the multiconfiguration Dirac-Fock equations that have to be solved self-consistently in the same way as their non-relativistic counterpart.

1.2 The representation of the atomic wave function

In second quantization representation, the spin-orbitals are created or annihilated by spherical tensor operators acting in angular momentum and spin space. A spin-orbital is created by operating with an electron creation operator $\mathbf{a}^{(ls)}$ on a vacuum state $|\,0\,\rangle$

$$\mathbf{a}^{(l\,s)}_{m_l\,m_s}\,|\,0\,\rangle = |\,l m_l s m_s\,\rangle\,. \tag{1.19}$$

The operator $\tilde{\mathbf{a}}^{(l\ s)}_{m_l m_s}$, obeying the Fano-Racah phase system, creates the vacuum state

$$\tilde{\mathbf{a}}^{(l\ s)}_{m_l m_s}\,|\,l m_l s m_s\,\rangle \;=\; (-1)^{l+s+m_l+m_s}\,\mathbf{a}^{\dagger\,(l\ s)}_{-m_l -m_s}\,|\,l m_l s m_s\,\rangle = |\,0\,\rangle\;, \tag{1.20}$$

where $\mathbf{a}^{\dagger\,(l\ s)}_{-m_l -m_s}$ is the hermitian conjugate of $\mathbf{a}^{(l\ s)}_{m_l m_s}$, called annihilation operator. As electrons are fermions, the creation and annihilation operators obey the following anti-commutation relations:

$$\left\{\mathbf{a}^{(l_1\ s_1)}_{m_{l_1} m_{s_1}}, \mathbf{a}^{(l_2\ s_2)}_{m_{l_2} m_{s_2}}\right\} \;=\; \left\{\mathbf{a}^{\dagger\,(l_1\ s_1)}_{m_{l_1} m_{s_1}}, \mathbf{a}^{\dagger\,(l_2\ s_2)}_{m_{l_2} m_{s_2}}\right\} = 0 \tag{1.21}$$

$$\left\{\mathbf{a}^{(l_1\ s_1)}_{m_{l_1} m_{s_1}}, \mathbf{a}^{\dagger\,(l_2\ s_2)}_{m_{l_2} m_{s_2}}\right\} \;=\; \delta\,(l_1 m_{l_1} s_1 m_{s_1}, l_2 m_{l_2} s_2 m_{s_2})\;. \tag{1.22}$$

A product wave function of equivalent electrons in a shell is created by repeated use of the creation operators, defining the phase by

$$\mathbf{a}^{(l\ \ s)}_{m_{l_k} m_{s_k}}\left[\,|\,l m_{l_1} s m_{s_1}\,\rangle|\ldots\rangle|\,l m_{l_{k-1}} s m_{s_{k-1}}\,\rangle|\,l m_{l_{k+1}} s m_{s_{k+1}}\,\rangle|\ldots\rangle|\,l m_{l_N} s m_{s_N}\,\rangle\right]$$
$$= (-1)^{k-1}\,|\,l m_{l_1} s m_{s_1}\,\rangle|\ldots\rangle|\,l m_{l_N} s m_{s_N}\,\rangle\;. \tag{1.23}$$

The mutual electron interaction couples the spin and angular momenta. If the non-central Coulomb repulsion prevails over the relativistic spin-orbit interaction, the angular momenta $\mathbf{l}$ of the N electrons couple to a resulting total momentum $\mathbf{L}$ and the spin momenta $\mathbf{s}$ to the final spin momentum $\mathbf{S}$. The angular momenta l and s of the Nth electron are coupled to its antisymmetric parent wave functions $|\,l^{N-1}L'S'\,\rangle$

$$|\,l^{N-1}L'S', ls, LSM_L M_S\,\rangle = \sum_{M'_L M'_S m_l m_s} \begin{bmatrix} L' & l & L \\ M'_L & m_l & M_L \end{bmatrix}\!\!\begin{bmatrix} S' & s & S \\ M'_S & m_s & M_S \end{bmatrix}$$
$$\times\,|\,l^{N-1}L'S'M'_L M'_S\,\rangle|\,l m_l s m_s\,\rangle\;. \tag{1.24}$$

The use of the conventional Clebsch-Gordan coupling coefficients (the expression in square brackets) assures the conservation of the angular symmetry [25].

The final wave function has to be antisymmetric under the exchange of any two electrons. To form a complete antisymmetric wave function $|\,nl^N LS\,\rangle$ for all N electrons,

a linear combination that assures the antisymmetry under the exchange of the Nth electron is used,

$$|\,l^N LSM_L M_S\,\rangle \;=\; \sum_{L'S'} \langle\, l^{N-1}(L'S')l\,|\,l^N LS\,\rangle\,|\,l^{N-1}L'S', l, LSM_L M_S\,\rangle\,. \qquad (1.25)$$

The expansion coefficients $\langle\, l^{N-1}(L'S')l\,|\,l^N LS\,\rangle$ are called coefficients of fractional parentage. The tensorial properties of the wave function and the creation operator allow to couple the creation operator to the wave function of $N-1$ electrons to the final momenta L and S

$$[\mathbf{a}^{(ls)} \times |\,l^{N-1}L'S'\,\rangle]^{(LS)}_{M_L M_S} = \sum_{M'_L M'_S\, m_l m_s} \mathbf{a}^{(l\ s)}_{m_l m_s}\,|\,l^{N-1}L'S'M'_L M'_S\,\rangle \times \begin{bmatrix} l & L' & L \\ m_l & M'_L & M_L \end{bmatrix} \begin{bmatrix} s & S' & S \\ m_s & M'_S & M_S \end{bmatrix}. \qquad (1.26)$$

By projecting Eq. 1.26 on the wave function $\langle\, l^N LSM_L M_S\,|$, the relationship

$$\langle\, l^N LS \,\|\, \mathbf{a}^{(ls)} \,\|\, l^{N-1}L'S'\,\rangle \;=\; (-1)^N\,(N[L,S])^{1/2}\langle\, l^N LS\,|\,l^{N-1}(L'S')l\,\rangle \qquad (1.27)$$

between the reduced matrix element of the creation operator and the coefficients of fractional parentage is obtained [41].

For $l > 1$ there can be more than one term with the same **L** and **S** quantum numbers. An additional symmetry is needed that serves to distinguish the terms. The Hamiltonian does not change the number of paired electrons, i.e. two electrons nl^2 coupled to a final momentum of $L = 0$ and $S = 0$. Such an electron pair is created or annihilated by the following operators, respectively,

$$q^{(1)}_1 \;= -\frac{i}{2}\Big[\mathbf{a}^{(ls)} \times \mathbf{a}^{(ls)}\Big]^{(00)}, \quad q^{(1)}_{-1} \;= -\frac{i}{2}\Big[\tilde{\mathbf{a}}^{(ls)} \times \tilde{\mathbf{a}}^{(ls)}\Big]^{(00)}. \qquad (1.28)$$

Together with the operator

$$q^{(1)}_0 \;= -\frac{i}{4}\left\{\Big[\mathbf{a}^{(ls)} \times \tilde{\mathbf{a}}^{(ls)}\Big]^{(00)} + \Big[\tilde{\mathbf{a}}^{(ls)} \times \mathbf{a}^{(ls)}\Big]^{(00)}\right\} \qquad (1.29)$$

these three operators meet the conditions for being irreducible components of a momentum operator $\mathbf{q}$, called quasispin. The z-component of $\mathbf{q}$ can be written as

$$q_z \;=\; -i\, q_0^{(1)} = [\mathbf{N} - \mathbf{N}_h]/4 \tag{1.30}$$

where $\mathbf{N} = [\mathbf{a}^{ls} \times \tilde{\mathbf{a}}^{(ls)}]^{(00)}$ counts the electrons in the pairing state and $\mathbf{N_h} = [\tilde{\mathbf{a}}^{ls} \times \mathbf{a}^{(ls)}]^{(00)}$ the missing ones (the holes). The quasispin of all pairing states in a shell can be coupled to the total quasispin momentum $\mathbf{Q}$:

$$\mathbf{Q}_1^{(1)} = -\frac{i}{2}\,(2l+1)^{1/2}\,[\mathbf{a}^{ls}\times\mathbf{a}^{(ls)}]^{(00)}; \tag{1.31}$$

$$\mathbf{Q}_{-1}^{(1)} = -\frac{i}{2}\,(2l+1)^{1/2}\,[\tilde{\mathbf{a}}^{ls}\times\tilde{\mathbf{a}}^{(ls)}]^{(00)}; \tag{1.32}$$

$$\mathbf{Q}_0^{(1)} = -\frac{i}{4}\,(4l+2)^{1/2}\left\{[\mathbf{a}^{ls}\times\tilde{\mathbf{a}}^{(ls)}]^{(00)} + [\tilde{\mathbf{a}}^{ls}\times\mathbf{a}^{(ls)}]^{(00)}\right\}. \tag{1.33}$$

The eigenvalue of the z-projection is related to the number of electrons in a shell,

$$M_Q \;=\; \frac{1}{2}(N - 2l + 1)\,. \tag{1.34}$$

As the quasispin operator $\mathbf{Q}$ commutes with $\mathbf{L}$ and $\mathbf{S}$, the states of the l^N configuration can be characterized by the eigenvalues of the operators $\mathbf{L}^2, L_z, \mathbf{S}^2, S_z, \mathbf{Q}^2$ and Q_z

$$|\, nlQLSM_QM_LM_S\rangle\,. \tag{1.35}$$

Instead of using the quasispin and its projection, an equivalent representation is given by

$$|\, nl^N\nu LSM_LM_S\rangle \tag{1.36}$$

using N and the seniority quantum number $\nu = 2l + 1 - 2Q$ as additional quantum numbers. Additional symmetries have to be used for $l > 2$; more details are found in [41] and the reference therein.

Acting with $\mathbf{a}^{(ls)}$ on a shell state, one electron is created and one hole is annihilated. Thereby the projection of the quasispin m_q is changed by one half, see Eq. 1.30. The annihilation operator decreases m_q by one half. The commutator relations between the

components of $\mathbf{q}$ and the creation and annihilation operators show, indeed, that $\mathbf{a}^{(ls)}$ and $\tilde{\mathbf{a}}^{(ls)}$ are components of an irreducible tensor of rank $q = 1/2$ in the quasispin space

$$[\mathbf{Q}^{(1)}_{\rho}, \mathbf{a}^{(q)}_{m}] = i\sqrt{q(q+1)}\begin{bmatrix} q & 1 & q \\ m & \rho & m+\rho \end{bmatrix}\mathbf{a}^{(q)}_{m+\rho}, \tag{1.37}$$

where

$$\mathbf{a}^{(q)}_{m} = \begin{cases} \mathbf{a}^{(ls)} & \text{for } m = 1/2 \\ \tilde{\mathbf{a}}^{(ls)} & \text{for } m = -1/2\,. \end{cases} \tag{1.38}$$

Second quantization operators can be expanded in terms of triple tensors in orbital, spin and quasispin space. The wave functions of a shell of equivalent electrons are classified using the quantum numbers L, S, Q, M_L, M_S and M_Q of the three commuting angular momenta in these spaces. Therefore the Wigner-Eckhart theorem [25] can be applied in all three spaces. The completely reduced matrix elements are independent of the shell occupation. The completely (in all three spaces) reduced matrix element of the creation operator is called reduced coefficient of fractional parentage. It is related to the coefficients of fractional parentage (Eq. 1.39) by [41]

$$\begin{aligned}\langle l^N \alpha QLS \,|\, l^{N-1}(\alpha_1 Q_1 L_1 S_1) l \rangle = (-1)^{N-1}(N[Q,L,S])^{(-1/2)} \\ \times \begin{bmatrix} Q_1 & 1/2 & Q \\ M_{Q_1} & 1/2 & M_Q \end{bmatrix} \langle\, l\alpha QLS \,|||\, \mathbf{a}^{(qls)} \,|||\, l\alpha_1 Q_1 L_1 S_1 \,\rangle\,. \end{aligned} \tag{1.39}$$

The main advantage of these reduced coefficients of fractional parentage over the usual ones is that they are independent of the shell occupation number N. Their number is thus much smaller. Furthermore, the quasispin methodology defines a consistent phase for all reduced coefficients of fractional parentage. Tables of their values exist in published version [38] and in electronic form [44].

With repeated use of Eq. 1.24, the shells can be coupled one to another to the final momenta $\mathbf{L}$ and $\mathbf{S}$,

$$\begin{aligned}|\,\gamma L M_L S M_S \,\rangle^s = |\, n_1 l_1^{N_1} \gamma_1 L_1 S_1, n_2 l_2^{N_2} \gamma_2 L_2 S_2, L_{12} S_{12}, n_3 l_3^{N_3} \gamma_3 L_3 S_3, L_{123} S_{123} \\ \cdots n_m l_m^{N_m} \gamma_m L_m S_m, L M_L S M_S \rangle\,, \end{aligned} \tag{1.40}$$

where additional quantum numbers are denoted by γ. This wave function is only antisymmetric in the permutation of electrons inside each shell. To antisymmetrize the wave function between different shell permutations, the following restricted permutations are used

$$|\gamma LM_L SM_S\rangle = \left(\frac{\prod_{a=1}^{m} n_a!}{N!}\right)^{1/2} \sum_{\mathcal{P}} (-1)^p \mathcal{P} |\gamma LM_L SM_S\rangle^s , \qquad (1.41)$$

where the sum is over all permutations $\mathcal{P}$, involving coordinate exchange only between two different subshells such that the coordinate number within each subshell remains in an increasing order. This wave function is called a configuration state function.

If the relativistic spin-orbit coupling is stronger than the non-symmetric part of the Coulomb interaction, the electron spins $\mathbf{l}$ and $\mathbf{s}$ couple to the total momentum $\mathbf{j}$. The Coulomb interaction couples the total $\mathbf{j}_k$ to the final momentum $\mathbf{J}$. To form antisymmetric states, the same formalism based on the relativistic reduced coefficients of fractional parentage is used. A shell is denoted by $|nlj^N J\rangle$. No additional symbols are necessary in this coupling scheme. For the final configuration state function, all shells are successively coupled to the final momentum $\mathbf{J}$ and additionally antisymmetrized by permutations between the shells.

A general configuration consists of groups of equivalent electrons

$$n_1 l_1^{N_1}\, n_2 l_2^{N_2} \cdots n_m l_m^{N_m} , \quad N = \sum_{a=1}^{m} N_a . \qquad (1.42)$$

From this configuration, the configuration state functions are formed and used as the $|\psi_i\rangle$ in Eq. 1.12 for the multiconfiguration approach to determine the radial orbitals and the mixing coefficients. Thereby, the atomic state function $|\Psi\rangle$ is obtained that is used in the calculation of the atomic properties.

2 The hyperfine structure operator

The expression for the hyperfine operators are derived in detail in [45]. These operators are transformed for this thesis to triple tensors in orbital $\mathbf{l}$, spin $\mathbf{s}$ and total spin $\mathbf{j}$ space using atomic units and the standard (Fano-Racah) phase system.

The tensorial expression of the electric interaction follows from the development of the electrostatic potential into spherical harmonics. With the definition of the nuclear electric multipole momentum Eq. 1.3, the electric multipole interaction operator has the form

$$\mathbf{T_e}^{(k)} \;=\; -i^k \sum_j r_j^{-k-1} \mathbf{C}_j^{(k)} \,. \tag{2.1}$$

As pointed out in [45], the contributions of the part of the electronic wave function that is inside the nucleus can be ignored. The detailed tensorial structure indicating the ranks in l, s and j spaces for one electron is given by the triple tensor

$$\mathbf{T_e}^{(k\,0\,k)} \;\equiv\; -i^k r^{-k-1} \mathbf{C}^{(k)} \,. \tag{2.2}$$

Following from that, $\mathbf{C}^{(k)}$ acts in the $\mathbf{l}$ space and there are no operators acting in the $\mathbf{s}$ space. The tensors of the electron part of the magnetic multipole interaction are the following:

$$\mathbf{T_m}^{(k)} = \sum_j \frac{1}{2}\alpha^2 r_j^{-k-2} \Bigg(i^k 2 \sqrt{\frac{2k-1}{k}} \left[\mathbf{C}_j^{(k-1)} \times \mathbf{L}_j^{(1)}\right]^{(k)} + i^{k+2} g_s \sqrt{(2k+3)(k+1)} \left[\mathbf{C}_j^{(k+1)} \times \mathbf{S}_j^{(1)}\right]^{(k)} \Bigg) \tag{2.3}$$

with gyromagnetic ratio $g_s = 2.00232$. The operator of the magnetic multipole interaction of one electron has two terms with different tensorial structure, namely

$$\mathbf{T_m}^{(k\,0\,k)} + \mathbf{T_m}^{(k+1\,1\,k)} \equiv \alpha^2 r^{-k-2} i^k \sqrt{\frac{2k-1}{k}} \left[\mathbf{C}^{(k-1)} \times \mathbf{L}^{(1)}\right]^{(k)} + \frac{g_s}{2}\alpha^2 r^{-k-2} i^{k+2} \sqrt{(2k+3)(k+1)} \left[\mathbf{C}^{(k+1)} \times \mathbf{S}^{(1)}\right]^{(k)} . \tag{2.4}$$

The first term acts in l and j spaces and has rank k, while the second has the rank $k+1$ in l space, the rank 1 in s space and the rank k in j space.

To arrive at Eq. 2.3 one has to assume that the electrons do not penetrate the nucleus. The s electrons, however, have a certain probability of being in the nucleus. This contribution depends essentially on the radial wave function at the nucleus and is the most difficult part to determine in hyperfine structure calculations. The Fermi contact contribution is a first-order effect for a point nucleus. An arbitrary distribution of the magnetization inside the nucleus can be assumed. In order to get higher-order effects, it is necessary to make more realistic assumptions about the nucleus. Such effects lead to the so-called hyperfine anomaly [46]. Although this is a small effect, it has been observed experimentally for the dipole interactions of s electrons in many cases. There are other nuclear size effects which may contribute to the hyperfine anomaly [45]. Without the hyperfine anomaly, the detailed calculation lead to the contact contribution

$$\begin{aligned} \mathbf{T_c}^{(k)} &= \sum_j 2\pi\alpha^2 g_s\, i^k\, \frac{k+1}{2k+1} \sqrt{\frac{2k-1}{k}}\, r_j^{-k+1}\, \delta(\mathbf{r}_j) \left[\mathbf{S}_j^{(1)} \times \mathbf{C}_j^{(k-1)}\right]^{(k)} \\ &\equiv \mathbf{T_c}^{(k-1\,1)\,k} \end{aligned} \tag{2.5}$$

where $\delta(\mathbf{r})$ is the three-dimensional delta function.

The spin-angular integration allows one to calculate the magnetic dipole constant A and electric quadrupole constant B in terms of the reduced matrix elements of the electron spherical tensors $\mathbf{T_m}^{(1)}$, $\mathbf{T_c}^{(1)}$ and $\mathbf{T_e}^{(2)}$ for any atom or ion with any number of open shells by:

$$A_J = \frac{\mu_I}{I} \frac{1}{\sqrt{J(J+1)(2J+1)}} \langle J \| \mathbf{T_m}^{(k_l\, k_s)\,1} + \mathbf{T_c}^{(k_l\, k_s)\,1} \| J \rangle \,, \tag{2.6}$$

$$B_J = Q \sqrt{\frac{4J(2J-1)}{(J+1)(2J+1)(2J+3)}} \langle J \| \mathbf{T_e}^{(k_l\, k_s)\,2} \| J \rangle \,. \tag{2.7}$$

The atomic state function is abbreviated by $|J\rangle$. These two constants are experimental measurable quantities, see Eq. I from the introduction.

2.1 Irreducible tensorial form in second quantization

The hyperfine structure operator is a one-particle operator. One electron of the bra function interacts with one electron of the ket function. The second quantization approach represents any one-particle operator by a sum over all possible single particle matrix elements $\langle i|f|j\rangle$. The creation a and annihilation $a^\dagger$ operators for the particles i and j define the operator attributes,

$$F = \sum_{i,j} a_i \, a_j^\dagger \, \langle i|f|j\rangle \, . \tag{2.8}$$

Spherical tensor operators play a central role in the atomic theory. They transform into each other according to their rank, defined by the space they are acting in. The creation and annihilation operators for an electron act in the orbital space of the electron l and its spin space s. As the one-particle operator acts in the same spaces, it has the ranks k_l and k_s ascribed, respectively. Applying the Wigner-Eckhart theorem on the matrix element in Eq. 2.8, the one-particle operator can be written as

$$F^{(k_l\,k_s)} = - \sum_{\substack{nlm_l\,m_s\,,\\ n'l'm_l'm_s'}} [k_l,k_s]^{-1/2} \begin{bmatrix} l' & k_l & l \\ m_l' & \lambda & m_l \end{bmatrix} \begin{bmatrix} s' & k_s & s \\ m_s' & \sigma & m_s \end{bmatrix} \times a^{(l\,s)}_{m_l\,m_s} \; a^{\dagger(l'\,s')}_{m_l'\,m_s'} \, \langle nls\|f^{(k_l\,k_s)}\|n'l's'\rangle \, . \tag{2.9}$$

Using the definition Eq. 1.20 for the annihilation operator allows one to couple the second quantization operators and express any spherical one-particle operator in the following compact form:

$$F^{(k_l\,k_s)} = -[k_l,k_s]^{-1/2} \Big[a^{(l\,s)} \times \tilde{a}^{(l'\,s')} \Big]^{(k_l\,k_s)} \langle nls\|f^{(k_l\,k_s)}\|n'l's'\rangle \, . \tag{2.10}$$

The creation and annihilation operators are components of a tensor in quasispin space as pointed out in Eq. 1.38. The operator F is given with additional quasispin space by

$$F^{(k_l\,k_s)} = -[k_l,k_s]^{-1/2} \Big[a^{(q\,l\,s)}_{1/2} \times a^{(q\,l'\,s')}_{-1/2} \Big]^{(k_l\,k_s)} \langle nls\|f^{(k_l\,k_s)}\|n'l's'\rangle \, . \tag{2.11}$$

This representation is universal for any one-particle operator, only the single electron reduced matrix element $\langle nls\|f^{(k_l\,k_s)}\|n'l's'\rangle$ defines the peculiarities of the operator.

The tensorial structure of the hyperfine structure operators are known (Eq. 2.2, Eq. 2.4, Eq. 2.5). The one-electron submatrix elements $\langle\, n_i l_i s \,\|\, \mathbf{f}^{(k_l k_s)} \,\|\, n_j l_j s \,\rangle$ for the electric quadrupole, magnetic dipole and the Fermi contact term are derived, now. The submatrix elements depend only on the values of the ranks in $\mathbf{l}$ and $\mathbf{s}$ spaces. The dependence on the value of rank in the $\mathbf{j}$ space is in the tensorial part of the formula. Therefore, in the treatment of one-electron submatrix elements for a physical operator only the values of the ranks in the $\mathbf{l}$ and $\mathbf{s}$ spaces are indicated. The expression $\mathbf{T}^{(k_l\, k_s)}$ for the notation of the submatrix element is used instead of $\mathbf{T}^{(k_l\, k_s)\, k_j}$ for the operator. The tensorial part of $\mathbf{F}^{(k_l k_s)}$ is called the pure spin-angular coefficient and is the same for any one-particle operator.

The electric multipole interaction operator Eq. 2.2 has the tensorial structure $k_l = k$ and $k_s = 0$. The one-electron submatrix element is

$$\langle\, nls \,\|\, \mathbf{T_e}^{(k0)} \,\|\, n'l's \,\rangle \;=\; -i^k \,\langle\, l \,\|\, \mathbf{C}^{(k)} \,\|\, l' \,\rangle\, \langle\, nl \,\|\, r^{-k-1} \,\|\, n'l' \,\rangle\,. \qquad (2.12)$$

It is not equal to zero if $l + k + l'$ is an even number.

The operator of the magnetic multipole interaction Eq. 2.4 has two terms with different tensorial structures. The first term acts in $\mathbf{l}$ and $\mathbf{j}$ spaces and has rank k, while the second has the rank $k+1$ in $\mathbf{l}$ space, rank 1 in $\mathbf{s}$ space and rank k in $\mathbf{j}$ space. Keeping in mind that

$$\langle\, l \,\|\Big[\mathbf{C}^{(k-1)} \times \mathbf{L}^{(1)}\Big]^{(k)} \|\, l' \,\rangle = \frac{i}{2}\,\langle\, l \,\|\, \mathbf{C}^{(k-1)} \,\|\, l' \,\rangle \times \sqrt{\frac{(l+l'+k+1)(l'+k-l)(l+k-l')(l+l'-k+1)}{k(2k-1)}}\,, \qquad (2.13)$$

the one-particle submatrix element has the form:

$$\langle\, nls \,\|\, \mathbf{T_m}^{(k0)} \,\|\, n'l's \,\rangle = \frac{1}{2}\,\alpha^2\, i^{k+1}\,\frac{1}{k}\,\langle\, l \,\|\, \mathbf{C}^{(k-1)} \,\|\, l' \,\rangle\, \langle\, nl \,\|\, r^{-k-2} \,\|\, n'l' \,\rangle \times \sqrt{(l+l'+k+1)(l'+k-l)(l+k-l')(l+l'k+1)}\,. \qquad (2.14)$$

Taking into account that, for $k = 1$, Eq. 2.13 becomes

$$\langle\, l \,\|\, \mathbf{L}^{(1)} \,\|\, l' \,\rangle \;=\; i\,\sqrt{l(l+1)(2l+1)}\,\delta(l,l')\,, \qquad (2.15)$$

the one-electron submatrix element of the operator $\mathbf{T}_m^{(10)}$ is equal to

$$\langle nls \| \mathbf{T}_m^{(10)} \| n'l's \rangle = -\frac{1}{2}\sqrt{l(l+1)(2l+1)}\,\delta(l,l')\,\langle nl\|r^{-3}\|n'l'\rangle\,. \quad (2.16)$$

The second term $\mathbf{T}_m^{(k+11)}$ in Eq. 2.4 has the general one-electron submatrix element

$$\langle nls \| \mathbf{T}_m^{(k+11)} \| n'l's \rangle = \frac{i^{k+3}}{2}\,\alpha^2\,g_s\,\langle l\|\mathbf{C}^{(k+1)}\|l'\rangle\langle nl\|r^{-k-2}\|nl'\rangle \times\sqrt{\frac{3}{2}(2k+3)(k+1)}\,. \quad (2.17)$$

It follows from here that for $\mathbf{T}_m^{(21)}$ the diagonal, with respect to the orbital momentum quantum number l, one-electron submatrix elements are

$$\langle nls \| \mathbf{T}_m^{(21)} \| n'ls \rangle = -\frac{\alpha^2}{2}\,g_s\sqrt{\frac{15l(l+1)(2l+1)}{(2l+3)(2l-1)}}\,\langle nl\|r^{-3}\|n'l\rangle\,. \quad (2.18)$$

This is in accordance with [47]. The off-diagonal (with respect to l), one-electron submatrix elements have the forms:

$$\langle nls \| \mathbf{T}_m^{(21)} \| n'(l-2)s \rangle = -\frac{3}{2}\,\alpha^2\,g_s\sqrt{\frac{5l(l-1)}{2(2l-1)}}\,\langle nl\|r^{-3}\|n'l-2\rangle \quad (2.19)$$

and

$$\langle nls \| \mathbf{T}_m^{(21)} \| n'(l+2)s \rangle = -\frac{3}{2}\alpha^2 g_s\sqrt{\frac{5(l+1)(l+2)}{2(2l+3)}}\,\langle nl\|r^{-3}\|n'l+2\rangle\,. \quad (2.20)$$

The Fermi-contact term has the tensorial structure $k_l = 0$ and $k_s = 1$. Using the relation $\langle nl\|4\pi r^2\delta(\mathbf{r})\|nl\rangle = \langle nl\|\delta(r)\|nl\rangle$ between the three-dimensional (from Eq. 2.5) and one-dimensional delta functions, the one-electron submatrix element can be written as

$$\langle nls \| \mathbf{T}_c^{(01)} \| n'l's \rangle = -\frac{\alpha^2}{2}g_s\sqrt{\frac{3(2l+1)}{2}}\,\langle nl\|\frac{2}{3}r^{-2}\delta(r)\|n'l\rangle\,\delta(l,0)\delta(l',0)\,. \quad (2.21)$$

This term is nonzero only for s electrons.

The one-electron submatrix element $\langle n_i l_i s_i \| \mathbf{T}^{(k_l k_s)} \| n_j l_j s_j \rangle$ of all three operators of the hyperfine interaction is necessary to obtain the explicit tensorial second quantization form of the hyperfine interaction operators. The main peculiarity of these expressions

is the use of the tensorial properties of the operators in orbital $\mathbf{l}$, spin $\mathbf{s}$ and quasispin $\mathbf{q}$ space. For instance, the final expressions of the electric multipole interaction operator in the coupled tensorial form of second quantization follows from Eq. 2.11 by inserting the one-electron submatrix element Eq. 2.12:

$$\mathbf{F_e} = \mathbf{T_e}^{(k)} = i^k \sum_{n_i l_i, n_j l_j} [k]^{-1/2} \langle l_i \| \mathbf{C}^{(k)} \| l_j \rangle \times \langle n_i l_i \| r^{-k-1} \| n_j l_j \rangle \left[\mathbf{a}_{1/2}^{(q\, l_i\, s)} \times \mathbf{a}_{-1/2}^{(q\ \ l_j\, s)} \right]^{(k0)k}. \quad (2.22)$$

In a similar way, the relevant expressions for the other hyperfine operators are found:

$$\mathbf{F_c} = \mathbf{T_c}^{(1)} = \frac{\alpha^2}{2\sqrt{2}} g_s \sum_{n_i l_i, n_j l_j} \sqrt{(2l_i+1)} \langle n_i l_i \| \frac{2}{3} r^{-2} \delta(r) \| n_j l_j \rangle \times \left[\mathbf{a}_{1/2}^{(q\, l_i\, s)} \times \mathbf{a}_{-1/2}^{(q\ \ l_j\, s)} \right]^{(01)1} \delta(l_i, 0)\delta(l_j, 0) \quad (2.23)$$

and

$$\begin{aligned} \mathbf{F_m} = \mathbf{T_m}^{(k)} = -i^{k+1} \frac{\alpha^2}{2k\sqrt{k}} \sum_{n_i l_i, n_j l_j} & \sqrt{(l_i + l_j + k + 1)(l_j + k - l_i)} \\ & \times \sqrt{(l_i + k - l_j)(l_i + l_j - k + 1)} \langle l_i \| \mathbf{C}^{(k-1)} \| l_j \rangle \\ & \times \langle n_i l_i \| r^{-k-2} \| n_j l_j \rangle \left[\mathbf{a}_{1/2}^{(q\, l_i\, s)} \times \mathbf{a}_{-1/2}^{(q\ \ l_j\, s)} \right]^{(k0)k} \\ & - \frac{1}{2} \alpha^2 i^{k+3} g_s \sqrt{\frac{(k+1)}{2}} \sum_{n_i l_i, n_j l_j} \langle l_i \| \mathbf{C}^{(k+1)} \| l_j \rangle \\ & \times \langle n_i l_i \| r^{-k-2} \| n_j l_j \rangle \left[\mathbf{a}_{1/2}^{(q\, l_i\, s)} \times \mathbf{a}_{-1/2}^{(q\ \ l_j\, s)} \right]^{(k+1\ 1)k}. \end{aligned} \quad (2.24)$$

In the following section the new hyperfine structure expressions Eq. 2.22, Eq. 2.23 and Eq. 2.24 are used for the efficient evaluation of the matrix elements of the hyperfine interaction operators for arbitrary electronic configurations.

2.2 The general expression for the matrix elements

In a configuration state function, the interacting electron is coupled to a shell. The shell, in turn, is coupled to the other shells. The decoupling of the electron can be done by applying graphical techniques. They are explained, for example, in [36]. Rather than

going into details, the calculation of the decoupling part $\mathcal{R}$ is illustrated by considering an example (without mentioning the phase). The general formula are summarized thereafter. The calculation follows the approach described in [37].

Each space is independent and therefore each space can be decoupled separately. The explicit calculations are done for one space only. For several spaces, one has to take the product of the decoupling elements, $\mathcal{R} = \mathcal{R}_L \cdot \mathcal{R}_S$ for LS-coupled wave functions, for example. In the following, the space is denoted by $\mathbf{L}$, a shell is abbreviated by $|\lambda\rangle$ and an electron by $|l\rangle$. The matrix element A of a one-particle operator with rank k in the $\mathbf{L}$ space acting on the shells a and b of configuration state functions with u shells then reads

$$\begin{aligned} A_{ab} = \langle \lambda_1\lambda_2 L_{12}\lambda_3 L_{123}\ldots\lambda_a L_{1\ldots a}\ldots\lambda_v L_{1\ldots v}\ldots\lambda_b L_{1\ldots b} \\ \ldots\lambda_{u-1}L_{1\ldots u-1}\lambda_u L\,|\,\mathbf{F}^{(k)}(a,b)\,|\,\lambda_1\lambda_2 L'_{12}\lambda_3 L'_{123}\ldots\lambda'_a L'_{1\ldots a} \\ \ldots\lambda_v L'_{1\ldots v}\ldots\lambda'_b L'_{1\ldots b}\ldots\lambda_{u-1}L'_{1\ldots u-1}\lambda'_u L'\rangle\,. \end{aligned} \tag{2.25}$$

The graphical representation of this matrix element is given in Fig. 1. Rules exist for cutting through the graph, connecting two loose ends or connecting three loose ends by a new vertex [25]. The main cutting lines are indicated in Fig. 1 by the dashed lines (I, II, III and IV). Cutting through line I and connecting the loose ends, the left part can successively be cut further into the delta function parts, see Fig. 2. This decoupling element amounts to

$$\mathcal{R}_I \;=\; \prod_{\alpha=1}^{a-1}\delta(L_\alpha, L'_\alpha)\,\delta(L_{12\ldots\alpha}, L'_{12\ldots\alpha})\,. \tag{2.26}$$

Cutting at line II through three lines, the loose ends are connected by a new vertex. The part that is cut free can be transformed into Fig. 3, which is essentially a 6j-symbol,

$$\mathcal{R}_{II} \;=\; (-1)^{L_{1\ldots a-1}+L_{1\ldots a}+L'_a+k_l}\left[L_a, L'_{1\ldots a}\right]^{1/2}\begin{Bmatrix} k & L'_a & L_a \\ L_{1\ldots a-1} & L_{1\ldots a} & L'_{1\ldots a}\end{Bmatrix}. \tag{2.27}$$

Cutting along III for all following parts ν, a product of 6j-symbols expression is obtained,

$$\mathcal{R}_{\mathrm{III}} = \prod_{\nu=a+1}^{b-1} (-1)^{l_a+L_\nu+L_{1\ldots\nu-1}+L'_{1\ldots\nu}} \left[L_{1\ldots\nu-1}, L'_{1\ldots\nu}\right]^{1/2} \left\{ \begin{array}{ccc} l_a & L'_{1\ldots\nu-1} & L_{1\ldots\nu-1} \\ L_\nu & L_{1\ldots\nu} & L'_{1\ldots\nu} \end{array} \right\}. \tag{2.28}$$

The part between the cutting lines III and IV leads to a 9j symbol as depicted in Fig. 4,

$$\mathcal{R}_{\mathrm{IV}} = [L_{1\ldots b-1}, L_b, L'_{1\ldots b}, k]^{1/2} \left\{ \begin{array}{ccc} L'_{1\ldots b-1} & l_a & L_{1\ldots b-1} \\ L'_b & l_b & L_{34} \\ L'_{1\ldots b} & k & L'_{1\ldots b} \end{array} \right\}. \tag{2.29}$$

In the part that is left over, similar to the part ν, all parts before $u-1$ are cut out to obtain a product of 6j-symbols,

$$\mathcal{R}_{\mathrm{V}} = \prod_{\nu=b+1}^{u-1} (-1)^{k+L_\nu+L_{1\ldots\nu-1}+L'_{1\ldots\nu}} \left[L_{1\ldots\nu-1}, L'_{1\ldots\nu}\right]^{1/2} \left\{ \begin{array}{ccc} k & L'_{1\ldots\nu-1} & L_{1\ldots\nu-1} \\ L_\nu & L_{1\ldots\nu} & L'_{1\ldots\nu} \end{array} \right\}. \tag{2.30}$$

The final part is again a 6j-symbol,

$$\mathcal{R}_{\mathrm{VI}} = (-1)^{k+L_u+L_{1\ldots u-1}+L'} \left[L_{1\ldots u-1}, L'\right]^{1/2} \left\{ \begin{array}{ccc} k & L'_{1\ldots u-1} & L_{1\ldots u-1} \\ L_u & L & L' \end{array} \right\}. \tag{2.31}$$

Any decoupling matrix for the one-particle operator $\mathcal{R}$ is given as a product of different parts of the $\mathcal{R}_x$. The analytical expressions for the decoupling matrices presented in this section are general and valid for any non-scalar one-particle operator (operator consisting of tensorial products of tensorial operators). For one interacting shell, the

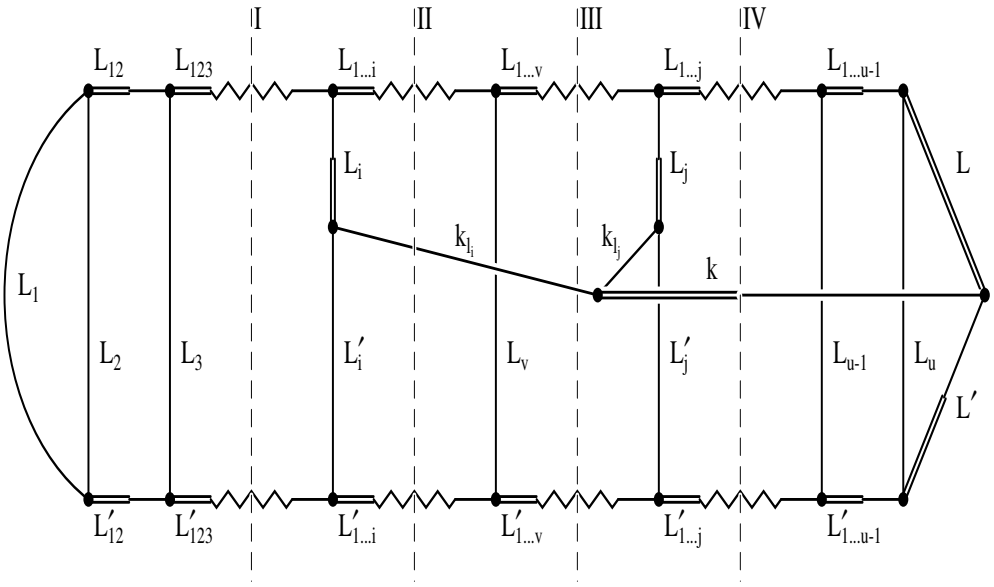

Fig 1. Graphical representation of the matrix element for a one-particle operator acting between two different shells i and j. The operator acts in orbital space with rank k, only. The configuration state functions have u shells. Cuts through the diagram are indicated by the dashed lines (I,II,III,IV).

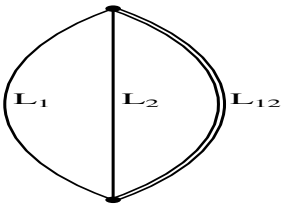

Fig 2. Delta function, obtained by the first parts left of cutting line I.

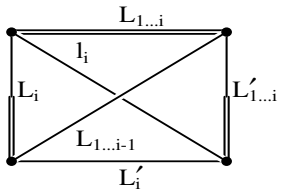

Fig 3. Part C1, obtained by cutting out the intermediate parts, 6j-symbol.

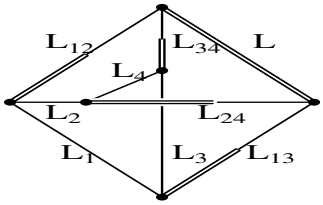

Fig 4. Part C4, obtained by cutting out the part between III and IV, 9j-symbol.

operators of second quantization act on the same shell denoted by a. The decoupling matrix has the expression:

$$\mathcal{R}(l_a, L_a, k_l) = [L_a]^{-1/2}\delta(L_1, L_1')\ldots\delta(L_{a-1}, L_{a-1}')\delta(L_{a+1}, L_{a+1}')\ldots\delta(L_u, L_u')$$
$$\times\begin{cases}\delta(L_1, L_1', k_l) & \text{for } u = 1\\ C_1 & \text{for } u = 2\\ C_1C_2(k_l, a+1, u-1)C_3 & \text{for } a < 3, u > 2\\ \delta(L_{12}, L_{12}')\ldots\delta(L_{12\ldots a-1}, L_{12\ldots a-1}') & \\ \quad\times C_1C_2(k_l, a+1, u-1)C_3 & \text{for } a > 3, a \neq u, u > 2\\ \delta(L_{12}, L_{12}')\ldots\delta(L_{12\ldots a-1}, L_{12\ldots a-1}')C_3 & \text{for } a = u, u > 2\,.\end{cases} \tag{2.32}$$

The notation $\delta(L_1, L_1', k_l)$ stands for the triangular condition. That is one if $|L_1 - L_1'| \leq k_l \leq L_1 + L_1'$ is fulfilled, and zero otherwise. The coefficient C_1 is

$$C_1 \;=\; (-1)^{\varphi}[L_a, T']^{1/2}\begin{Bmatrix} k_l & L_a' & L_a \\ J & T & T'\end{Bmatrix}, \tag{2.33}$$

where the values of parameters φ, J, T and T' occurring in expression Eq. 2.33 are given in Table 1. The remaining two coefficients are

Table 1. Parameters for C_1 of Eq. 2.33

u	a	φ	J	T	T'
2	1	$L_1 + 2L_1' - L_2 - L' + k_l$	L_2	L	L'
2	2	$L_1 + L + L_2' + k_l$	L_1	L	L'
$u \neq 2$	1	$L_1 + 2L_1' - L_2 - L_{12}' + k_l$	L_2	L_{12}	L_{12}'
$u \neq 2$	2	$L_1 + L_{12} + L_2' + k_l$	L_1	L_{12}	L_{12}'
$u \neq 2$	$a > 2$	$L_{12\ldots a-1} + L_{12\ldots a} + L_a' + k_l$	$L_{12\ldots a-1}$	$L_{12\ldots a}$	$L_{12\ldots a}'$

$$C_2(k_l, k_{min}, k_{max}) = \begin{cases} \prod_{i=k_{min}}^{k_{max}} (-1)^{k_l+L_i+L_{12\ldots i-1}+L'_{12\ldots i}} [L_{12\ldots i-1}, L'_{12\ldots i}]^{1/2} \\ \qquad \times \begin{Bmatrix} k_l & L'_{12\ldots i-1} & L_{12\ldots i-1} \\ L_i & L_{12\ldots i} & L'_{12\ldots i} \end{Bmatrix} & \text{for } k_{min} \le k_{max} \\ 0 & \text{for } k_{min} > k_{max} \end{cases} \tag{2.34}$$

and

$$C_3 \;=\; (-1)^{\varphi} [J, L']^{1/2} \begin{Bmatrix} k_l & J' & J \\ j & L & L' \end{Bmatrix}, \tag{2.35}$$

where the parameters φ, j, J and J' are given in Table 2.

Table 2. Parameters for C_2 and C_3 of Eq. 2.34 and Eq. 2.35

u	φ	j	J	J'
$u \neq a$	$k_l + L_u + L_{12\ldots u-1} + L'$	L_u	$L_{12\ldots u-1}$	$L'_{12\ldots u-1}$
a	$k_l - L_{12\ldots u-1} + 2L_u + L'_u - L$	$L_{12\ldots u-1}$	L_u	L'_u

In the case of two interacting shells, one operator of second quantization acts upon a shell α and the second one acts upon β. The shells a and b are defined in the following equation by $a = \min\{\alpha, \beta\}$ and $b = \max\{\alpha, \beta\}$. The decoupling element is given by

$$\begin{aligned}\mathcal{R}(l_a, L_a, l_b, L_b, k_l) = (-1)^{\zeta}[L_a, L_b]^{-1/2}&\delta(L_1, L_1')\ldots\delta(L_{a-1}, L_{a-1}')\delta(L_{a+1}, L_{a+1}')\\ &\ldots\delta(L_{b-1}, L_{b-1}')\delta(L_{b+1}, L_{b+1}')\ldots\delta(L_u, L_u')\\ \times\begin{cases} C_4(K_{12}, K_{12}', k_l) & \text{for } a = 1, b = 2, u = 2\\ C_4(K_{12}, K_{12}', k_l)C_3 & \text{for } a = 1, b = 2, u = 3\\ C_4(K_{12}, K_{12}', k_l)C_2(k_l, 3, u-1)C_3 & \text{for } a = 1, b = 2, u > 3\\ C_1C_2(K_{12}, a+1, b-1)C_4(K_{12}, K_{12}', k_l) & \\ \quad\times C_2(k_l, b+1, u-1)C_3 & \text{for } a < 3, b > 2, b \neq u\\ C_1C_2(K_{12}, a+1, b-1)C_4(K_{12}, K_{12}', k_l) & \text{for } a < 3, b > 2, b = u\\ \delta(L_{12}, L_{12}')\ldots\delta(L_{12\ldots a-1}, L_{12\ldots a-1}')C_1 & \\ \quad\times C_2(K_{12}, a+1, b-1)C_4(K_{12}, K_{12}', k_l) & \\ \quad\times C_2(k_l, b+1, u-1)C_3 & \text{for } a \geq 3, b > 2, b \neq u\\ \delta(L_{12}, L_{12}')\ldots\delta(L_{12\ldots a-1}, L_{12\ldots a-1}')C_1 & \\ \quad\times C_2(K_{12}, a+1, b-1)C_4(K_{12}, K_{12}', k_l) & \text{for } a \geq 3, b = u\,. \end{cases}\end{aligned} \tag{2.36}$$

If $\alpha < \beta$ in Eq. 2.36 then $K_{12} = l_\alpha$ and $K_{12}' = l_\beta$. If $\alpha > \beta$ then $K_{12} = l_\beta$ and $K_{12}' = l_\alpha$. The phase factor ζ is

$$\zeta \;=\; \begin{cases} 0 & \text{for } \alpha < \beta\\ l_a + l_b - k_l & \text{for } \alpha > \beta \end{cases} \tag{2.37}$$

and the additional coefficient C_4 is defined as

$$C_4(k_1, k_2, k_l) \;=\; [J_1, J_2, J_3', k_l]^{1/2}\begin{Bmatrix} J_1' & k_1 & J_1\\ J_2' & k_2 & J_2\\ J_3' & k_l & J_3 \end{Bmatrix}. \tag{2.38}$$

The values of the parameters J_1, J_1', J_2, J_2', J_3 and J_3' that occur in Eq. 2.38 are given in Table 3.

Table 3. Parameters for C_4 in Eq. 2.38

a	b	u	J_1	J_1'	J_2	J_2'	J_3	J_3'
1	2	$u \neq b$	L_1	L_1'	L_2	L_2'	L_{12}	L_{12}
1	2	b	L_1	L_1'	L_2	L_2'	L	L
$a \neq 1$	$b \neq q2$	b	$L_{1\ldots u-1}$	$L'_{1\ldots u-1}$	L_u	L_u'	L	L′
in all other cases			$L_{1\ldots b-1}$	$L'_{1\ldots b-1}$	L_b	L_b'	$L_{1\ldots b}$	$L'_{1\ldots b}$

After the interacting shells are decoupled, the matrix element Eq. 2.25 can be written as

$$A_{ab} = \prod_x \mathcal{R}_x \langle n_a l_a s \| f^{(k_l k_s)} \| n_b l_b s \rangle \times \langle n_a l_a s\, L_a S_a \| \left[\mathbf{a}^{(q\, l_a\, s)}_{1/2} \times \mathbf{a}^{(q\, l_b\, s)}_{-1/2} \right]^{(k_l k_s)} \| n_b l_b s\, L_b S_b \rangle \,. \quad (2.39)$$

The tensorial part

$$\langle n_a l_a s\, L_a S_a \| \left[\mathbf{a}^{(q\, l_a\, s)}_{1/2} \times \mathbf{a}^{(q\, l_b\, s)}_{-1/2} \right]^{(k_l k_s)} \| n_b l_b s\, L_b S_b \rangle \quad (2.40)$$

is efficiently evaluated in quasispin space. If the operator acts on two different shells a and b, the creation and annihilation operators decouple and leading to the expression for Eq. 2.40 in quasispin space of

$$\langle l_a s\, L_a S_a \| \left[\mathbf{a}^{(q\, l_a\, s)}_{1/2} \times \mathbf{a}^{(q\, l_b\, s)}_{-1/2} \right]^{(k_l k_s)} \| n_b l_b s\, L_b S_b \rangle = \langle l_a^{N_a}\, \alpha_a Q_a L_a S_a M_Q \| \mathbf{a}^{(q\, l_a\, s)}_{1/2} \| l_a^{N'_a}\, \alpha_a Q_a L_a S_a M'_Q \rangle \times \langle l_b^{N_b}\, \alpha_b Q_b L_b S_b M_Q \| \mathbf{a}^{(q\, l_a\, s)}_{-1/2} \| l_b^{N'_b}\, \alpha_b Q_b L_b S_b M'_Q \rangle \,. \quad (2.41)$$

By applying the Wigner-Eckhart theorem in quasispin space the submatrix elements of operators of type $\mathbf{a}^{(q\ l)}_{m_q}$ are obtained in the form

$$\langle l^N\, \alpha Q L S M_Q \| \mathbf{a}^{(q\ l\, s)}_{m_q} \| l^{N'}\, \alpha' Q' L' S' M'_Q \rangle = -\left[Q\right]^{-1/2} \begin{bmatrix} Q' & 1/2 & Q \\ M'_Q & m_q & M_Q \end{bmatrix} \langle l\, \alpha Q L S \| \mathbf{a}^{(q\, l\, s)} \| l\, \alpha' Q' L' S' \rangle \,. \quad (2.42)$$

The last factor is the matrix element, reduced in all spaces, of the tensor $\mathbf{a}^{(q\,ls)}$. It is proportional to the so-called completely reduced coefficient of fractional parentage, compare Eq. 1.39.

If the operator acts on the same shell a, the tensorial expression is the compound operator

$$\begin{aligned}\langle nl^N\,\alpha QLSM_Q \| \left[\mathbf{a}^{(q\ \ ls)}_{m_{q_1}} \times \mathbf{a}^{(q\ \ ls)}_{m_{q_2}}\right]^{(k_l k_s)} \| nl^{N'}\,\alpha' Q' L' S' M'_Q\rangle \\ = \sum_{k_q, m_q} \left[Q\right]^{-1/2} \begin{bmatrix} q & q & k_q \\ m_{q_1} & m_{q_2} & m_q \end{bmatrix} \begin{bmatrix} Q' & k_q & Q \\ M'_Q & m_q & M_Q \end{bmatrix} \\ \times \langle nl\,\alpha QLS \| \boldsymbol{W}^{(k_q\,k_l\,k_s)} \| nl\,\alpha' Q' L' S'\rangle\,, \quad (2.43)\end{aligned}$$

where $\langle nl\,\alpha QLS \| \boldsymbol{W}^{(k_q\,k_l\,k_s)} \| nl\,\alpha' Q' L' S'\rangle$ denotes the completely reduced matrix element of the tensorial operator $\boldsymbol{W}^{(k_q\,k_l\,k_s)}(nl,nl) = \left[\mathbf{a}^{(q\,ls)} \times \mathbf{a}^{(q\,ls)}\right]^{(k_q k_l k_s)}$ in quasispin space. In terms of the fully reduced coefficients of fractional parentage

$$\langle l\,\alpha QLS \| \mathbf{a}^{(q\,ls)} \| l\,\alpha' Q' L' S'\rangle \quad (2.44)$$

one finds

$$\begin{aligned}\langle nl\,\alpha QLS \| \boldsymbol{W}^{(k_q\,k_l\,k_s)} \| nl\,\alpha' Q' L' S'\rangle = (-1)^{Q+L+S+Q'+L'+S'+k_q+k_l+k_s} \left[k_q, k_l, k_s\right]^{1/2} \\ \times \sum_{\alpha'' Q'' L'' S''} \begin{Bmatrix} q & q & k_q \\ Q' & Q & Q'' \end{Bmatrix} \begin{Bmatrix} l & l & k_l \\ L' & L & L'' \end{Bmatrix} \begin{Bmatrix} s & s & k_s \\ S' & S & S'' \end{Bmatrix} \\ \times \langle l\,\alpha QLS \| \mathbf{a}^{(q\,ls)} \| l\,\alpha'' Q'' L'' S''\rangle \langle l\,\alpha'' Q'' L'' S'' \| \mathbf{a}^{(q\,ls)} \| l\,\alpha' Q' L' S'\rangle\,. \quad (2.45)\end{aligned}$$

The decoupling of the interacting electrons from their shells amounts to simple expressions proportional to the completely reduced coefficients of fractional parentage. These are the standard quantities behind this approach.

In order to evaluate the hyperfine splitting of the atomic energy levels $E_{hfi}(IJF)$, the submatrix elements of the operator $\mathbf{T}^{(k)}$ with respect to the wave functions having,

in general, an arbitrary number of electronic shells is needed. In the case where the electronic wave function of the atom is given by a configuration state expansion

$$|\Psi(LS)J\rangle \;=\; \sum_i c_i\,|\psi_i(L_iS_i)J\rangle \tag{2.46}$$

the electronic submatrix elements can be written as follows:

$$\begin{aligned}\langle\Psi(LS)J\|\mathbf{F}^{(k_l\,k_s)\,k}\|\Psi'(L'S')J'\rangle &= \sum_{i,j} c_i\,c_j\,\langle\psi_i(L_iS_i)J\|\mathbf{F}^{(k_l\,k_s)\,k}\|\psi'_j(L'_jS'_j)J'\rangle \\ &= \sum_{i,j} c_i\,c_j \begin{Bmatrix} L'_j & S'_j & J' \\ k_l & k_s & k \\ L_i & S_i & J \end{Bmatrix} \sqrt{[k,J,J',L_i,S_i]}\,\langle\psi_i(L_iS_i)\|\mathbf{F}^{(k_l\,k_s)}\|\psi'_j(L'_jS'_j)\rangle\,. \end{aligned} \tag{2.47}$$

Both submatrix elements, diagonal and off-diagonal with respect to the electronic configurations of the operators under consideration are needed, as can be seen from Eq. 2.46 and Eq. 2.47.

The matrix elements of the one-particle non-scalar operator $\mathbf{F}^{(k_l\,k_s)}$ between configuration state functions with u open shells,

$$\begin{aligned}|\psi_u(LS)\rangle = |&n_1l_1^{N_1}L_1S_1\,n_2l_2^{N_2}L_2S_2L_{12}S_{12}\ldots n_al_a^{N_a}L_aS_aL_{1\ldots a}S_{1\ldots a} \\ &\ldots n_bl_b^{N_b}L_bS_bL_{1\ldots b}S_{1\ldots b}\ldots n_ul_u^{N_u}L_uS_uLS\rangle\end{aligned} \tag{2.48}$$

can be expressed as a sum over one-electron contributions

$$\langle\psi_u(LS)\|\mathbf{F}^{(k_l\,k_s)}\|\psi'_u(L'S')\rangle \;=\; \sum_{n_a,l_a,n_b,l_b} \langle\psi_u(LS)\|F(n_al_a,n_bl_b)\|\psi'_u(L'S')\rangle\,, \tag{2.49}$$

where

$$\begin{aligned}
\langle \psi_u(LS) \| F(n_a l_a, n_b l_b) \| \psi'_u(L'S') \rangle = (-1)^{\Delta+1} [k_l, k_s]^{-1/2} \\
\times \mathcal{R}(l_a, l_b, L_a, L_b, L'_a, L'_b, k_l) \mathcal{R}(s, S_a, S_b, S'_a, S'_b, k_s) \Big\{ \delta(n_a l_a, n_b l_b) \\
\times \langle l_a^{N_a} \alpha_a Q_a M_{Q_a} L_a S_a \| \left[\mathbf{a}_{1/2}^{(q\, l_a\, s)} \times \mathbf{a}_{-1/2}^{(q\, l_a\, s)} \right]^{(k_l k_s)} \| l_a^{N_a} \alpha_a Q_a M_{Q_a} L_a S_a \rangle \\
+ (1 - \delta(n_a l_a, n_b l_b)) \langle l_a^{N_a} \alpha_a Q_a M_{Q_a} L_a S_a \| \mathbf{a}_{1/2}^{(q\, l_a\, s)} \| l_a^{N'_a} \alpha_a Q_a M_{Q_a} L_a S_a \rangle \\
\times \langle l_b^{N_b} \alpha_b Q_b M_{Q_b} L_b S_b \| \mathbf{a}_{-1/2}^{(q\, l_b\, s_b)} \| l_b^{N'_b} \alpha_b Q_b M_{Q_b} L_b S_b \rangle \Big\} \\
\times \langle n_a l_a s \| \mathbf{T}^{(k_l k_s)} \| n_b l_b s \rangle \, . \qquad (2.50)
\end{aligned}$$

The decoupling parts $\mathcal{R}$ are given in the form of 3nj-symbols, delta functions and phase factors. The tensorial parts are given by the creation and annihilation operator expressions and are related to the completely reduced coefficients of fractional parentage. The additional phase factor Δ arises from the reordering needed to match the decoupled creation and annihilation operators in the Bra and Ket vectors and is given by

$$\Delta = \begin{cases} 0 & n_a l_a = n_b l_b \\ 1 + \sum_{r=\min(a,b)}^{\max(a,b)-1} N_r & n_a l_a \neq n_b l_b \, . \end{cases} \qquad (2.51)$$

To calculate the hyperfine structure from an atomic state function with any number of open shells in LS-coupling, one has to evaluate Eq. 2.47. In detail, one has to calculate

- the decoupling matrices $\mathcal{R}(l_a, l_b, L_a, L_b, L'_a, L'_b, k_l)$ and $\mathcal{R}(s_a, s_b, S_a, S_b, S'_a, S'_b, k_s)$, Eq. 2.32 and Eq. 2.36;
- the submatrix elements of irreducible tensor operators $\langle l_a^{N_a} \alpha_a Q_a M_{Q_a} L_a S_a \| \left[\mathbf{a}_{1/2}^{(q\, l_a\, s)} \times \mathbf{a}_{-1/2}^{(q\, l_a\, s)} \right]^{(k_l k_s)} \| l_a^{N'_a} \alpha'_a Q'_a M'_{Q'_a} L'_a S'_a \rangle$ and $\langle l^N \alpha Q M_Q L S \| \mathbf{a}_{\pm 1/2}^{(q\ l\, s)} \| l^{N'} \alpha Q M'_Q L S \rangle$ based on the standard quantities and the definitions Eq. 2.42, Eq. 2.43 and Eq. 2.45;
- the phase factor Δ, Eq. 2.51;
- and the one-electron submatrix elements $\langle n_a l_a s \| \mathbf{T}^{(k_l k_s)} \| n_b l_b s \rangle$, Eq. 2.12, Eq. 2.16, Eq. 2.17 and Eq. 2.21.

2.3 Explicit expressions for a two-shell system

The matrix element for a two-shell system can be written in a general way using Eq. 2.49 and Eq. 2.50 as

$$\begin{aligned}
&\langle n_1 l_1{}^{N_1}\alpha_1 L_1 S_1\, n_2 l_2{}^{N_2}\alpha_2 L_2 S_2\, LS \,\|\, \mathbf{F}^{(k_l k_s)} \,\|\, n_1' l'{}^{N_1'}\alpha_1' L_1' S_1'\, n_2' l'{}^{N_2'}\alpha_2' L_2' S_2'\, L'S' \rangle \\
&\qquad \equiv \mathbf{F}^{(k_l k_s)}(12;1'2') = (-1)^{\Delta+1}\left[k_l, k_s\right]^{1/2} \\
&\times \Big[\mathcal{R}(1,1')\mathbf{f}^{(k_l k_s)}(1,1')\,\langle 1 \,\|\, \left[\mathbf{a}_{1/2}^{(q\,l\,s)} \times \mathbf{a}_{-1/2}^{(q\,l\,s)}\right]^{(k_l k_s)} \,\|\, 1'\rangle \\
&+ \mathcal{R}(2,2')\mathbf{f}^{(k_l k_s)}(2,2')\,\langle 2 \,\|\, \left[\mathbf{a}_{1/2}^{(q\,l\,s)} \times \mathbf{a}_{-1/2}^{(q\,l\,s)}\right]^{(k_l k_s)} \,\|\, 2'\rangle \\
&+ \mathcal{R}(1,2')\mathbf{f}^{(k_l k_s)}(1,2')\,\langle 1 \,\|\, \mathbf{a}_{1/2}^{(q\,l\,s)} \,\|\, 1'\rangle\langle 2 \,\|\, \mathbf{a}_{-1/2}^{(q\,l\,s)} \,\|\, 2'\rangle \\
&\qquad + \mathcal{R}(2,1')\mathbf{f}^{(k_l k_s)}(2,1')\,\langle 2 \,\|\, \mathbf{a}_{1/2}^{(q\,l\,s)} \,\|\, 2'\rangle\langle 1 \,\|\, \mathbf{a}_{-1/2}^{(q\,l\,s)} \,\|\, 1'\rangle\Big]. \qquad (2.52)
\end{aligned}$$

The examination of the the coupled creation and annihilation expressions leads directly to three distinct cases: $N_1 = N_1'$ and $N_2 = N_2'$, $N_1 = N_1' - 1$ and $N_2 = N_2' + 1$ and $N_1 = N_1' + 1$ and $N_2 = N_2' - 1$. The matrix elements of other combinations of the occupation numbers are zero. In the first case where $N_1 = N_1'$ and $N_2 = N_2'$, by evaluating the decoupling parts $\mathcal{R}(1,1')$ and $\mathcal{R}(2,2')$ using Eq. 2.32 one ends up with

$$\begin{aligned}
&\mathbf{F}^{(k_l k_s)}(12;1'2') = (-1)^{\Delta+1}[k_l, k_s]^{-1/2} \\
&\times \left[\begin{Bmatrix} k_l & L_1' & L_1 \\ L_2 & L & L' \end{Bmatrix}\begin{Bmatrix} k_s & S_1' & S_1 \\ S_2 & S & S' \end{Bmatrix}\mathbf{f}^{(k_l k_s)}(1,1')\,\langle 1 \,\|\, \left[\mathbf{a}_{1/2}^{(q\,l\,s)} \times \mathbf{a}_{-1/2}^{(q\,l\,s)}\right]^{(k_l k_s)} \,\|\, 1'\rangle\right. \\
&\times \delta(L_2, L_2')\delta(S_2, S_2')(-1)^{L_1 - 2L_1' - L_2 - L' - k_l + S_1 - 2S_1' - S_2 - S' - k_s}[L', S']^{1/2} \\
&+ \begin{Bmatrix} k_l & L_2' & L_2 \\ L_1 & L & L' \end{Bmatrix}\begin{Bmatrix} s & S_2' & S_2 \\ S_1 & S & S' \end{Bmatrix}\mathbf{f}^{(k_l k_s)}(2,2')\,\langle 2 \,\|\, \left[\mathbf{a}_{1/2}^{(q\,l\,s)} \times \mathbf{a}_{-1/2}^{(q\,l\,s)}\right]^{(k_l k_s)} \,\|\, 2'\rangle \\
&\times \left.\delta(L_1, L_1')\delta(S_1, S_1')(-1)^{L_1 - L - L_2' - k_l + S_1 - S - S_2' - k_s}[L', S']^{1/2}\right]. \qquad (2.53)
\end{aligned}$$

Further simplifications occur if one shell (here the first one) is closed. Then $L_1 = S_1 = L_1' = S_1' = 0$, $L_2 = L, S_2 = S, L_2' = L'$ and $S_2' = S'$. The 6j-coefficient before $\mathbf{f}^{(k_l k_s)}(1,1')$ evaluates to zero if k_l or k_s is not equal to zero. The two 6j-coefficients before $\mathbf{f}^{(k_l k_s)}(2,2')$ have simple expressions

$$\begin{Bmatrix} k_l & L' & L \\ 0 & L & L' \end{Bmatrix} = (-1)^{L'+L+k_l}\delta(k_l, L, L')[L', L]^{-1/2} \qquad (2.54)$$

and analog for S. In the case of a closed first shell with $N_2 = N_2'$ the phase $\Delta = 0$ and the matrix elements evaluate to

$$\mathbf{F}^{(k_l k_s)}(12;1'2') = \delta(k_l, L, L')\delta(k_s, S, S')(-1)^{L+L'+k_l+S+S'+k_s} \times [L, k_l, S, k_s]^{-1/2} \mathbf{f}^{(k_l k_s)}(2, 2') \langle 2 \| \left[\mathbf{a}_{1/2}^{(q\,l\,s)} \times \mathbf{a}_{-1/2}^{(q\,l\,s)} \right]^{(k_l k_s)} \| 2' \rangle \,. \quad (2.55)$$

Expressing the coupled creation and annihilation operator part in terms of the completely reduced coefficients of fractional parentage $\langle \gamma \| \mathbf{a}^{(q\,l\,s)} \| \gamma' \rangle$ with $\gamma = l\alpha QLS$ leads to

$$\begin{aligned}
\mathbf{F}^{(k_l k_s)}(12;1'2') &= \delta(k_l, L, L')\delta(k_s, S, S')(-1)^{L+L'+k_l+S+S'+k_s}[L, k_l, S, k_s]^{-1/2} \\
&\times \mathbf{f}^{(k_l k_s)}(2, 2') \sum_{k_q, m_q} \begin{bmatrix} q & q & k_q \\ m_{q1} & m_{q2} & m_q \end{bmatrix} \begin{bmatrix} Q' & k_q & Q \\ M_Q' & m_q & M_Q \end{bmatrix} \\
&\times [k_q, k_l, k_s]^{1/2} [Q]^{-1/2} (-1)^{Q_2+L_2+S_2+Q_2'+L_2'+S_2'+k_q+k_l+k_s} \\
&\sum_{\alpha'', Q'', L'', S''} \begin{Bmatrix} q & q & k_q \\ Q' & Q & Q'' \end{Bmatrix} \begin{Bmatrix} l & l & k_l \\ L' & L & L'' \end{Bmatrix} \begin{Bmatrix} s & s & k_s \\ S' & S & S'' \end{Bmatrix} \\
&\times \langle l_2 \alpha_2 Q_2 L_2 S_2 \| \mathbf{a}^{(q\,l\,s)} \| l_2 \alpha'' Q'' L'' S'' \rangle \\
&\times \langle l_2 \alpha'' Q'' L'' S'' \| \mathbf{a}^{(q\,l\,s)} \| l_2 \alpha_2' Q_2' L_2' S_2' \rangle \,.
\end{aligned} \quad (2.56)$$

The last step is to use the definition of the hyperfine structure submatrix elements with appropriate ranks k_l and k_s to evaluate the submatrix element $\mathbf{f}$. For the orbital term the ranks are $k_l = 1$ and $k_s = 0$ and $\mathbf{f}$ is given by Eq. 2.16. For the diagonal hyperfine interaction matrix element between a closed shell 1 and the second shell $2 \equiv |\, 3d^4\, {}^3_4P \,\rangle$ the coupled operators of second quantization evaluate to $-3/\sqrt{10}$. All together the result is

$$\begin{aligned}
T_m^{(10)}(1, 3d^4\, {}^3_4P; 1, 3d^4\, {}^3_4P) &= \frac{1}{2\sqrt{30}} \sqrt{l(l+1)(2l+1)}\, \langle nl \| r^{-3} \| nl \rangle \\
&= \frac{1}{2} \langle 3d \| r^{-3} \| 3d \rangle \,.
\end{aligned} \quad (2.57)$$

The radial integral must be evaluated with wave functions obtained, for example, in a multiconfiguration Hartree-Fock calculation or treated as adjustable parameters in a semiempirical approach.

The general expression of the matrix elements of the hyperfine structure operator was derived. This expression was based on second quantization, the concept of quasispin, graphical methods and the smallest set of standard quantities, the completely reduced coefficients of fractional parentage. The expression is valid for any open shell atomic wave function of symmetry adapted configuration state functions in Russel-Sandars (LS) coupling. The special case of a two shell system was considered explicitly.

3 Implementation of the expression in computer programs

The formula to calculate the hyperfine structure splitting constants A and B for a general multiconfiguration atomic state functions was derived in the last chapter. Two computer programs to calculate the hyperfine constants from a multiconfiguration atomic state function have been developed during the work on this thesis.

The programs have to evaluate the general formula Eq. 2.50. The pure spin-angular factor of the matrix element between the electron $n_a l_a$ of the configuration state function $\langle \psi_u(LS)|$ and the electron $n_b l_b$ of the configuration state function $|\psi'_u(L'S')\rangle$ is thus derived. The decoupling parts $\mathcal{R}_x$ are calculated by Eq. 2.32 if $a = b$ or Eq. 2.36 if $a \neq b$. To evaluate the coefficients C_x, additional procedures for the $3nj$-symbols are used. The tensorial parts are evaluated by Eq. 2.42 and Eq. 2.45. The standard quantities of the completely reduced coefficients of fractional parentage are taken from their tabulated values.

The special hyperfine structure submatrix elements are evaluated, one for the electric quadrupole interaction (Eq. 2.12), two for the magnetic dipole interaction (Eq. 2.16 and Eq. 2.17) and one for the contact term (Eq. 2.21).

For a bra and ket configuration state function, the hyperfine contributions of all electrons in turn have to be obtained and summed up, see Eq. 2.49. The additional decoupling factor due to the coupled angular momentum $\mathbf{L}$ with the spin momentum $\mathbf{S}$ to the final momentum $\mathbf{J}$ is evaluated, compare Eq. 2.47.

In the multiconfiguration approximation, the atomic state function $|\Psi(LS)J\rangle$ is a linear combination of configuration state functions $|\psi_i(L_iS_i)J\rangle$ and their weights c_i. Thus, for every combination of the configuration state functions i and j the hyperfine contribution has to be evaluated and multiplied by the appropriate weights, see Eq. 2.47.

The results define the $\langle J \| \mathbf{T}^{(k_l\, k_s)\, k} \| J \rangle$ part of Eq. 2.6 and Eq. 2.7. They are multiplied by the nuclear factor μ or Q to get the A and B factors.

More detailed information can be found in the source codes. In order to use this algorithm, functions for the $3nj$-symbols and Clebsch-Gordan coefficients, as well as for the reduced coefficients of fractional parentage, are needed. Furthermore, a way to extract the quantum numbers from atomic state functions must be given and procedures that calculate the radial parts.

3.1 Implementation in the symbolic environment of MAPLE

MAPLE is a powerful programming language based on symbolic programming – the unifying idea is that every element can be represented as a symbolic expression. Symbolic programming has come to the forefront of computing as the next large-scale change in programming paradigms after the concept of object-oriented programming. MAPLE's rich symbolic programming language is designed from the ground up for manipulation of structured expressions. When solving an equation using symbolic programming, one can give the input just as on paper, without manual reduction to "computer friendly" form. One then can get not only numerical results, but also closed form solutions, perhaps including parameters that can be further manipulated as optimized or solved for. MAPLE incorporates a high-level programming language that allows the user to define his own procedures. These can be grouped into packages of specialized functions and loaded on demand. MAPLE can be used in batch mode for solving complex problems and developing algorithms or interactively allowing its use as a quick "pocket calculator". During the past years an atomic application development system based on the standard quantities of the angular momentum theory and the atomic shell model has been developed in MAPLE. It is made up of the RACAH and the JUCYS packages.

The RACAH package is designed as an environment for the symbolic manipulation, simplification and computation of any number of $3nj$-symbols and Clebsch-Gordan coefficients as well as various integrals over spherical harmonics. Additional symbols and functions from the angular momentum theory and their fast and reliable computation are defined [48–51], too. The JUCYS package mainly contains quantities from the atomic shell model [52, 53]. It is based on the concept of quasispin and second quantization (in a tensorial form) for the classification of operators and wave functions. All expressions, therefore, have an unified convention and notation for the standard quantities. Both packages include about 300 procedures, from which about 10 are sufficient for daily work. Detailed information about the arguments and functions can be obtained from the user manual coming with the package. A brief description of the versions of RACAH and JUCYS are presented in the paper [54].

The procedures of the JUCYS and the RACAH packages are extended [54, 55] in this thesis. Next to the implementation of the complete reduced coefficients of fractional parentage, a short but powerful notation is introduced for the creation and annihilation

operators as well as for the products of such operators and their reduced matrix elements. For one open shell, the evaluation of the spin-angular coefficients of one- and two-particle physical operators are possible. All the coefficients and the matrix elements from above are equally supported for both LS— and jj—coupled operators and functions. The RACAH package is enlarged for complex atoms with several open shells. The concept of configuration state function and atomic state functions is implemented. Then the spin-angular integration (for one-body interaction) is extended to the many open shell case in LS—coupling. The general approach outlined in the last chapter is used to evaluate the matrix elements up to the radial part and the reduced matrix element.

The concept of symbolic programming is followed that allows for an almost literal translation of theoretical formulas and their evaluation. With these extensions, all the procedures for calculating the hyperfine structure matrix elements are implemented [55]. The algorithm for hyperfine structure calculations is programmed in a new package, called HFS [56]. The experience gained from the investigations on the hyperfine structure of Niobium [5] was used to design data-structures and procedures that are of use for the experimentalist, too. It was installed at the Universität Kassel, Fachbereich Physik[†]. The algorithm that is used is the same as the one for the large scale *ab initio* approach shown in the next section.

The semiempirical approach treats the radial parameters left over after spin-angular integration as adjustable parameters. In a least square fit approximation they are fitted to the experimental A and B factors. Both approaches are implemented in the package, allowing a combined tackling of hyperfine structure problems in an environment with unified definitions.

The extensions made to the RACAH and JUCYS package are tabulated in Table 4. The MAPLE input commands and its output is typeset in the following as:

```
> Input;

  Output
```

To use these functions, the atomic structure packages must be loaded into MAPLE:

```
> with(Racah):with(Jucys):with(HFS):

  Welcome to Racah - Mindaugas!
  Welcome to Jucys!  - II
```

[†]http://www.physik.uni-kassel.de/fritzsche/programs.html

Table 4. MAPLE functions for computing the spin-angular coefficients, matrix elements for any one-particle operator and the hyperfine structure. Apart from these main functions, a few auxiliary procedures are provided in order to facilitate the communication with and within atomic structure programs RACAH and JUCYS and to evaluate the $3nj$-symbols. All functions are explained in detail in the interactive help.

Function	Description
asf_LS(),asf_jj()	Represents a LS- or jj-coupled atomic state function.
csf_LS(),csf_jj()	Represents a LS- or jj-coupled configuration state function.
csf_tabulate()	Extracts the quantum numbers of a configuration state function.
Racah_rcfp()	Returns the reduced coefficients of fractional parentage in $LS-$ or $jj-$coupling.
Racah_shell_coefficients()	Returns the (reduced) matrix element of the tensorial operator $\left[\mathbf{a}_{m_{q1}}^{(q\gamma)} \times \mathbf{a}_{m_{q2}}^{(q\gamma)}\right]^{(k)}$ or $\left[\left[\mathbf{a}_{m_{q1}}^{(q\gamma)} \times \mathbf{a}_{m_{q2}}^{(q\gamma)}\right]^{(k_1)} \times \left[\mathbf{a}_{m_{q3}}^{(q\gamma)} \times \mathbf{a}_{m_{q4}}^{(q\gamma)}\right]^{(k_2)}\right]^{(k)}$ in LS- or jj-coupling, respectively.
Racah_angular_coefficient()	Returns the pure spin-angular coefficients for one- or two-particle operators of a single open shell in LS- or jj-coupling and of one-particle operators with any open shell in LS-coupling.
hfs_submatrix()	Returns the hyperfine structure submatrix element with the tensor structure of rank k_l in orbital and k_s in spin space.
hfs_environment()	Defines the nuclear data for the hyperfine structure.
hfs_A(),hfs_B()	Expresses the A or B factor in its spin-angular and radial parts for an atomic state function.
hfs_fit()	Does the hyperfine structure parameterization for all given levels. All spin-angular parameters are calculated and a least square fit of the unknown radial parameters to obtain theoretical A and B factors is performed.
hfs_energy()	Calculates the hyperfine level energies.
hfs_intensity()	Calculates the relative intensities of all hyperfine lines arising from the two given levels.
hfs_plot()	Plots a scheme of the splitting between two fine structure states.

The atomic state functions, the configuration state functions and the shells are defined in close analogy to the general string notation of these quantities. Together with further informations about a fine structure level, the electronic part is defined by a level_LS() data-structure. A shell $|\,nl^N\alpha\ LS\,\rangle$ is defined by the shell_LS($[n,l]$, N, α, L, S) command. The quantum numbers are standard: n for principal, l for orbital, L for the coupled angular and S for the coupled spin momentum quantum numbers. N is the occupation number and α stands for all additional quantum numbers needed for a unique classification of the state (v, w). The command csf_LS() keeps the information of a configuration state function together. Using the additional argument *check* tests if the shells are correct and if all couplings fulfill the triangle condition $|\,a-b\,| \le c \le a+b$. To define a configuration state function of two shells, say $4d^4\,{}^5D$ and $5s^1\,{}^2S$ coupled to ${}^6D_{3/2}$ in MAPLE one would define the symbol D6_5D_3_2 as a configuration state function:

```
> D6_5D_3_2 := csf_LS (shell_LS( "4d^4 5^D"), shell_LS( "5s^1 2^S"), 2, 5/2,
  3/2, check);

  D6_5D_3_2 := csf_LS( shell_LS( [4,2], 4, 4, 2, 2), shell_LS( [5,0], 1, 1, 0,
  1/2), 2, 5/2, 3/2)
```

The last three numbers are the final $L = 2$, $S = 5/2$ and $J = 3/2$ quantum numbers. MAPLE checks if the shells and their coupling are valid and returns the shell in numeric representation. In a multiconfiguration approximation, an atomic wave function is defined as a linear combination of m configuration state functions. The command asf_LS() defines an atomic state function in MAPLE:

```
> P4_3P4_3_2 := csf_LS( shell_LS( "4d^4 3^P_4"), shell_LS("5s^1
  2^S"),1,3/2,3/2):

> asf_D6 := asf_LS (D6_5D_3_2, 0.995, P4_3P4_3_2, 0.061);

  asf_D6 := asf_LS( csf_LS( shell_LS( [4,2],4,4,2,2), shell_LS( [5,0], 1, 1,
  0, 1/2), 2, 5/2, 3/2), 0.995, csf_LS( shell_LS( [4,2], 4, 4, 1, 1),
  shell_LS( [5,0], 1, 1, 0, 1/2) ,1 ,3/2 ,3/2), 0.061)
```

The asf_LS() is a list of configuration state functions followed by their mixing coefficients. To hold the information about a fine structure level together, the structure level_LS() is defined. Any keyword together with any data-structure can be set, erased or returned. Giving the level designation as a name for the structure, one can store additional data. For instance, the hyperfine structure of the level ${}^6D_{3/2}$ of the configuration $4d^4 5s$ at an energy of 12300 cm^{-1} is examined. The A and B factors with errors are obtained using laser-induced fluorescence (LIF). One can define the following structure[†]:

[†]The units of the quantities are not stored. The package follows the general convention and treats fine structure in [cm^{-1}] and hyperfine structure in [MHz].

```
> d4s1_D6_3_2 := level_LS (Energy=12300, A=852.543, B=-64.572, Aerr=0.002,
  Berr=0.041, Method="LIF"):
```

To work with the quantum numbers, the command csf_tabulate() exists. It creates a table of all quantum numbers of a configuration state function:

```
> Ket:= csf_tabulate( P4_3P4_3_2 ):
```

and allows one to extract the table entries simply by:

```
> [Ket[l][1],Ket[Q][1],Ket[L][1],Ket[S][1],Ket[mQ][1]];

  [2, 1/2, 1, 1, 1/2]
```

The atomic state functions for an atom can be stored in a file and read in. The electronic part is then defined in MAPLE and can be used efficiently for further work.

The calculation of the spin-angular integration requires the computation of a large number of Clebsch-Gordan and $3nj$-symbols. The corresponding existing procedures have been optimized for computation speed [57].

As pointed out, the JUCYS package is based on the completely reduced coefficients of fractional parentage. To obtain a reduced coefficient of fractional parentage, the procedure Racah_rcfp(l,Q,L,S,Q',L',S') is used:

```
> Racah_rcfp(2,3/2,1,1,1,3,3/2,algebraic);

  8.197560616
```

which is equivalent to the matrix element

$$\langle\, 3d^3\,{}^4F_3 \,|||\, \mathbf{a}^{(1/2\,2\,1/2)}_{1/2} \,|||\, 3d^2\,{}^3P_4 \,\rangle \;=\; 8.197560616\,. \tag{3.1}$$

The next building block is the matrix element of the tensor $\boldsymbol{W}^{(k_l\,k_s)}$. To evaluate this tensor, for example

$$\langle\, 3d^3\,{}^4F \,|||\, \left[\mathbf{a}^{(q\,2\,s)}_{1/2} \times \mathbf{a}^{(q\,2\,s)}_{-1/2}\right]^{(10)} \,|||\, 3d^d\,{}^4F \,\rangle\,, \tag{3.2}$$

one would type in MAPLE:

```
> Racah_shell_coefficients(W_LS( a_LS(2, 1/2), a_LS( 2, -1/2), 1, 0),
  shell_LS( "3d3 4F"), shell_LS( "3d3 4F");

  -4.098780311
```

The close analogy with the general formula is preserved. The missing part for the spin-angular integration is the decoupling parts. The formulas are implemented allowing one

to calculate the spin angular coefficient for any one-particle operator in LS-coupling. The command Racah_angular_coefficient() calculates the angular coefficient up to the reduced matrix element. First one indicates by F to calculate a one-particle operator. Then the ranks follow, $[k_l, k_s, k] = [0, 1, 1]$ in this example. The following argument is the atomic state function. The optional argument *check* tests if the atomic state function is valid. The final argument defines the output format:

```
> Racah_angular_coefficient( "F", [0,1,1], asf_LS( csf_LS( shell_LS( "3d3
  4F"), shell_LS( "4s1 2S"), 3, 2, 3), 1, check), float);

  [-0.6274950218, "F([0,1,1], 3, 2, "3d^34s^1", 3, 2, "3d^34s^1")"],
  [-0.4677071738, "F([0,1,1], 4, 0, "3d^34s^1", 4, 0, "3d^34s^1")"]
```

The following result (after rounding the sixth digit) is obtained

$$\langle\, 3d^3\,{}^4F\; 4s^1\,{}^2S\;\; {}^2F_3 \,\|\, \mathbf{F}^{(01)1} \,\|\, 3d^3\,{}^4F\; 4s\;{}^2S\;\; {}^2F_3 \,\rangle$$
$$= -0.627495\,\langle\, 3d \,\|\, \mathbf{f}^{(01)} \,\|\, 3d \,\rangle - 0.467707\,\langle\, 4s \,\|\, \mathbf{f}^{(01)} \,\|\, 4s \,\rangle\ . \quad (3.3)$$

Each angular coefficient is given, followed by a string that indicates the type (F for one-particle operator), the ranks $[k_l, k_s, k]$ and the quantum numbers n, l of the bra shell followed by the bra configuration and the same for the ket shell. This string defines the symbol for the reduced matrix element.

The extensions so far are generally adaptive for any one-particle operator in atomic systems. The special nature of the hyperfine structure operator is given by its reduced matrix elements. Functions to evaluate them up to the radial part are defined and are bundled together with some additional functions into the HFS package for hyperfine structure examinations. The HFS package is distributed with a file *niobium.txt* that defines the atomic state functions of the nine low-lying levels in Niobium. They are obtained in [58]. An extract of this file is given in Fig. 5. The ground state, for example, is defined by the symbol D6_1_2. The experimental values of the A and B factors are stored, in addition. A file of this kind defines the atomic state functions for the HFS package. It is loaded into MAPLE by:

```
> read("niobium.txt"):
```

Having set up the level structure of the atom, the nuclear data have to be defined. These data are supplied using the command hfs_environment(). For Niobium, the nuclear spin is $9/2\,\hbar$, the magnetic dipole moment in nuclear magnetons is $\mu = 6.1705\,\mu_N$ and the electric quadrupole moment is $Q = -0.36$ barn [58]. In MAPLE the same units are used, so one defines:

```
D6_1_2:=level_LS(Name="(5D)6D 1/2",A=1868.218,Aerror=0.002,Energy=0, Asf=asf_LS(
csf_LS(shell_LS([4, 2],4,4,2,2),shell_LS([5, 0],1,1,0,1/2),2,5/2,1/2), .99261,
csf_LS(shell_LS([4, 2],4,4,1,1),shell_LS([5, 0],1,1,0,1/2),1,3/2,1/2), .7934e-1,
csf_LS(shell_LS([4, 2],4,2,1,1),shell_LS([5, 0],1,1,0,1/2),1,3/2,1/2), -.7737e-1,
csf_LS(shell_LS([4, 2],4,4,2,1),shell_LS([5, 0],1,1,0,1/2),2,3/2,1/2), -.935e-2,
csf_LS(shell_LS([4, 2],4,4,2,2),shell_LS([5, 0],1,1,0,1/2),2,3/2,1/2), .723e-2,
csf_LS(shell_LS([4, 2],4,4,0,0),shell_LS([5, 0],1,1,0,1/2),0,1/2,1/2), .499e-2,
csf_LS(shell_LS([4, 2],4,0,0,0),shell_LS([5, 0],1,1,0,1/2),0,1/2,1/2), -.340e-2,
csf_LS(shell_LS([4, 2],4,4,1,1),shell_LS([5, 0],1,1,0,1/2),1,1/2,1/2), .281e-2,
csf_LS(shell_LS([4, 2],4,2,1,1),shell_LS([5, 0],1,1,0,1/2),1,1/2,1/2), -.278e-2,
csf_LS(shell_LS([4, 2],3,3,1,3/2),shell_LS([5, 0],2,0,0,0),1,3/2,1/2), -.4737e-1,
csf_LS(shell_LS([4, 2],3,3,1,1/2),shell_LS([5, 0],2,0,0,0),1,1/2,1/2), -.364e-2));

D6_3_2:=level_LS(Name="(5D)6D 3/2",A=852.543,Aerror=0.003, B=-64.572,Berror=0.41,
       Energy=154.2, Asf=asf_LS(
csf_LS(shell_LS([4, 2],4,4,2,2),shell_LS([5, 0],1,1,0,1/2),2,5/2,3/2), .99493,
csf_LS(shell_LS([4, 2],4,4,1,1),shell_LS([5, 0],1,1,0,1/2),1,3/2,3/2), .6140e-1,
csf_LS(shell_LS([4, 2],4,2,1,1),shell_LS([5, 0],1,1,0,1/2),1,3/2,3/2), -.6142e-1,
csf_LS(shell_LS([4, 2],4,4,2,1),shell_LS([5, 0],1,1,0,1/2),2,3/2,3/2), -.1849e-1,
csf_LS(shell_LS([4, 2],4,4,2,2),shell_LS([5, 0],1,1,0,1/2),2,3/2,3/2), .1219e-1,
csf_LS(shell_LS([4, 2],4,4,3,1),shell_LS([5, 0],1,1,0,1/2),3,3/2,3/2), .1318e-1,
csf_LS(shell_LS([4, 2],4,2,3,1),shell_LS([5, 0],1,1,0,1/2),3,3/2,3/2), -.734e-2,
csf_LS(shell_LS([4, 2],4,4,1,1),shell_LS([5, 0],1,1,0,1/2),1,1/2,3/2), .296e-2,
csf_LS(shell_LS([4, 2],4,2,1,1),shell_LS([5, 0],1,1,0,1/2),1,1/2,3/2), -.279e-2,
csf_LS(shell_LS([4, 2],4,4,2,1),shell_LS([5, 0],1,1,0,1/2),2,1/2,3/2), -.3e-4,
csf_LS(shell_LS([4, 2],4,4,2,0),shell_LS([5, 0],1,1,0,1/2),2,1/2,3/2), -.166e-2,
csf_LS(shell_LS([4, 2],4,2,2,0),shell_LS([5, 0],1,1,0,1/2),2,1/2,3/2), .106e-2,
csf_LS(shell_LS([4, 2],3,3,3,3/2),shell_LS([5, 0],2,0,0,0),3,3/2,3/2), .2223e-1,
csf_LS(shell_LS([4, 2],3,3,1,3/2),shell_LS([5, 0],2,0,0,0),1,3/2,3/2), -.3646e-1,
csf_LS(shell_LS([4, 2],3,3,1,1/2),shell_LS([5, 0],2,0,0,0),1,1/2,3/2), -.393e-2,
csf_LS(shell_LS([4, 2],3,3,2,1/2),shell_LS([5, 0],2,0,0,0),2,1/2,3/2), .160e-2,
csf_LS(shell_LS([4, 2],3,1,2,1/2),shell_LS([5, 0],2,0,0,0),2,1/2,3/2), -.41e-3));

...
```

Fig 5. Extract of the HFS input file of the atomic fine structure level of Niobium as obtained in [58].

```
> hfs_environment (I=9/2, mu=6.1705, Q=-0.36);
```

The hyperfine structure spectrum arising between two fine structure levels can be simulated. It will typically look like Fig. 6:

```
> hfs_environment (I=1);

> D4S1 := level_LS (A=100, B=30, Energy=12034,
  Asf = asf_LS( csf_LS( shell_LS( "1s^1 2^S"), shell_LS("2p^1 2^P"), 1,1,2),
  1)):

> D3S2 := level_LS (A=300, B=20, Energy=14034,
  Asf=asf_LS (csf_LS (shell_LS("1s^2 1^S"), shell_LS("2p^2 1^D"), 2,0,2),
  1)):

> hfs_plot (D4S1, D3S2, 400, info);
```

The lines are simulated using Gauss functions with supplied full width at half minimum (here 400 MHz) and relative intensities. A scheme of the hyperfine structure levels and the transition lines between them is sketched on top of the plot. The optional argument *info* types out the information about the hyperfine structure as shown on the right side of Fig. 6.

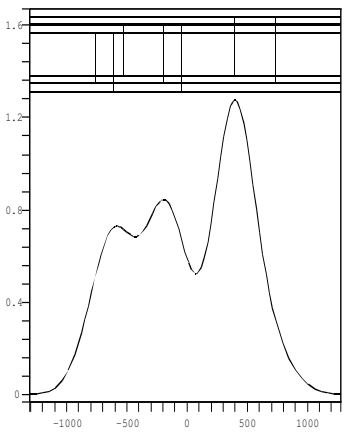


```
Hyperfine structure, fwhm : 400.0
Nuclear Spin: 1.0
Angular moment upper level: 2.0
Angular moment lower level: 2.0
Hyperfine parameter:
Upper level: A:300.000, B:20.000
Lower level: A:100.000, B:30.000
Lines:
Energy   : -611.250000  Lower level: -266.250    Upper level: -877.500
Intensity: 0.450000     F:1.0 F: 1.0
Energy   : -758.750000  Lower level: -118.750    Upper level: -877.500
Intensity: 0.150000     F:2.0 F: 1.0
Energy   :  -46.250000  Lower level: -266.250    Upper level: -312.500
Intensity: 0.150000     F:1.0 F: 2.0
Energy   : -193.750000  Lower level: -118.750    Upper level: -312.500
Intensity: 0.694444     F:2.0 F: 2.0
Energy   : -527.500000  Lower level:  215.000    Upper level: -312.500
Intensity: 0.155556     F:3.0 F: 2.0
Energy   :  728.750000  Lower level: -118.750    Upper level:  610.000
Intensity: 0.155556     F:2.0 F: 3.0
Energy   :  395.000000  Lower level:  215.000    Upper level:  610.000
Intensity: 1.244444     F:3.0 F: 3.0
```

Fig 6. Output of the command hfs_plot(). On the left side the simulated hyperfine structure is given, on the right side the text output.

The theoretical expression for the A and B factors can be split into a sum where each term of the sum is a product of a spin-angular coefficient times a radial integral. This expansion can be used in the semiempirical analysis of the hyperfine structure or *ab initio* calculations.

The matrix element $\langle \gamma LSJ \| \mathbf{F}^{(k_l,k_s)k_j} \| \gamma' L'S'J' \rangle$ up to the reduced matrix element $\langle nls \| \mathbf{f}^{(k_l,k_s)} \| n'l's' \rangle$ is integrated by a call to the procedure Racah_angular_coefficient(). Historically, the coupling scheme normally used for hyperfine structure is SL-coupling while LS-coupling is normally used for the fine structure. This leads to an additional phase factor. Therefore the coupling scheme has to be defined. Depending on the approach (either semiempirical or *ab initio*) the hyperfine structure reduced matrix elements have different definitions [21, 47]. These definitions are set using the hfs_environment(). The possibilities are summarized in Table 5.

The hyperfine submatrix elements can be expressed by spin-angular factor α times a radial parameter a. If Nuclear in hfs_environment() is set to true, the nuclear data are multiplied to the spin-angular data and only the pure radial coefficients are used as parameters. In Table 6 the different definitions of the hyperfine submatrix elements are compiled. Giving the ranks $[k_l, k_s]$ followed by $[n, l]$ of the bra and ket electron, hfs_submatrix() returns this expression:

```
> hfs_submatrix ([1,0],[2,1],[2,1]);
```

Table 5. The possible settings for hfs_environment() and their explanations are summarized. The units are indicated in square brackets. Each keyword defines the entry as given by the definition.

Keyword	Entry	Definition
I	I	Nuclear spin [$\hbar$]
MU	μ	Magnetic dipole moment [$e\hbar/(2m_p)$]
Q	Q	Electric quadrupole moment [barn]
COUPLING	"SL" / "LS"	Coupling scheme being used
APPROACH	"abinitio" / "semiempirical"	The approach being used
NUCLEAR	"true" / "false"	Defines the radial part with or without the nuclear data

$-2\sqrt{3}$ a_01(2, 1, 2, 1)

Setting Nuclear to true one obtains:

```
> hfs_environment (Nuclear=true);
```

```
> hfs_submatrix ([1,0],[2,1],[2,1]);
```

$-95.41068\sqrt{3}\,\frac{\text{MU\_NUC}}{\text{I\_NUC}}$ a_01(2, 1, 2, 1)

All procedures are at hand to parameterize the A and B factors into their spin-angular parts α and the radial parameters a:

```
> CSF := csf_LS (shell_LS("2p^2 3^P"), shell_LS("3p^2 3^P"), 1,1,1):
```

```
> hfs_A (CSF);
```

```
0.2500000007 a_01(2, 1, 2, 1, "2p^2 3p^2", "2p^2 3p^2")
+ 0.2500000007 a_01(3, 1, 3, 1, "2p^2 3p^2", "2p^2 3p^2")
+ 0.1250000002 a_12(2, 1, 2, 1, "2p^2 3p^2", "2p^2 3p^2")
+ 0.1250000002 a_12(3, 1, 3, 1, "2p^2 3p^2", "2p^2 3p^2")
+ 0.2499999999 a_10(2, 1, 2, 1, "2p^2 3p^2", "2p^2 3p^2")
+ 0.2499999999 a_10(3, 1, 3, 1, "2p^2 3p^2", "2p^2 3p^2")
```

The radial parameters are given by the name $a_{k_l k_s}$. In round brackets, the n and l values for the bra and ket electron are given, respectively. To distinguish the radial

Table 6. The definition of the magnetic dipole (α) and electric quadrupole (β) submatrix elements. g_s is the electronic g factor, μ_I the magnetic dipole moment, Q the electric quadrupole moment and I the nuclear spin. ($*$): The contact term in the *ab initio* approach is only defined for $l = 0$, otherwise the submatrix element is zero. This is not the case in the semiempirical approach.

Ab initio	Semiempirical	Nuclear	Semiempirical, nuclear
$\alpha_l = -2\sqrt{2l(l+1)(2l+1)}$	$\alpha^{(01)} = \frac{1}{2}\alpha_l$	$\frac{\mu_I}{I}\alpha_l$	$2\frac{\mu_I}{I}\alpha^{(01)}$
$\alpha_d = -g_s\sqrt{\frac{30l(l+1)(2l+1)}{2(2l+3)(2l-1)}}$	$\alpha^{(12)} = \frac{1}{g_s}\alpha_d$	$\frac{\mu_I}{I}\alpha_d$	$2\frac{\mu_I}{I}\alpha^{(12)}$
$\alpha_c = -g_s\sqrt{\frac{3}{2}(2l+1)}$ $(*)$	$\alpha^{(10)} = \frac{1}{g_s}\alpha_c$	$\frac{\mu_I}{I}\alpha_c$	$\frac{4}{3}\frac{\mu_I}{I}\alpha^{(10)}$
$\beta_q = \sqrt{\frac{2l(l+1)(2l+1)}{(2l+3)(2l-1)}}$	$\beta^{(02)} = \beta_q$	$Q_I\beta_q$	$Q_I\beta^{(02)}$
	$\beta^{(13)} = \sqrt{\frac{3}{10}}$		$Q_I\beta^{(13)}$
	$\beta^{(11)} = \sqrt{\frac{3}{10}}$		$Q_I\beta^{(11)}$

parameters arising from different configurations, bra and ket configurations are given, too. The output for the A factor in the example translates to

$$\begin{aligned} A \;\equiv\; & \langle\, 2p^2\ {}^3P\ 3p^2\ {}^3P\ {}^3P_1 \,\|\, T_m + T_c \,\|\, 2p^2\ {}^3P\ 3p^2\ {}^3P\ {}^3P_1 \,\rangle \\ =\; & 0.250a_{01}^{2p,2p} + 0.250a_{01}^{3p,3p} + 0.125a_{12}^{2p,2p} + 0.125a_{12}^{3p,3p} \\ & +0.250a_{10}^{2p,2p} + 0.250a_{10}^{3p,3p}\,. \end{aligned} \tag{3.4}$$

If the A factors are known for more levels than the radial parameters, they can be least square fit to the experimental data.

To test the hyperfine package and show its capabilities, a semiempirical hyperfine structure analysis for Niobium was performed. The fine structure analysis has been done [58] for the two low-lying even-parity configurations $4d^4\,5s$ and $4d^3\,5s^2$. The mixing coefficients were obtained by diagonalizing the energy matrix using a series of pure SL states. The A and B factors for these nine levels $4d^4\,5s\ {}^6D$ and $4d^3\,5s^2\ {}^4F$ of ^{93}Nb are known experimentally. The level_LS() data-structure is defined in the file *niobium.txt*, see Fig. 5. The hfs_environment() is defined:

```
> hfs_environment( Coupling="SL", Approach="semiempirical", Nuclear=false,
  mu=6.1436, Q=-.37, I=9/2);
```

The radial parts $a^{nl}_{k_s k_l}$ and $b^{nl}_{k_s k_l}$ are least square fit to the observed hyperfine structure splittings

$$A_J = \sum_{nl} \left[\alpha^{nl}_{01} a^{nl}_{01} + \alpha^{nl}_{12} a^{nl}_{12} + \alpha^{nl}_{10} a^{nl}_{10} \right] \tag{3.5}$$

and

$$B_J = \sum_{nl} \left[\beta^{nl}_{02} b^{nl}_{02} + \beta^{nl}_{13} b^{nl}_{13} + \beta^{nl}_{11} b^{nl}_{11} \right] . \tag{3.6}$$

With the package HFS this can be done using the procedure hfs_fit(). Parsing the level_LS() as arguments for hfs_fit(), one has to define whether to fit to the magnetic dipole factor A or the electric quadrupole factor B:

```
> hfs_fit (D6_1_2, D6_3_2, D6_5_2, D6_7_2, D6_9_2, F4_3_2, F4_5_2, F4_7_2, F4_9_2,
  'A');
```

```
> hfs_fit(D6_1_2, D6_3_2, D6_5_2, D6_7_2, D6_9_2, F4_3_2, F4_5_2, F4_7_2, F4_9_2,
  'B');
```

The results are summarized in Table 7 and Table 8. The result for the radial parameters for the A and B factors calculated by HFS are in agreement with the results obtained by [58].

Table 7. Least square fit approximation of the magnetic dipole interaction for the $4d^4 5s\ ^6D$ and $4d^3 5s^2\ ^4F$ state. Δ is the difference of the observed A_{exp} minus the calculated A_{calc} factor. The obtained results are compared to the ones calculated by Büttgenbach [58].

Spin-angular factors

Level	$a_{01}^{4d}(4d^3 5s^2)$	$a_{01}^{4d}(4d^4 5s^1)$	$a_{10}^{4d}(4d^3 5s^2)$	$a_{10}^{4d}(4d^4 5s^1)$	$a_{10}^{5s}(4d^4 5s^1)$	$a_{12}^{4d}(4d^3 5s^2)$	$a_{12}^{4d}(4d^4 5s^1)$
(5D)6D 1/2	-0.001478279	-1.321586561	0.003735445	1.842770750	0.476563156	-0.000555595	0.304409019
(5D)6D 3/2	0.001158735	0.134768269	0.000682942	0.683936681	0.179461621	0.000115643	-0.172819131
(5D)6D 5/2	0.002242638	0.343179604	0.000315293	0.519365825	0.134900523	-0.000304605	-0.145624940
(5D)6D 7/2	0.003642260	0.412207363	0.001132718	0.464426645	0.118592401	-0.000040083	-0.046795100
(5D)6D 9/2	0.005573288	0.442718391	0.002763661	0.438755133	0.110184034	0.000399950	0.073846555
4F 3/2	1.476251035	0.118324065	-0.551164448	-0.028836952	-0.014567145	-0.085247166	-0.006111646
4F 5/2	0.891435130	0.077389061	0.026895615	0.002510185	0.001762129	-0.045139377	-0.003213829
4F 7/2	0.693092017	0.067567335	0.215181330	0.016169418	0.007993658	-0.007920321	-0.001455079
4F 9/2	0.598758966	0.067757217	0.295587084	0.026216937	0.011674442	0.046331098	-0.000133540

Radial parameters

Radial parameter	This work [MHz]	From [58] [MHz]
$a_{01}^{4d}(4d^3 5s^2)$	395.1(2)	395.39(0.25)
$a_{01}^{4d}(4d^4 5s^1)$	351.49(3)	351.67(0.58)
$a_{10}^{4d}(4d^3 5s^2)$	-224(9)	-225.84(1.97)
$a_{10}^{4d}(4d^4 5s^1)$	-501(2)	-511.47(30.47)
$a_{10}^{5s}(4d^4 5s^1)$	6658(7)	6700(118)
$a_{12}^{4d}(4d^3 5s^2)$	234(3)	238.34(3.19)
$a_{12}^{4d}(4d^4 5s^1)$	275.5(1)	276.08(2.17)

A factors

Level	A_{calc} [MHz]	A_{exp} [58] [MHz]	Δ [MHz]	from [58] [MHz]
(5D)6D 1/2	1868(8)	1868.218(2)	0.218	1868.217
(5D)6D 3/2	852(4)	852.543(3)	0.543	852.573
(5D)6D 5/2	719(3)	719.476(2)	0.476	719.414
(5D)6D 7/2	690(3)	690.198(2)	0.198	690.248
(5D)6D 9/2	691(2)	691.614(3)	0.614	691.580
4F 3/2	644(1)	644.160(54)	0.16	644.91
4F 5/2	372.4(4)	372.485(2)	0.085	372.485
4F 7/2	292.2(5)	292.202(2)	0.002	292.203
4F 9/2	269.5(8)	269.632(3)	0.132	269.631

Table 8. Least square fit approximation of the electric quadrupole interaction for the $4d^45s\,^6D$ and $4d^35s^2\,^4F$ state. Δ is the difference of the observed B_{exp} minus the calculated B_{calc} factor. The obtained results are compared to the ones calculated by Büttgenbach [58].

Spin-angular factors

Level	$b_{02}^{4d}(4d^35s^2)$	$b_{02}^{4d}(4d^45s^1)$	$b_{11}^{4d}(4d^35s^2)$	$b_{11}^{4d}(4d^45s^1)$	$b_{13}^{4d}(4d^35s^2)$	$b_{13}^{4d}(4d^45s^1)$
(5D)6D 3/2	-0.0001536878	0.2832387083	0.0000124163	0.0440101216	0.0000010217	-0.0372590873
(5D)6D 5/2	0.0002299041	0.2032209510	0.0001451145	0.0798037553	0.0000099833	0.0234194366
(5D)6D 7/2	-0.0009020775	-0.0935163490	0.0006659198	0.1165656655	-0.0001496518	0.0605109743
(5D)6D 9/2	-0.0023457386	-0.5628877300	0.0018183489	0.1555875843	0.0002907346	-0.0380143472
4F 3/2	-0.1304114064	0.0059884604	-0.0437416130	-0.0008953975	-0.0470374052	0.0030294340
4F 5/2	-0.1257660152	0.0067755168	0.0519457218	-0.0030618788	-0.0488107596	0.0036645801
4F 7/2	-0.1713143764	0.0084160970	0.1281733799	-0.0041316140	-0.0288742116	0.0028341163
4F 9/2	-0.2495139724	0.0087687680	0.1986457521	-0.0042408072	0.0311364960	-0.0037472748

Radial parameters

Radial parameter	This work [MHz]	from [58] [MHz]
$b_{02}^{4d}(4d^35s^2)$	-256(1)	-263.58(2.85)
$b_{02}^{4d}(4d^45s^1)$	-232.1(8)	-232.04(0.17)
$b_{11}^{4d}(4d^35s^2)$	17.4(8)	7.25(3.45)
$b_{11}^{4d}(4d^45s^1)$	3(4)	2.62(0.54)
$b_{13}^{4d}(4d^35s^2)$	-36(1)	-30.64(3.49)
$b_{13}^{4d}(4d^45s^1)$	-28(3)	-27.53(1.16)

B factors

Level	B_{calc} [MHz]	B_{exp} [58] [MHz]	Δ [MHz]	from [58] [MHz]
(5D)6D 3/2	-64.5(5)	- 64.572(41)	-0.072	-64.541
(5D)6D 5/2	-47.6(6)	- 47.605(39)	0.005	-47.651
(5D)6D 7/2	20.6(7)	20.475(75)	-0.125	20.587
(5D)6D 9/2	133(1)	132.754(116)	-0.246	132.690
4F 3/2	32.8(2)	32.800(128)	0.0	34.0
4F 5/2	33.2(2)	33.341(38)	0.141	33.341
4F 7/2	45.1(3)	44.928(47)	-0.172	44.928
4F 9/2	64.4(4)	64.315(130)	0.015	64.313

3.2 Implementation for the ATSP package

The multiconfiguration Hartree-Fock code MCHF determines radial functions that define the orbitals of configuration states in the expansion of a non-relativistic wave function of a many-electron atom or ion. This code has been combined with others that perform angular and radial integrations to form an atomic-structure package ATSP for the prediction of atomic properties [6].

A Fortran HFS program [47] exists for the ATSP package. The integration over the spin-angular variables is based on the scheme outlined in [59]. This spin-angular integration is replaced by the approach outlined in Chapter 2. The reduced coefficients of fractional parentage, the matrix element of the $\boldsymbol{W}^{(k_q\, k_l\, k_s)}$ tensor and the $3nj$-symbols are taken from the Fortran library SAI [60].

The ATSP package was installed on the BENDROSIOS FIZIKOS KATEDROS cluster at Vilnius Pedagogical University, division of general physics. This five node cluster has AMD Athlon(tm) XP 2800+ processors with 2079.581 MHz CPU. The unpublished new version of the MCHF atomic-structure package [61], based on dynamic memory allocation, sparse matrix methods, and the new angular library is used for the multiconfiguration Hartree-Fock calculations.

The new hyperfine program and the installation of the ATSP package were tested on two small cases. First, the hyperfine structure of the ground state of Lithium was calculated, compare [62]. As the hyperfine structure of Lithium is only given by the contact term, the other submatrix elements were tested by the hyperfine structure calculation of Beryllium [63]. The results agreed with the ones calculated using the new version of the hyperfine structure program.

The available computing power and the refined programs allow to use a very detailed method for the hyperfine structure calculation. In the following chapter the method is explained on the calculation of Vanadium. The approach is automated by a script that handles the communication between the modules of the ATSP or GRASP package. The case specific data are supplied in form of three files. The script then calls the required modules, monitors their states and outputs the results of the hyperfine structure calculation. This is explained in more detail at the end of the next chapter.

Without the new refinements and advanced computing capacities, the calculations performed would not have been feasible.

4 Multiconfiguration *ab initio* calculations

Application of the multiconfiguration approach to a complex many-electron atom is hampered by the vast number of configuration state functions that contribute to the atomic state function. The unlimited atomic state function consists of all of them, including the unbound solutions. A first truncation is made by looking at the energy separation of the different fine structure levels. Levels that lie energetically close are chosen as reference set while the others can be ignored. The orbitals of the reference sets are called spectroscopic. The correlation to these orbitals is introduced by partly substituting them with correlation orbitals. These orbitals are only defined by their angular symmetry and do not necessarily have the correct number of nodes as the spectroscopic orbitals do. The substitutions define the additional configuration state functions. Their admixture is determined in the self consistent procedure. A manageable number of these configuration state functions has to be determined in order to represent the most important correlations that take place.

The important configuration state functions are identified from the structure of the operators that are involved. The hyperfine structure is a single-particle operator. As a result, single substitutions of the electron orbitals with correlation ones give the main contribution. Double substitutions are most important for the Coulomb operator. Triple and higher substitutions do not interact directly and have less influence. A reasonable point of departure is, therefore, to limit the number of substitutions to double at most.

The correlations can be divided into three types. Outer electrons are less tightly bound and interact strongly with each other. They are called valence electrons, the correlation between them is called valence correlation. The radial orbitals undergo changes compared to the Hartree-Fock or Dirac-Fock orbitals. Inner electrons are tightly bound. They do not change from their (Dirac-)Hartree-Fock radial orbitals and define the core. Substitutions of core orbitals with the correlation orbitals lead to the core correlation. Correlations of the third type take place between core and valence orbitals, the core-valence correlation. The electrons near the nucleus are so tightly bound and screened by the outer electrons that they do not experience correlations. They define the closed orbitals and their substitutions are ignored.

The usual approach, outlined in [13], is to calculate the three correlation types part by part. In turn, more correlation orbitals are included until convergence is obtained. The correlation orbitals from previous calculations are kept fixed. Selected substitutions

are taken into account and configuration state function with a weight lower than a certain cutoff are ignored, a technique called condensing. These calculations aim to obtain most of the orbital relaxations to the correlations that take place. In a second calculation, all orbitals are held fixed and a calculation with a larger configuration state function space is performed. This configuration interaction calculation includes more correlations but neglects further orbital relaxation.

This thesis is based on this calculation scheme. The correlations are introduced in finer steps allowing to observe the influence of the correlation orbitals on the magnetic dipole interaction for each spectroscopic orbital. That involves to calculate for each orbital in turn multiconfigurational the wave function and thereafter the hyperfine structure. This is repeated for an increasing number of correlation orbitals with the same symmetry. Compared with other hyperfine structure calculations a substantially increased number of calculations have to be done.

The win of such step by step evaluation is threefold. First, convergence problems in the self consistent procedure are minimized as only small changes are introduced within each step. Second, the procedure allows to filter out correlations that have less influence on the hyperfine structure. For complex many-electron atoms this approximation is an inescapable necessity. Third, the step by step calculation allows to observe the contribution and convergence of the different correlations. As correlations often compensate in hyperfine structure only the step by step calculation can detect this.

The three correlation types (core, valence and core-valence) are therefore divided into correlation groups for each spectroscopic orbital. The configuration state functions of a group are included into the multiconfiguration approximation, the wave function is determined and the hyperfine structure is calculated. If this group of configuration state functions does not change the A factor by more than a certain limit, the group is ignored. The substitution of the next orbital(s) with correlation orbitals of the same layer is included.

Each layer consists of a number of correlation orbitals of different symmetry, labeled by the Greek letters ($\alpha, \beta, \gamma, \delta, \epsilon$ and ζ). For each of these layers, the valence and the correlation orbitals of the layer are varied in the self-consistent procedure. The core and old correlation orbitals are held fixed if the next layer is included.

The following notation is used to term the correlation groups. The type of correlation is abbreviated by V,C and CV for valence, core and core-valence correlation, respectively. For double substitutions in the cases of valence and core correlations, the letter is doubled. The correlation layer is followed by the orbitals that are substituted by the correlation orbitals. V(α)4s means single substitution of the valence 4s orbital with correlation orbitals of layer α. Double core substitution of the two orbitals 2s and 2p with two different correlation orbitals of layer β are denoted by CC($\beta\beta$)2s2p. If the same correlation orbital is used for the substitution, only one layer will be indicated, CC(β)2s2p.

4.1 The hyperfine structure of Vanadium

Vanadium belongs to the iron group elements. The hyperfine structure data of many transitions of these elements are presently needed in various fields of astrophysics. Ignoring hyperfine structure effects and isotopic shifts when considering line formation processes may result in a considerable overestimation of solar and stellar abundances and in the wavelength shifts of saturated lines [64].

Natural Vanadium has only one stable isotope $^{51}V(99.75\%, I^\pi = \frac{7}{2}^-)$ together with an extremely long-lived isotope, $^{50}V(0.25\%, I^\pi = 6^+)$, that has a half-life of 1.5×10^{17} years. The high spins and the complicated electronic energy levels that occur in all transition elements result in extensive hyperfine structure in the atomic spectra. Vanadium ^{51}V has a nuclear magnetic dipole moment of $\mu_I = 5.1487057(2)\ \mu_b$ (μ_b Bohr magneton) and a small electric quadrupole moment in the range of $-0.052(10)$ barn to $-0.033(10)$ barn, the most exact value being $Q = -0.043$ barn. The values are taken from the table in [20].

Childs and Goodmann [65] measured the hyperfine structure of the ground state with an atomic-beam magnetic-resonance technique. Several hyperfine structure splittings, among them the ground state splitting, were analyzed in a semiempirical approach [66].

Semiempirical analysis has shown that the electron core in the low even-parity configurations behave non-relativistic and the departure from the LS-limit is very small [67]. Hyperfine anomaly is not observed. A multiconfiguration Hartree-Fock approach therefore seems promising.

The ground term of Vanadium is $3d^3\,{}^4_3F\,4s^2\,{}^4F$, forming the four levels $^4F_{3/2}$ (the atomic ground state), $^4F_{5/2}$, $^4F_{7/2}$ and $^4F_{9/2}$. The next term, $3d^4\,{}^5D\,4s\,{}^6D$, is about

Table 9. The single configuration Hartree-Fock calculation of the hyperfine structure of the ground state of Vanadium, $3d^3\ {}^4_3F\ 4s^2\ {}^4F$. For each J, the contribution to the A factor of the orbital, spin-dipole and contact term are given. The total A and B factor is compared with the experimental measurements (Exp.) [65] and the semiempirical results (Sem.) [66] .

		single configuration Hartree-Fock				Exp.	Sem.
	J	Orbital [MHz]	Spin-dipole [MHz]	Contact [MHz]	Total [MHz]	from [65] [MHz]	from [66] [MHz]
A	3/2	594.101	−50.982	0.0	543.119	560.048	547.923
A	5/2	360.704	−24.884	0.0	335.820	321.227	321.575
A	7/2	282.905	−6.744	0.0	276.162	249.740	255.368
A	9/2	247.542	11.801	0.0	259.344	227.132	237.025

$2000\,\mathrm{cm}^{-1}$ away. Term mixing can thus be ignored and the configuration state function space is limited to one reference configuration state function.

In Table 9 the single configuration Hartree-Fock results of the hyperfine structure are compared with the experimental results [65] and the semiempirical calculated values [66]. The agreement with the experimental value is good. The Hartree-Fock calculation, however, has no contact contribution as all ns shells are closed. If correlation is taken into account, the open 3d shell will polarize the s shells. Therefore the good agreement of the single configuration Hartree-Fock results with the experimental ones is accidental and indicates a compensation of the polarization effect between the ns shells. The single configuration Hartree-Fock calculation deviates from the experimental results by 3% for $J = 3/2$, 4.6% for $J = 5/2$, 11% for $J = 7/2$ and 14% for $J = 9/2$. In comparison the semiempirical analysis [66] represents the experimental values with a deviation of 2% for $J = 3/2$, 0.1% for $J = 5/2$ and 2% for $J = 7/2$. The largest deviation being 4.4% for $J = 9/2$.

4.2 Multiconfiguration Hartree-Fock calculation

The radial parts of the Hartree-Fock orbitals are given in Fig. 7. Three regions are separated by the dotted lines. The near nucleus region is dominated by the 1s orbital. This orbital is screened well by the other orbitals and tide bound to the nucleus. If this orbital can be kept closed, that is the influence of correlation on this orbital can be ignored, is discussed. The valence electrons, 3s, 3p, 3d and 4s are located in the far nucleus region. They are less tightly bound and as Fig. 7 shows, their orbital wave functions strongly overlap. The correlation, therefore, has a dominant effect on these orbitals. As the valence electrons are in the far nucleus region their direct influence on the hyperfine structure is small. Indirectly, however, the 3d shell polarizes the closed s shells. That has a large net effect on the contact contribution. This is analyzed next. The region in the middle is formed by the core orbitals 2s and 2p. To estimate their correlation effects, the core correlation is analyzed in the multiconfiguration Hartree-Fock and configuration interaction calculation based on the wave functions obtained in the valence correlation calculation. The correlations are then studied together in a multiconfiguration Hartree-Fock calculation and refined in a configuration interaction calculation.

The correlation is introduced by adding the following layers of correlation orbitals:

α : p, d, f orbitals.

β : p, d, f, g orbitals.

γ : p, d, f, g, h orbitals.

δ : p, d, f, g, h i orbitals.

ϵ: p, d, f, g, h i orbitals.

ζ: p, d, f, g, h i orbitals.

Configuration state functions that arise from substitutions with the $n = 3$ orbitals are included into layer α.

An overview of the influence of correlation on the Vanadium ground state and an estimation for the contribution of the 1s shell was obtained, first. In Table 10 the results for the A factor with $J = 3/2$ obtained by single substitutions with increasing

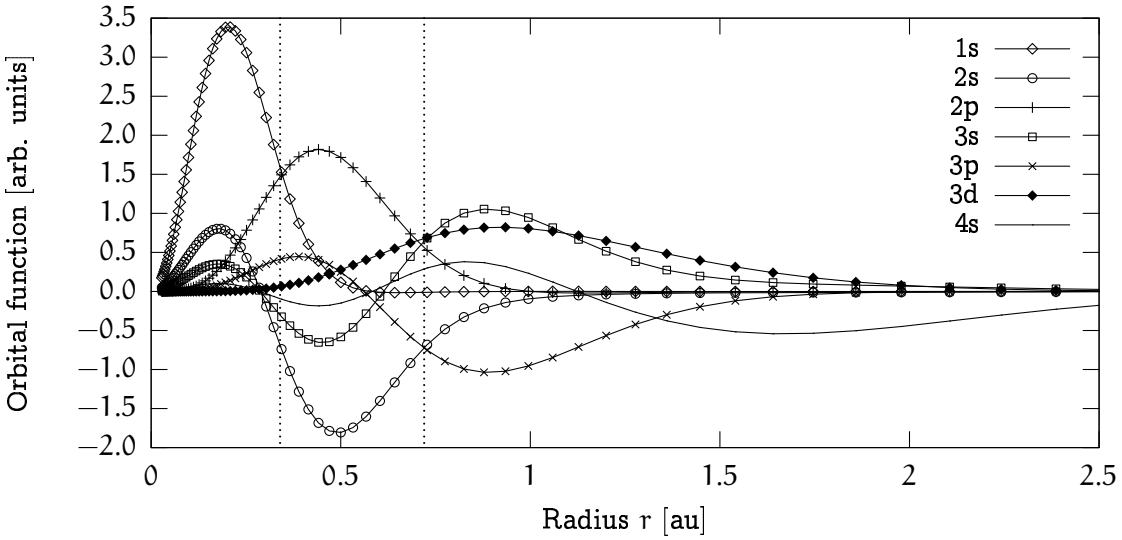

Fig 7. The radial orbital functions for each orbital obtained by single configuration Hartree-Fock calculation. A rough classification of closed, core and valence region is indicated by the vertical dotted lines.

layers of correlation orbitals are given. The calculation denoted by open 1s included core excitations from the 1s shell, 1399 configuration state functions were included. The calculation denoted by closed 1s excluded these excitations and consisted of 1256 configuration state functions.

Three important results were obtained. First, the hyperfine structure constant A converged well within 1 MHz after layer δ had been included. The final A factor was around 40 MHz too high compared to the experimental value. Second, the exclusion of single excitations from the 1s shell introduced an error of less than 3.3 MHz, that is less than 0.5% on the calculated value. The influence of the 1s shell was similar for the other J values. Third, the most varying contribution was given by the contact term. Starting with -8 MHz for layer α, it decreased to -96 MHz with correlation of layer β included, raised to 78 MHz with layer γ and converged to 74 MHz. To get more accurate results and to gain further insight into the correlation effects, a more detailed approach is necessary that also includes double substitutions.

Table 10. The results for J = 3/2 of single substitutions with increasing layers for all electrons (open 1s) are compared with the results of single substitutions keeping the 1s shell closed (closed 1s). The difference is noted. The contributions of the orbital, spin-dipole and contact terms to the A factor is listed and the total A factor is given.

Layer	Case	Orbital [MHz]	Spin-dipole [MHz]	Contact [MHz]	A factor [MHz]
α	open 1s	602.235	−52.149	−8.022	542.064
	closed 1s	602.236	−52.171	−7.951	542.114
	difference	−0.001	0.021	−0.071	−0.050
β	open 1s	574.341	−46.326	−101.490	426.525
	closed 1s	574.343	−46.364	−96.326	431.653
	difference	−0.002	0.038	−5.164	−5.128
γ	open 1s	572.242	−46.482	81.982	607.743
	closed 1s	572.243	−46.520	78.470	604.194
	difference	−0.001	0.038	3.512	3.550
δ	open 1s	572.062	−46.468	76.614	602.208
	closed 1s	572.063	−46.504	73.381	598.940
	difference	−0.001	0.036	3.232	3.268
ϵ	open 1s	571.778	−46.384	76.567	601.961
	closed 1s	571.777	−46.411	73.347	598.713
	difference	0.001	0.028	3.219	3.248
ζ	open 1s	571.752	−46.375	77.196	602.573
	closed 1s	571.752	−46.403	74.406	599.755
	difference	0.0	0.028	2.790	2.818

The valence correlation was studied in detail. The aim was to obtain a configuration state function space that is limited to the most important valence correlations for the A factor. At the same time the error in the calculation due to this limitation was estimated.

The largest configuration state function space of the valence correlation that is feasible within the computing capacities includes all groups up to layer δ, all V(ϵ) and some lower VV($\epsilon\epsilon$). The configuration state function space of almost 30 000 functions was divided into 189 correlation groups. The configuration state function space was enlarged by one group, the wave function was obtained and the A factor was calculated. If the change of the A factor was larger or equal to a given limit, this group was included in the calculation for the next group. Five different limits were set: $0, 0.5, 1, 3$ and 5 MHz. These calculations took about two month to complete. As a result, the detailed picture

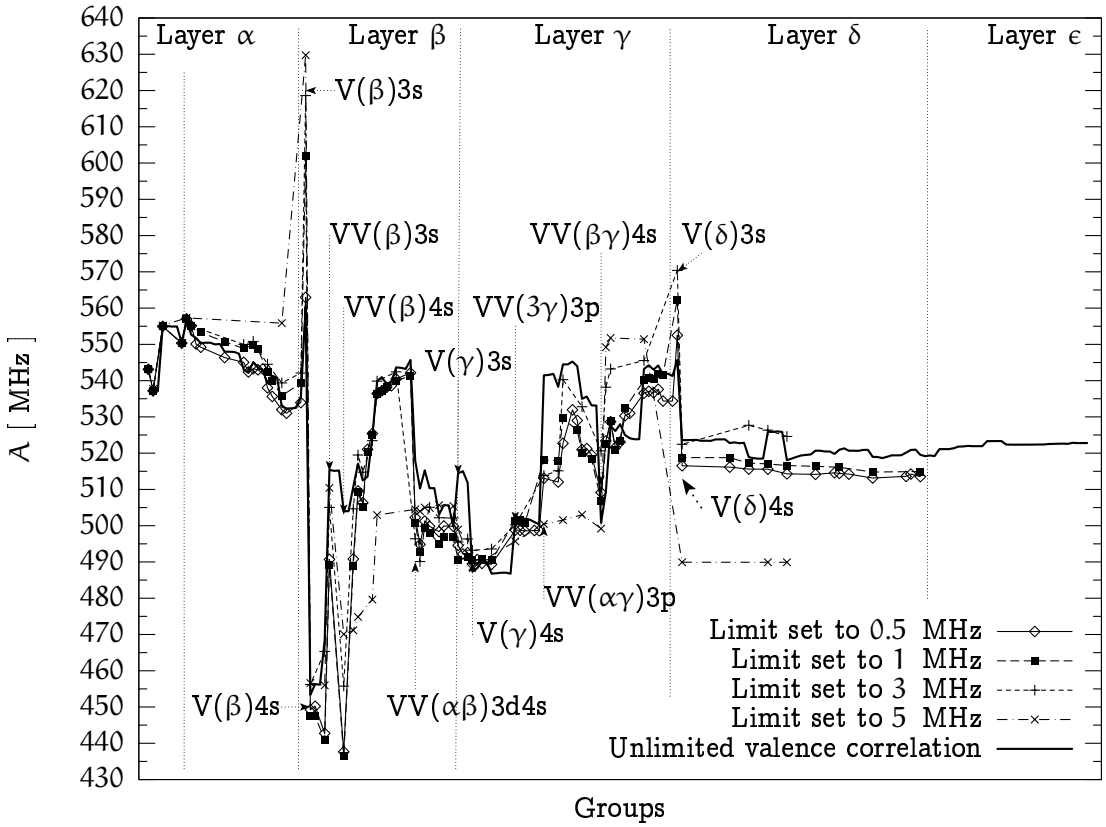

Fig 8. The valence correlation effects on the A factor for $J = 3/2$. The value of the A factor in dependence of increasing valence correlation groups (in total 189 groups) is given. Five different limitation values are set: $0, 0.5, 1, 3$ and $5\,\mathrm{MHz}$. The complete calculation is done until the number of configuration state functions is around 30 000, that is at part of the layer ϵ groups. Significant groups are indicated in the figure.

of the valence correlation was obtained, see Fig. 8 for $J = 3/2$. For all J, the correlations between layer $n = 3$ and α mainly affect the orbital term. The changes of the A factor are dominated by the contact contributions. Strong compensation is observed between the V3s group that increases the A factor and the V4s group that decreases A substantially. A similar compensation is observed for the VV3s and VV4s groups, however with far less influence. Major correlations occur within layer β and γ and are saturated with layer δ. As a result the restriction to groups of maximum layer δ captures all single and double valence correlations.

The final results of the hyperfine structure constants are given in Table 11. The limited calculations are compared with the unlimited calculation up to layer δ. As

Table 11. Result of the limited valence calculation, $J = 3/2$. The limitation value is indicated by x. The calculation indicated by † includes parts of layer ϵ. In the column Δ the difference between A_x and A_0 is given. The number of configuration state functions is listed in the second column (Csf) and the percentage deviation from A_0 in the final column.

Limit x [MHz]	Csf	A_x [MHz]	Δ [MHz]	Percentage [%]
0	25069	519.53		
$0^\dagger$	29929	522.80	−3.27	0.6
0.5	15870	513.53	6.0	1.2
1	12630	514.93	4.6	0.9
3	6333	524.61	−5.08	1.0
5	4587	489.93	29.6	5.7

Fig. 8 shows, the influence of layer ϵ was below the limit. However, layer ϵ increased the A factor for the unlimited calculation by 3 MHz. The limitation to layer δ therefore underestimated the A factor.

The threshold of 5 MHz omitted important correlations and deviated from the unlimited calculation by 30 MHz. The limit of 3 MHz deviated by 5 MHz from the complete calculation, only a small part of layer δ was included. Setting the limit to 1 MHz groups deviated by 5 MHz from the complete calculation and allowed one to half the number of configuration state functions from 25 069 to 12 630 for layer δ. No improvement was gained by the 0.5 MHz limit. The limit to groups above the 1 MHz amounted to 0.2% of the experimental value for the A factor. As a result, the deviation from the unlimited calculation was 1%. The limitation to layer δ underestimated this calculation by 8 MHz or 2%. In good approximation the valence correlation was calculated within an upper error of 2% if the limited configuration state function space of groups that have changed the A factor by more than 1 MHz was used. The error was dominated by the truncation of the space to layer δ and underestimated the A factor for $J = 3/2$.

The applied method allowed to limit the correlation groups from 189 groups to 77 most important ones if the limit is set to 0.2% of the experimental value. An error of

2% on the calculation was thereby introduced and the number of configuration state functions was truncated to one half.

The limited configuration state function space for the core correlation was studied next. To estimate whether the core correlation has its main influence due to orbital variation or due to the mixing coefficients, this type of correlation was calculated in two different ways: in a multiconfiguration Hartree-Fock calculation and in the configuration interaction approach using the wave functions from the previous valence calculation.

The valence calculation showed that double substitutions are important. The ground state of Vanadium has seven shells. Taking double substitutions from all shells into account led to configuration state functions with nine shells. The atomic structure package, however, allows at most eight shells in a configuration state function definition, closed shells excluded. The 1s shell substitutions contributed less than 4 MHz for $J = 3/2$, see Table 10. That was less than the double substitutions included so far contributed and less than the error of the calculation of 8 MHz. Therefore 1s shell substitutions were excluded.

In the first calculations the core correlation groups were added to the Hartree-Fock approximation, allowing all new orbitals to vary. The final number of configuration state functions was 10 540 setting up 49 groups. The core and core-core groups with substitutions to the same layer showed correlation effects as can be seen in Fig. 9. The influence is dominated by the contact contribution. The C(β)2s group had most influence, raising A by 130 MHz. Substitutions from two different layers were unimportant. The final A factor was 642 MHz.

There was poor convergence with layer ϵ for the multiconfiguration calculation as can be seen in Table 12. Each subsequent layer undid partly the change introduced by the layer before. A careful estimation of the change with layer ζ would be around 25 MHz or 5% of the calculated value. This layer, however, could not be included into following combined valence and core correlation calculations as the configuration state function space was too large.

Table 12. Result of the core correlation multiconfiguration Hartree-Fock calculation. The change of the hyperfine structure contributions after including a group is given for the orbital, spin-dipole and contact contribution to the A factor and of the total A factor.

Group	Orbital [MHz]	Spin-dipole [MHz]	Contact [MHz]	Total [MHz]
C(α)2s	−0.027	−0.523	−0.336	−0.885
C(β)2s	0.035	−0.376	130.094	129.753
C(γ)2s	−0.008	0.345	−20.803	−20.466
C(δ)2s	0.005	−0.683	26.309	25.631
C(ϵ)2s	−0.001	0.663	−10.730	−10.068
C(α)2p	−32.925	6.084	0.0	−26.840
C(β)2p	2.254	−0.056	−0.001	2.197
C(γ)2p	−7.477	1.0	0.570	−5.907
C(δ)2p	1.268	0.164	0.023	1.455
C(ϵ)2p	3.227	−0.571	−0.041	2.615
CC(α)2s	0.076	−0.024	−0.002	0.051
CC(β)2s	0.164	−0.039	15.895	16.020
CC(γ)2s	−0.564	0.119	−20.427	−20.872
CC(δ)2s	0.856	−0.210	18.010	18.656
CC(ϵ)2s	−0.244	0.189	−18.227	−18.282
CC(α)2p	−1.957	0.537	0.284	−1.136
CC(β)2p	5.481	−1.021	5.233	9.693
CC(γ)2p	0.932	0.435	−10.030	−8.662
CC(δ)2p	1.315	−0.547	−4.481	−3.713
CC(ϵ)2p	0.030	0.081	2.178	2.289

In the second calculation, the core groups were included in a configuration interaction calculation, using the orbitals from the previous valence calculation with 1 MHz limit. The results are shown in Fig. 10. The single core excitations were again clearly visible, double substitutions became unimportant. The increase by the C(β)2s group was down to 60 MHz. The final A factor was 604 MHz. The core-core groups changed the hyperfine structure by less than 5 MHz in total, with the main changes well below 2 MHz. The core 2p groups converged within 1 MHz and contributed mainly to the orbital term. The orbital and spin-dipole contribution converged for the 2s groups. The contact term showed no clear convergence. However, the change from layer β to γ and δ was clearly reduced and one could estimate the change due to layer ϵ to be less than 10 MHz. For all J values the configuration interaction calculation converged within 2% of the calculated value.

Comparing the two calculations, clear orbital correlations are visible for the 2p and 2s orbitals. While the C groups all change in the same direction in the configuration interaction calculation, this is not the case when the orbitals are allowed to vary. The C2p groups converge well and have their main influence on the orbital term. The CC2p groups are of minor importance and are orbital correlation in nature, only. Together with the C2s and CC2s groups they form the limited core correlation configuration state function space.

In both calculations, the two configuration state functions obtained by substitution of one 2s electron by one s electron of the second correlation layer, βs,

$$2s^1{}^2_1S\ 3d^3{}^4_3F\ {}^3F\ \beta s^2_1S\ {}^4F \tag{4.1}$$

and

$$2s^1{}^2_1S\ 3d^3{}^4_3F\ {}^5F\ \beta s^2_1S\ {}^4F \tag{4.2}$$

have a huge impact on the A factor. The two configuration state functions contributed to the contact term, both through orbital and mixing correlation. There was no compensation with the following layers for this contribution.

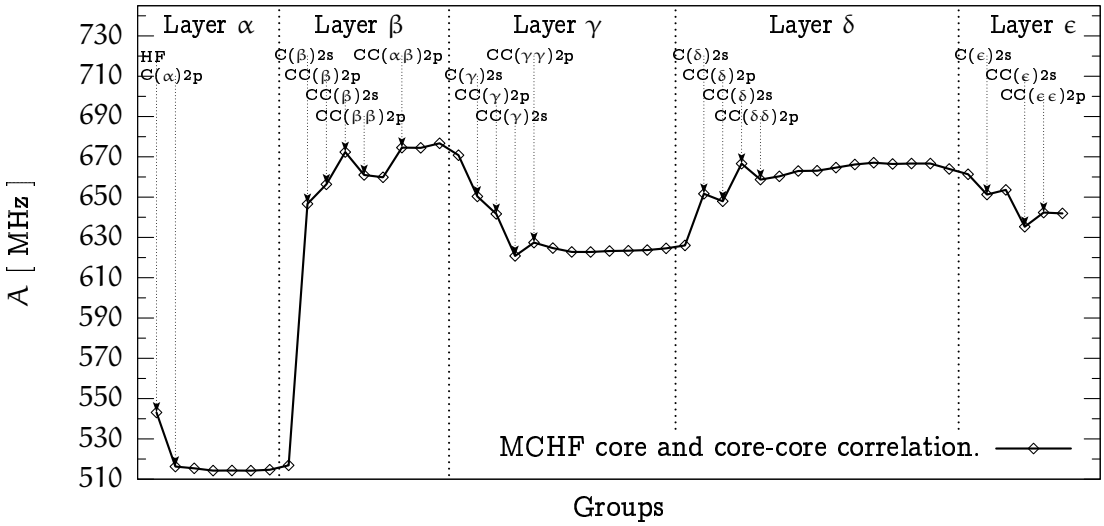

Fig 9. Multiconfiguration Hartree-Fock calculation of the A factor for the core correlation only. The A factor follows the change of the contact term.

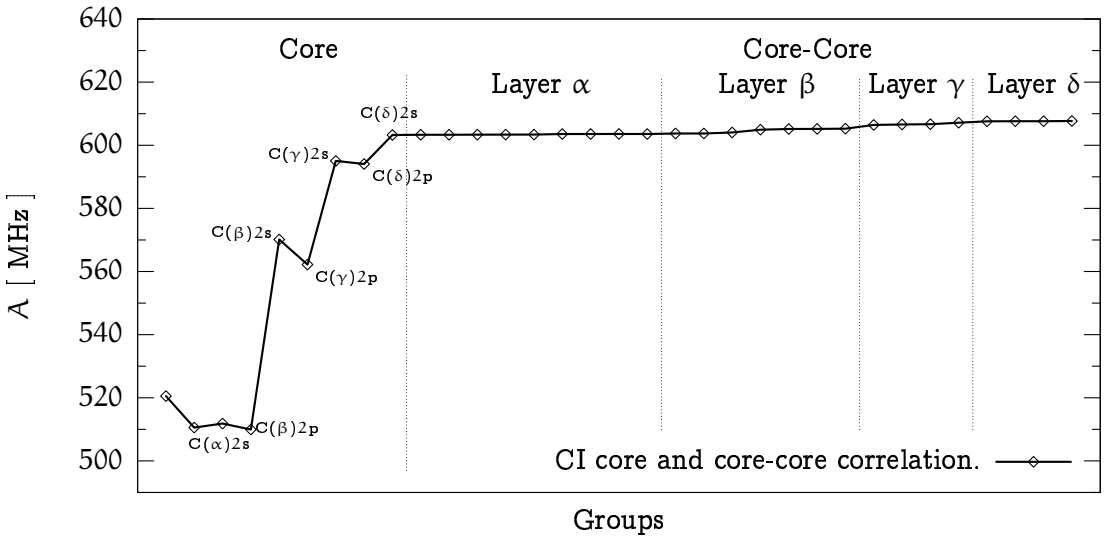

Fig 10. Configuration interaction calculation of the core correlation. The valence and correlation orbitals from the valence calculation limited to 1 MHz were used.

The correlations were studied together in a multiconfiguration Hartree-Fock calculation. Only groups of the limited valence and core configuration state function space were used. A total of 93 most important correlation groups from the valence and core correlation calculations done before form the configuration state function space, including part of layer ϵ. That amounted to a total of 14 133 configuration state functions. After the valence and core groups of one layer have been included, their orbitals were held fixed for the following groups of the next layers.

Four different calculations were performed to study the influence of the two configuration state functions Eq. 4.1 and Eq. 4.2. In Fig. 11 they are compared with the valence correlation calculation. The arrows indicate the most significant deviations between the calculations. These calculations took about two month calculation time.

The first calculation included both of the two configuration state functions. The final A factor was 620 MHz (I). The second calculation omitted the configuration state function Eq. 4.1. The final A factor was 580 MHz (II). For the third calculation, all configuration state functions from the C(n)2s groups were ignored. The final A factor was 506 MHz (III). In the final calculation, both configuration state functions, Eq. 4.1 and Eq. 4.2 were omitted. The final A factor was 540 MHz (IV).

The orbital, spin-dipole and quadrupole term were not affected and had the same dependence on the groups in all four calculations. The deviation of the different calculations was due to the contact contribution, only. This contact contribution was mainly given by the correlation of the 2s shell. The influence was dominated by the admixture of the correlation βs orbitals of the two configuration state functions Eq. 4.1 and Eq. 4.2 with a weight of 0.0009274 and -0.0004695, respectively. From a total of 14133 configuration state functions the introduced correlation of these two changed the A factor by 80 MHz.

The exclusion of these two functions led to a very different behavior of the correlations from layer γ on compared with the other calculations. All valence groups with double substitutions with one orbital from layer β showed no correlation any more. Correlation occurred with the following layer δ that were stronger compared to the other cases. The core groups of layer ϵ showed stronger correlations, too.

The detailed calculations allowed to estimate the error due to the convergence of certain correlation groups. This error was 5% on the calculated A factor and dominated by the 2s core correlation. It is given by the value in the round brackets in Table 13.

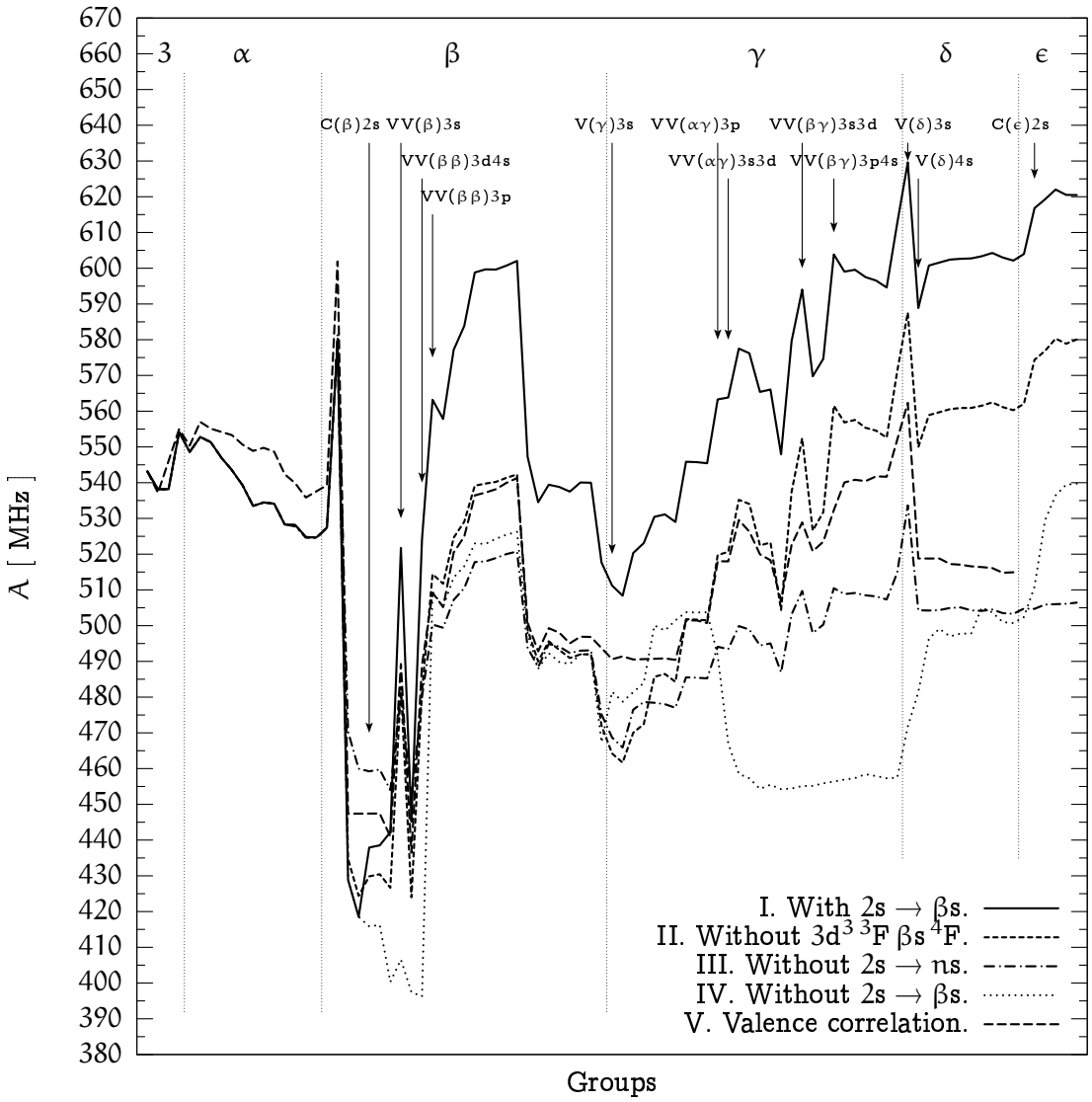

Fig 11. The correlations for the A factor in the multiconfiguration Hartree-Fock calculation using the limited valence and core configuration state function space. The configuration state functions are divided into 93 groups. After the configuration state functions of one group are included, the hyperfine structure factor A is calculated out of the new atomic state function. Valence and core correlations are included within each layer. The influence of the C(β)2s group is observed in different calculations: **I.** With the C(β)2s group, **II.** Without the configuration state function $3d^{3}{}^{3}F\beta s\,{}^{4}F$ of the C(β)2s group, **III.** Without any configuration state functions from the C(n)2s groups, **IV.** Without the two configuration state functions of the C(β)2s group, **V.** Valence correlation, only.

Contributions from the 1s shell and from triple or higher substitutions were estimated to be less than 2%.

Combining core and valence correlation led to an overestimation of 15% from the experimental value. Without correlation of the 2s orbital the A factor for $J = 3/2$ deviated by -10%. Ignoring the configuration state function Eq. 4.1 led to a deviation of 4% over the experimental value, ignoring also the other configuration state function underestimates A by -4%.

The C(βs)2s group led to a significant deviation from the experimental result. Higher substitutions than double could compensate that influence bringing the A factor closer to the experimental value. However all s correlation orbitals were included with double substitutions. Furthermore the weights of these two configurations is small, so matrix elements with triple or higher substitutions contribute far less and could compensate for only a part of the orbital relaxation.

Another reason for the dominant influence of the C(βs)2s group could be that relativistic effects were not taken fully into account. The complete relativistic multiconfiguration Dirac-Fock calculation in the next section will refute this.

More work has to be done to conclude that maybe the numerical procedure used to calculate the electron probability at the nucleus has to be improved.

The different behavior of the group dependency observed when the two configuration state functions were ignored together with the convergence pattern of the groups suggest yet another possibility. Ignoring the C(βs)2s group meant that correlations of the other orbitals were included first and the C(βs)2s group was included as C(γs)2s. That altered the correlation with the 2s orbital and excluded the strong polarization. In other words, including the 2s polarization before other correlations have occurred introduced a strong βs polarization orbital. The following correlation orbitals of the next layer could not change this fixed orbital. That led to the bad convergence of the C2s groups and the overestimation of the A factor.

Therefore the introduction of the core 2s correlation had to be done only after more correlations had been introduced. This is sustained by the fact that the calculation without the two configuration state functions Eq. 4.1 and Eq. 4.2 agreed within the estimated error of 5% with the experimental value. Under these assumptions the two configuration state functions were ignored for the following calculations.

The core-valence correlation was added in configuration interaction. The correlations converged fast and they contributed less than 1% to the A factor. The change, except

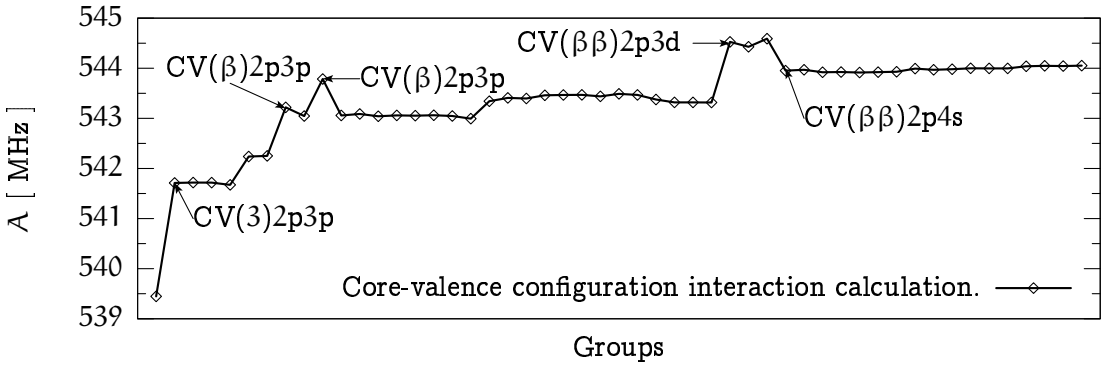

Fig 12. Based on the calculations without the C(βs)2s group, the core-valence correlation was included as configuration interaction calculation, using only CV(n) and CV(nn) groups.

for a few groups was well below 2 MHz, see Fig. 12. In a final configuration interaction calculation the 88 valence groups that had been eliminated from the configuration state function space were included, again group by group. These calculations took one month of time.

Good convergence was obtained for the orbital, spin-dipole and quadrupole terms. As one can see in Fig. 13, except for three groups, the changes were less than 2 MHz. The last jump of less than 2 MHz occurred at layer δ.

The result of the multiconfiguration Hartree-Fock calculation without the two configuration state functions of the C(βs)2s group and the following configuration interaction calculation with extended configuration state function space are given in Table 13.

Relativistic contributions to these results were obtained in Breit-Pauli approximation. All seven additional configuration state functions that were possible from the configuration $3d^3 4s^2$ were added to the configuration state function space. The expansion coefficients for the atomic wave function in intermediate LSJ coupling were obtained by the program BPCI [68]. The weights of the admixed terms were below 0.002. As can be seen in Table 13, relativistic effects in Breit-Pauli approximation were negligible.

Compared with the experimental result, the obtained values for the A factor were in good agreement with the experiment. The overall deviation was less than 2%. Except for $J = 5/2$, the multiconfiguration calculations were in better agreement than the semiempirical values.

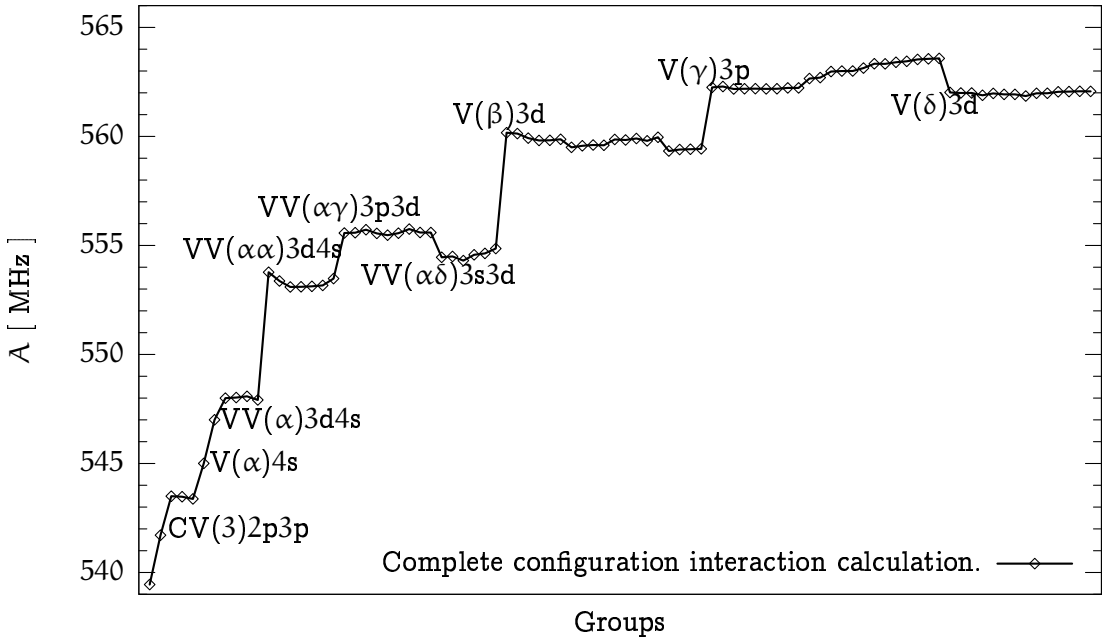

Fig 13. The core-valence configuration interaction calculation was extended by the groups left out in the multiconfiguration Hartree-Fock calculation.

Table 13. The hyperfine structure of the ground state of Vanadium, $3d^3\ ^3F\ 4s^2\ ^4F$. Comparison of the experimental data (Exp.) [67] and semiempirical calculation (Sem.) [66] with the calculated A factors. The Hartree-Fock (HF), limited multiconfiguration Hartree-Fock (MCHF), the configuration interaction calculation (CI) and Breit-Pauli corrections (CI+BP) are given. The last row lists the number of configuration state functions (Csf).

J	HF [MHz]	MCHF [MHz]	CI [MHz]	CI+BP [MHz]	Exp. [67] [MHz]	Sem. [66] [MHz]
3/2	543	540(27)	562(28)	561	560.069(2)	547.923
5/2	336	320(16)	322(16)	323	321.251(3)	321.575
7/2	276	256(13)	252(13)	253	249.752(2)	255.368
9/2	259	237(12)	230(12)	230	227.136(1)	237.025
Csf	1	13296	29052	29059		

4.3 Multiconfiguration Dirac-Fock calculation

To test the method in the full relativistic framework and to further investigate the core correlation, similar calculations in multiconfiguration Dirac-Fock approximation were performed. The package for multiconfiguration Dirac-Fock calculations, GRASP [7], was used for the calculations.

The configuration state functions $|\psi_i\rangle$ of the atomic state function (Eq. 1.12) were defined using the notation

$$|\psi_i\rangle = |[n_1 l_{1j_1}]^{N_1} J_1\, [n_2 l_{2j_2}]^{N_2} J_2\, J_{12}\, [n_3 l_{3j_3}]^{N_3} J_3\, J_{123}\, \ldots\rangle\,. \tag{4.3}$$

The relativistic subshells were regarded as belonging to the same correlation group as in the multiconfiguration Hartree-Fock case. The shell $3d^3$, for example, splits into four relativistic subshells $[3d_{5/2}]^3$, $[3d_{5/2}]^2\,[3d_{3/2}]$, $[3d_{5/2}]\,[3d_{3/2}]^2$ and $[3d_{3/2}]^3$. Substitutions from these four subshells were again denoted by V3d. The set of correlation layers included all orbitals of given l symmetry. That allows one to use the same method as in the multiconfiguration Hartree-Fock calculations. The configuration state functions of each correlation group were added in turn with increasing correlation orbital layer and the atomic state function was determined self-consistently. The hyperfine structure was calculated after one group was included.

The reference set was obtained by the Dirac-Fock calculation and verified by transformation of the atomic state function from jj- into LS-coupled wave functions. The transformation matrices were evaluated with the program LSJ [69]. The Dirac-Fock calculation was based on all possible configuration state functions of the configuration $3d^3 4s^2\,{}^4F$ that could couple to the given J value. The transformations showed that the wave functions were almost purely LS-coupled:

$$\begin{aligned}
{}^4F_{3/2} &= -0.5998\,[3d_{3/2}]^2 2[3d_{5/2}]\tfrac{5}{2}\,\tfrac{3}{2}\,[4s_{1/2}]^2\,\tfrac{3}{2} + 0.5900\,[3d_{3/2}]^3\tfrac{3}{2}[4s_{1/2}]^2 2\,\tfrac{3}{2} \\
&\quad +0.3915\,[3d_{3/2}]\tfrac{3}{2}[3d_{5/2}]^2 2\,\tfrac{3}{2}\,[4s_{1/2}]^2\,\tfrac{3}{2} \\
&\quad -0.3309\,[3d_{3/2}]\tfrac{3}{2}[3d_{5/2}]^2\,\tfrac{3}{2}\,[4s_{1/2}]^2\,\tfrac{3}{2} \\
&\quad -0.1714\,[3d_{5/2}]^3\tfrac{3}{2}[4s_{1/2}]^2 2\,\tfrac{3}{2} \qquad (4.4) \\
&= -0.999876\; 3d^3\,{}^4_3F\; 4s^2\,{}^4F_{3/2} - 0.013356\; 3d^3\,{}^2_3D\; 4s^2\,{}^2D_{3/2} \\
&\quad +0.008387\; 3d^3\,{}^2_1D\; 4s^2\,{}^2D_{3/2} + 0.000181\; 3d^3\,{}^2_3P\; 4s^2\,{}^2P_{3/2} \\
&\quad -0.000021\; 3d^3\,{}^4_3P\; 4s^2\,{}^4P_{3/2}\,. \qquad (4.5)
\end{aligned}$$

$$
\begin{aligned}
{}^4\mathrm{F}_{5/2} &= 0.8218\ [3\mathrm{d}_{3/2}]^2 2[3\mathrm{d}_{5/2}]\tfrac{5}{2}\ \tfrac{5}{2}\ [4\mathrm{s}_{1/2}]^2\ \tfrac{5}{2} + 0.3670\ [3\mathrm{d}_{3/2}]^3\tfrac{5}{2}[4\mathrm{s}_{1/2}]^2\ \tfrac{5}{2} \\
&\quad -0.2741\ [3\mathrm{d}_{3/2}]^2[3\mathrm{d}_{5/2}]\tfrac{5}{2}\ \tfrac{5}{2}\ [4\mathrm{s}_{1/2}]^2\ \tfrac{5}{2} \\
&\quad -0.2661\ [3\mathrm{d}_{3/2}]\tfrac{3}{2}[3\mathrm{d}_{5/2}]^2 2\ \tfrac{5}{2}\ [4\mathrm{s}_{1/2}]^2\ \tfrac{5}{2} \\
&\quad -0.2096\ [3\mathrm{d}_{3/2}]\tfrac{3}{2}[3\mathrm{d}_{5/2}]^2 4\tfrac{5}{2}[4\mathrm{s}_{1/2}]^2\ \tfrac{5}{2} \qquad (4.6) \\
&= -0.999939\ 3\mathrm{d}^3\ {}^4_3\mathrm{F}\ 4\mathrm{s}^2\ {}^4\mathrm{F}_{5/2} - 0.009026\ 3\mathrm{d}^3\ {}^2_3\mathrm{D}\ 4\mathrm{s}^2\ {}^2\mathrm{D}_{5/2} \\
&\quad +0.005699\ 3\mathrm{d}^3\ {}^2_1\mathrm{D}\ 4\mathrm{s}^2\ {}^2\mathrm{D}_{5/2} + 0.002851\ 3\mathrm{d}^3\ {}^2_3\mathrm{F}\ 4\mathrm{s}^2\ {}^2\mathrm{F}_{5/2} \\
&\quad -0.000052\ 3\mathrm{d}^3\ {}^4_3\mathrm{P}\ 4\mathrm{s}^2\ {}^4\mathrm{P}_{5/2}\,. \qquad (4.7)
\end{aligned}
$$

$$
\begin{aligned}
{}^4\mathrm{F}_{7/2} &= 0.8421\ [3\mathrm{d}_{3/2}]\ \tfrac{3}{2}\ [3\mathrm{d}_{5/2}]^2 4\ \tfrac{7}{2}\ [4\mathrm{s}_{1/2}]^2\ \tfrac{7}{2} \\
&\quad +0.4557\ [3\mathrm{d}_{3/2}]^2 2[3\mathrm{d}_{5/2}]\tfrac{5}{2}\ \tfrac{5}{2}\ [4\mathrm{s}_{1/2}]^2\ \tfrac{7}{2} \\
&\quad -0.2884\ [3\mathrm{d}_{3/2}]\tfrac{3}{2}[3\mathrm{d}_{5/2}]^2 2\ \tfrac{7}{2}\ [4\mathrm{s}_{1/2}]^2\ \tfrac{7}{2} \qquad (4.8) \\
&= -0.999950\ 3\mathrm{d}^3\ {}^4_3\mathrm{F}\ 4\mathrm{s}^2\ {}^4\mathrm{F}_{7/2} + 0.003347\ 3\mathrm{d}^3\ {}^2_3\mathrm{F}\ 4\mathrm{s}^2\ {}^2\mathrm{F}_{7/2} \\
&\quad +0.009454\ 3\mathrm{d}^{\mathrm{d}}\ {}^2_3\mathrm{G}\ 4\mathrm{s}^2\ {}^2\mathrm{G}_{7/2}\,. \qquad (4.9)
\end{aligned}
$$

$$
\begin{aligned}
{}^4\mathrm{F}_{9/2} &= 0.6791\ [3\mathrm{d}_{3/2}]^2 2[3\mathrm{d}_{5/2}]\tfrac{5}{2}\ \tfrac{9}{2}\ [4\mathrm{s}_{1/2}]^2\ \tfrac{9}{2} \\
&\quad -0.6717\ [3\mathrm{d}_{3/2}]\tfrac{3}{2}[3\mathrm{d}_{5/2}]^2 4\ \tfrac{9}{2}\ [4\mathrm{s}_{1/2}]^2\ \tfrac{9}{2} \\
&\quad -0.2960\ [3\mathrm{d}_{5/2}]^3\tfrac{9}{2}[4\mathrm{s}_{1/2}]^2\ \tfrac{9}{2} \qquad (4.10) \\
&= -0.999785\ 3\mathrm{d}^3\ {}^4_3\mathrm{F}\ 4\mathrm{s}^2\ {}^4\mathrm{F}_{9/2} + 0.020747\ 3\mathrm{d}^3\ {}^2_3\mathrm{G}\ 4\mathrm{s}^2\ {}^2\mathrm{G}_{9/2} \\
&\quad -0.000315\ 3\mathrm{d}^3\ {}^2_3\mathrm{H}\ 4\mathrm{s}^2\ {}^2\mathrm{H}_{9/2}\,. \qquad (4.11)
\end{aligned}
$$

For each J value these configuration state functions were used as reference set.

As in the multiconfiguration Hartree-Fock approximation, first single substitutions with the reference set for core and valence orbitals were included to raising correlation layers. In Table 14 the results of the A factor for substitutions including 1s (A_{1s}) and excluding this substitutions ($A_{\mathrm{no\ 1s}}$) for raising correlation layers are compared. Convergence within 2 MHz was obtained with layer δ. That was in the range of the 1s shell correlation contribution. As a result this shell could be kept closed for all further calculations, introducing an error of less than 0.4%. The relativistic influence, estimated by comparing the results with the multiconfiguration Hartree-Fock calculation showed that the influence is below 1%.

Table 14. Results of the A factor in the single substitution calculation for $J = 3/2$. The results with substitutions of the 1s shell (A_{1s}) and without ($A_{no\ 1s}$) were compared with the multiconfiguration Hartree-Fock calculation with no 1s substitutions ($A_{MCHF,no\ 1s}$, see Table 10). The experimental value is $A = 560.048$ MHz [65]. The number of configuration state functions is given in the Csf column.

Layer	Csf	A_{1s} [MHz]	Csf	$A_{no\ 1s}$ [MHz]	Csf	$A_{MCHF,\ no\ 1s}$ [MHz]
DF/HF	5	540	5	539	1	548
$3, \alpha$	865	535	789	517	137	542
β	1946	420	1742	411	309	432
γ	3191	607	2877	607	525	604
δ	4450	601	4014	603	757	599
ϵ	5707	602	5149	603	1005	599
ζ	6962	602	6284	604	1256	600

The multiconfiguration Dirac-Fock calculation was performed for each J value separately. The limit on the configuration state function group was set to 0.2% on the experimental A value, that is 1 MHz for $J = 3/2$. The single and double substitutions of the valence and core electrons without 1s shell substitutions were divided into 273 groups. After each group, the hyperfine structure was determined from the new atomic wave function. Once all groups of one layer were included, this orbitals were held fixed and only the valence and new layer orbitals were varied. The results of the calculations are given in Fig. 14. Groups that change A below the limit of 0.2% are indicated by the small dots and were ignored. The groups above the limit are marked by the diamond symbol and were used in the calculation that followed. These intensive calculations took about three month of time.

More than 600 000 interacting configuration state functions span the configuration state function space for the ground state of Vanadium for single and double core and valence substitutions by five correlation layers with the highest possible symmetry of $l = i$. The core-valence configuration state functions more than doubled this space. The restriction to groups that change the A factor by more than 0.2% limited the number of groups for layer δ from 71 down to 12 groups, and similar for the other J values. This reduction of the configuration space, however, was not enough and additional condensing

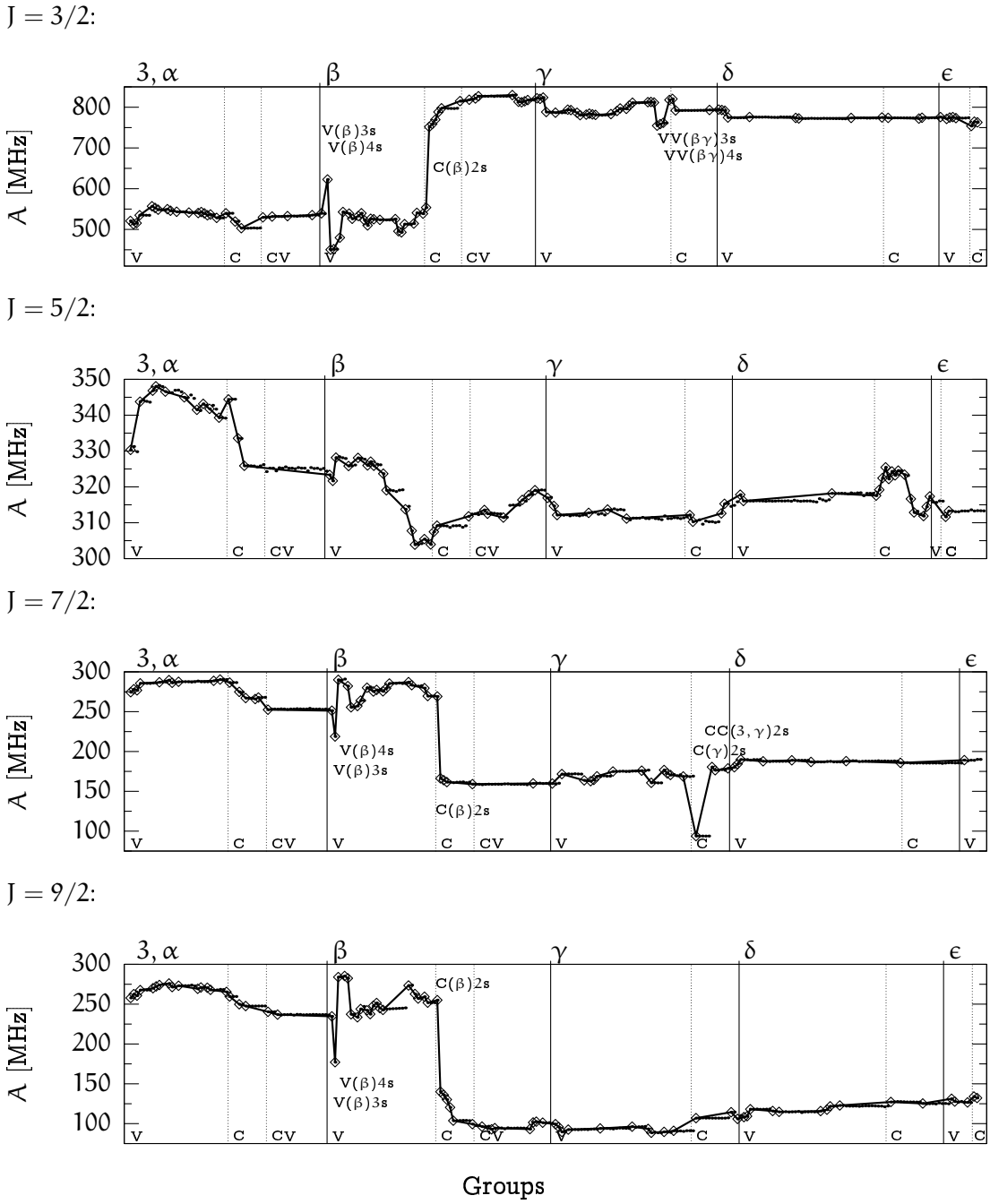

Fig 14. The A factor dependence on the correlation groups in multiconfiguration Dirac-Fock approximation. The groups that change the A factor by less than 0.2% are given by the small dots, the groups above 0.2% are given by the diamond symbols. The layers are indicated on top. Vertical lines separate the correlation groups that are abbreviated by V for valence, C for core and CV for the core-valence groups.

was used. The truncation was set that the deviation was 1% between the uncondensed multiconfiguration calculation and the configuration interaction calculation based on the wave functions of the condensed multiconfiguration calculation.

The level $J = 3/2$ showed the strongest correlation, followed by $J = 7/2$ and $J = 9/2$. The level with $J = 5/2$ showed very weak correlation. The influence of the core-valence groups became negligible after layer γ. Two properties were the same for all J values. First, the compensation of the 3s and 4s single valence groups was visible in the beginning of the layer β groups. Second, there was a huge influence of the C(β)2s group. Some major changes occurred that were different for each J and all of them almost compensated within the layer. The number of important groups shrank considerable from layer δ on.

In order to estimate the convergence of the correlation groups and detect their influence, the change of the A factor was analyzed for the groups used. The valence correlation groups converged well within 1% with layer ϵ. For $J = 3/2$, the core group seemed to converge with layer δ. However some groups of layer ϵ, probably due to the severe condensing, had an influence of around 20 MHz. For $J = 5/2$ and $J = 7/2$ convergence within 5 MHz was obtained. The core correlation for $J = 9/2$ seemed converged well with layer δ but layer ϵ changed A by 10 MHz. Observing the trend with which the change of each layer diminished, convergence within 2% for the core groups was justified, except for $J = 3/2$ with an error of 4%.

The approximation so far did not lead to agreement with the experiment, see Table 15. The calculated A factor for $J = 3/2$ was 763 MHz, the experimental result was 560 MHz. That was a deviation of 36% of the experimental value while the estimated error was only 4%. A similar result was observed in the multiconfiguration Hartree-Fock approach. Only $J = 5/2$ was near the estimated error, the case that did not show much correlation.

The approximation was extended in configuration interaction approximation by including configuration state functions of the limited groups that had been ignored due to condensing. The wave functions were taken from the calculations before.

First, only the valence groups were used. After all valence groups of one layer were included, the mixing coefficients of the atomic state function were determined and the hyperfine structure was calculated. Thereafter, the atomic state function was condensed. The cut-off was set so that the condensed calculation changed the A factor by less than

Table 15. Result of the relativistic multiconfiguration approximation of the A factors. For each J, the single configuration Dirac-Fock calculation (DF) and the limited multiconfiguration Dirac-Fock calculation (MCDF) are compared to the experimental results [65]. The deviation from the experimental value is given (Δ) and the percentage deviation (Percentage). In round brackets the estimated error on the calculation is indicated, 4% for $J = 3/2$ and 2% for the other J values.

J	DF [MHz]	MCDF [MHz]	Exp. [65] [MHz]	Δ [MHz]	Percentage [%]
3/2	520.91	762(30)	560.069(2)	-202	-36
5/2	330.32	313(6)	321.251(3)	8	3
7/2	274.46	189(4)	249.752(2)	60	24
9/2	257.83	132(3)	227.136(1)	95	42

0.2%. As these calculations needed a lot of computation time, no detailed calculation was performed for each group. The calculations, shown in Fig. 15 took one month to complete. Convergency below 1% compared to the calculated value was achieved. Partial compensation took place between the change of layer β and the two following layers.

The core groups were added to the configuration state function space of the valence correlations. This was done in detail adding each group in turn. The A factor after the groups were included is shown in Fig. 16 to Fig. 19. Layer ϵ was omitted to include more configuration state functions of the lower layers.

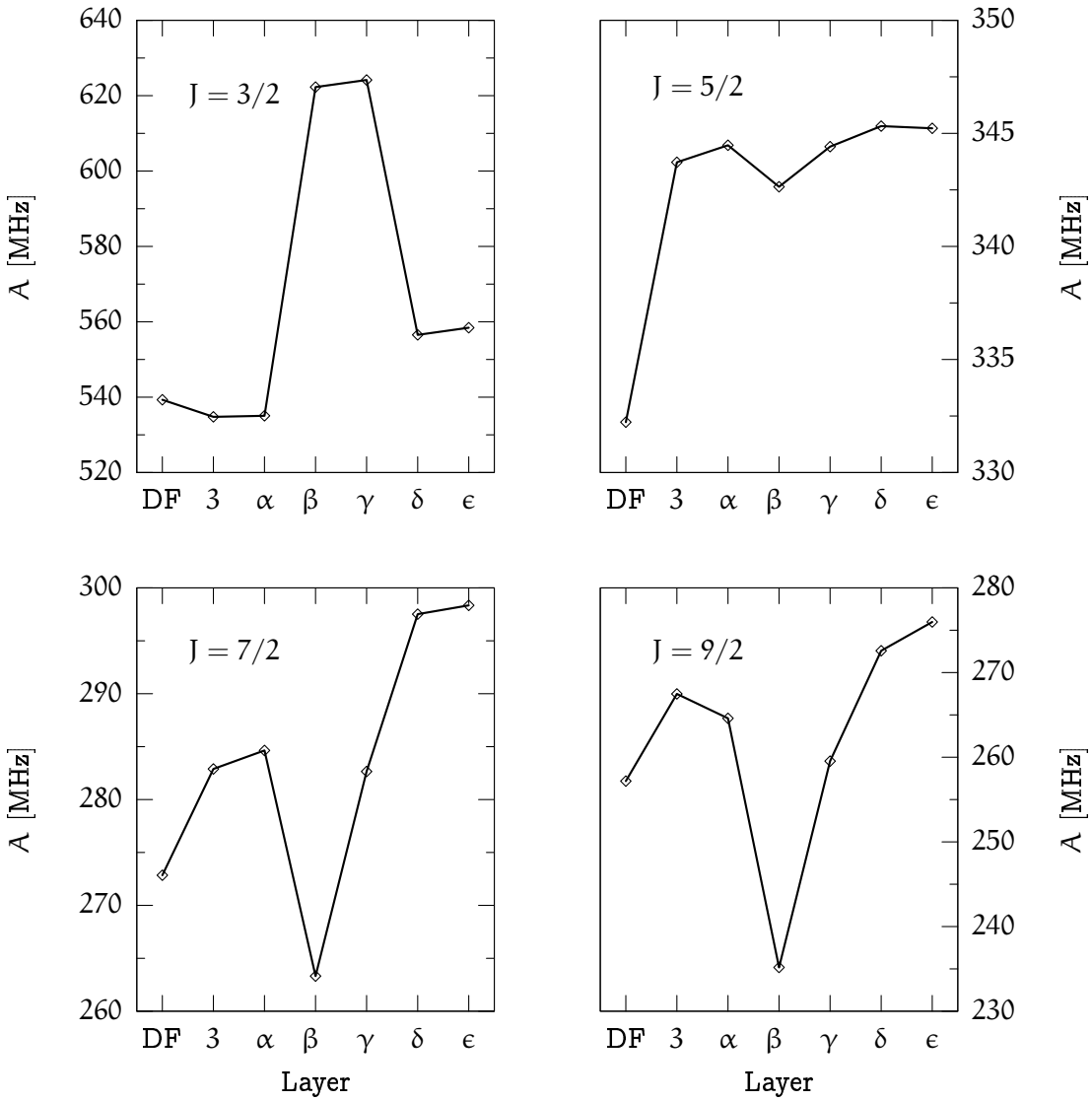

Fig 15. The A factor for the configuration interaction calculation using valence correlation groups, only.

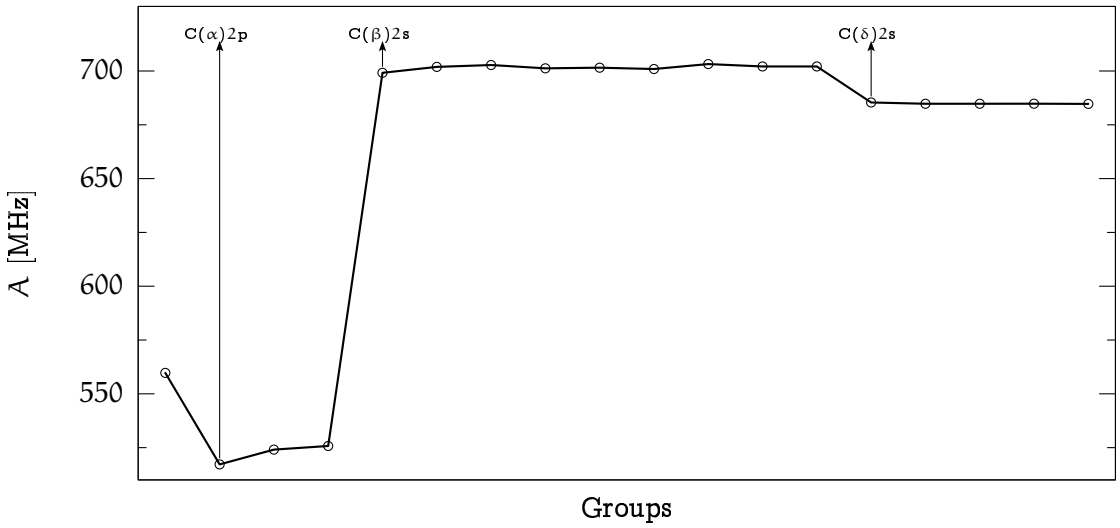

Fig 16. The A factor for $J = 3/2$ for the core groups. Detailed configuration interaction calculation after the valence groups had been included.

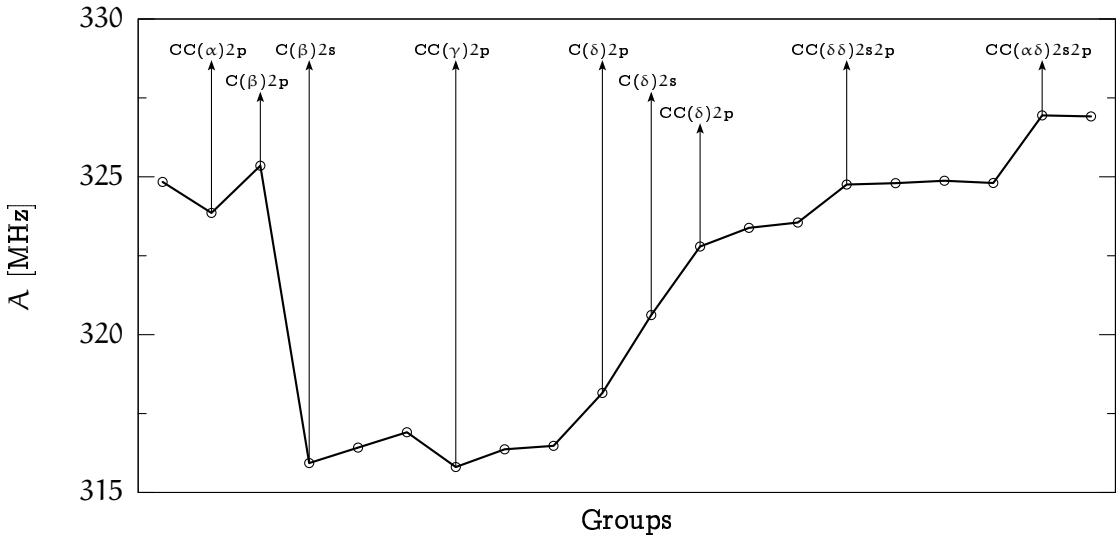

Fig 17. The A factor for $J = 5/2$ for the core groups. Detailed configuration interaction calculation after the valence groups had been included.

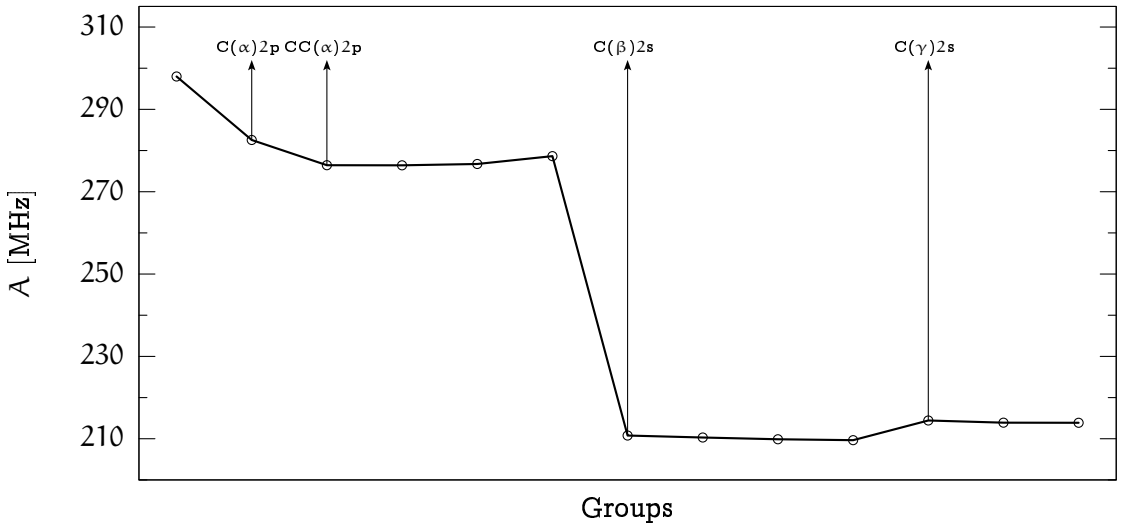

Fig 18. The A factor for $J = 7/2$ for the core groups. Detailed configuration interaction calculation after the valence groups had been included.

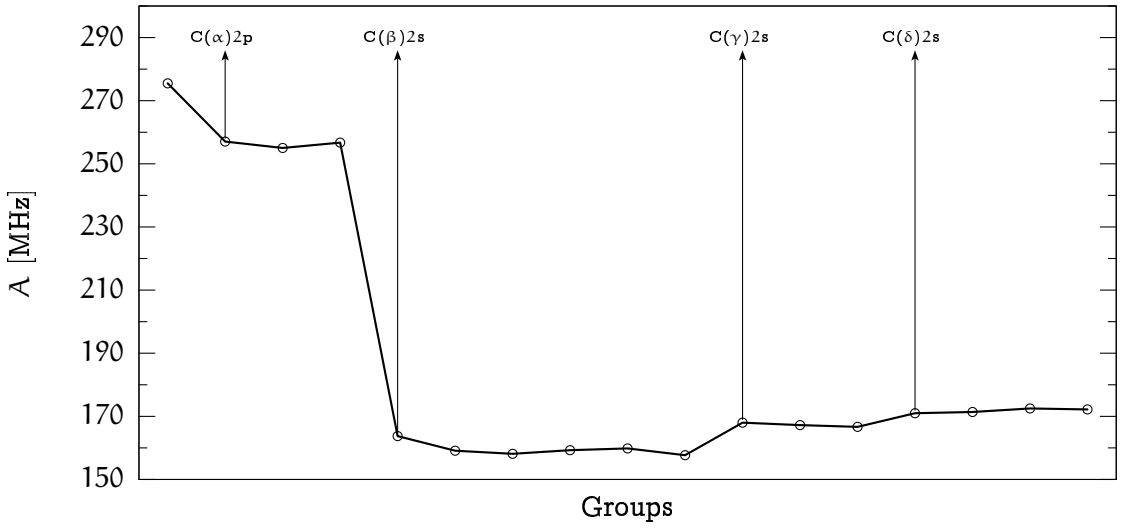

Fig 19. The A factor for $J = 9/2$ for the core groups. Detailed configuration interaction calculation after the valence groups had been included.

Table 16. Result of the relativistic multiconfiguration calculation of the A factor. The multiconfiguration calculation, the valence configuration interaction and the core configuration interaction calculation are compared with the experimental results [65]. The errors are indicated in the round brackets.

J	DF [MHz]	MCDF [MHz]	V-CI [MHz]	C-CI [MHz]	Exp. [MHz]
3/2	520.91	762.86	558(6)	685(27)	560.069(2)
5/2	330.32	313.27	345(3)	327(6)	321.251(3)
7/2	274.46	189.20	298(3)	214(4)	249.752(2)
9/2	257.83	132.16	275(3)	172(4)	227.136(1)

The C2s groups had the main influence on the A factor. The C(β)2s group dominated over the others. The convergence of this group was not good and it was the main source of error. The last change was around 4% of the calculated value for $J = 3/2$, for all other J around 2%. The results for the A factor are summarized in Table 16. The estimated error for the configuration interaction calculations (CI) is given in round brackets. For $J = 5/2$ agreement with the experiment was obtained. The other J values were off the error limits. The deviation from the experiment was with 25% the highest for $J = 9/2$.

The assigned error is much smaller than the deviation from the experimental result. This points out that, as in the multiconfiguration Hartree-Fock approximation, further effects have to be considered as a source of error.

In the multiconfiguration Hartree-Fock approach the C(βs)2s configuration state functions were ignored to obtain good agreement with the experiment. In the multiconfiguration Dirac-Fock approximation, the C(βs)2s group could be divided into four subgroups, depending on the occupation of the $3d^3$ subshells, $[3d_{3/2}]^{N_1}[3d_{5/2}]^{N_2}$ with $N_1 + N_2 = 3$.

In Table 17 the calculations without configuration state functions of the subgroups of C(βs)2s are tabulated. The percentage deviation from the experimental value is indicated in the error column. The error due to the calculation is 2% (4% for $J = 3/2$).

For $J = 3/2$, very good agreement was obtained if the $[3d_{3/2}][3d_{5/2}]^2$ subgroup of C(βs)2s was ignored. The influence of the $[3d_{5/2}]^3$ subgroup was below the error of the calculation, therefore no information was obtained about whether this group was to be

Table 17. The influence of the C(βs)2s subgroups on the A factor is tabulated. The deviation of the A factor from the experimental value is denoted by ΔA. The error is given in the percentage deviation from the experimental value. Due to condensing, the subgroups $[3d_{3/2}][3d_{5/2}]^2$ and $[3d_{3/2}]^3$ were already eliminated for $J = 7/2$ and $J = 9/2$.

J	Type	A [MHz]	ΔA [MHz]	Error [%]
3/2	Experimental	560.069		
	Calculation	685	-124.931	22.3
	Without subgroups of C(βs)2s			
	$[3d_{3/2}]^2[3d_{5/2}]$	607	-46.931	8.4
	$[3d_{3/2}][3d_{5/2}]^2$	564	-3.931	0.7
	$[3d_{3/2}][3d_{5/2}]^2, [3d_{5/2}]^3$	562	-1.931	0.3
	$[3d_{3/2}][3d_{5/2}]^2, [3d_{3/2}]^3$	467	-93.069	16.6
	$[3d_{3/2}][3d_{5/2}]^2, [3d_{3/2}]^2[3d_{5/2}]$	509	51.069	9.1
5/2	Experimental	321.251		
	Calculation	327	-5.749	1.8
	Without subgroups of C(βs)2s			
	$[3d_{3/2}]^2[3d_{5/2}]$	318	3.251	-1.0
	$[3d_{3/2}][3d_{5/2}]^2$	318	3.251	-1.0
	$[3d_{3/2}][3d_{5/2}]^2, [3d_{5/2}]^3$	318	3.251	-1.0
	$[3d_{3/2}][3d_{5/2}]^2, [3d_{3/2}]^3$	318	3.251	-1.0
	$[3d_{3/2}][3d_{5/2}]^2, [3d_{3/2}]^2[3d_{5/2}]$	309	12.251	-3.8
7/2	Experimental	249.752		
	Calculation	214	35.752	-14.3
	Without subgroups of C(βs)2s			
	$[3d_{3/2}]^2[3d_{5/2}]$	228	21.752	-8.7
	$[3d_{3/2}][3d_{5/2}]^2$	270	-20.248	8.1
	$[3d_{3/2}][3d_{5/2}]^2, [3d_{5/2}]^3$	270	-20.248	8.1
	$[3d_{3/2}][3d_{5/2}]^2, [3d_{3/2}]^3$	—	—	—
	$[3d_{3/2}][3d_{5/2}]^2, [3d_{3/2}]^2[3d_{5/2}]$	284	-34.248	13.7
9/2	Experimental	227.136		
	Calculation	172	55.136	-24.3
	Without subgroups of C(βs)2s			
	$[3d_{3/2}]^2[3d_{5/2}]$	180	47.136	-20.8
	$[3d_{3/2}][3d_{5/2}]^2$	225	2.136	-0.9
	$[3d_{3/2}][3d_{5/2}]^2, [3d_{5/2}]^3$	282	-54.864	24.2
	$[3d_{3/2}][3d_{5/2}]^2, [3d_{3/2}]^3$	—	—	—
	$[3d_{3/2}][3d_{5/2}]^2, [3d_{3/2}]^2[3d_{5/2}]$	233	-5.864	2.6

Table 18. Hyperfine structure factor A for the ground state of Vanadium. The calculated values are compared with the experimental values (Exp.) [65] and the semiempirical results (Sem.) [66]. The single configuration Hartree-Fock (HF), the multiconfiguration Hartree-Fock (MCHF) excluding the C(βs)2s group, the configuration interaction calculation with the extended configuration state function space (MCHF+CI) and additional Breit-Pauli correction (MCHF+BPCI) are listed. For the multiconfiguration Dirac-Fock calculation the reference Dirac-Fock calculation (DF), the multiconfiguration Dirac-Fock including the C(βs)2s $[3d_{3/2}][3d_{5/2}]^2$ subgroup and configuration interaction calculation with extended configuration state function space (MCDF+CI) and the calculation excluding this subgroup (MCDF+CI,excl.) are listed. In round brackets, the estimated error on the calculation is given.

	A factor [MHz]			
Calculation	$J = 3/2$	$J = 5/2$	$J = 7/2$	$J = 9/2$
HF	543	336	276	259
MCHF	540(27)	320(16)	256(13)	237(12)
MCHF+CI	562(28)	322(16)	252(13)	230(12)
MCHF+BPCI	561	323	253	230
DF	521	330	274	258
MCDF+CI	685(27)	327(6)	214(4)	172(4)
MCDF+CI,excl.	564(23)	318(6)	270(5)	225(5)
Exp. [65]	560.069(2)	321.251(3)	249.752(2)	227.136(1)
Sem. [66]	547.923	321.575	255.368	237.025

included or not. For $J = 5/2$, the percentage error compared with the experimental value was 1.8%. That was in the estimated error of 2% of the calculation. Ignoring of the same subgroup as for $J = 3/2$ lowered the result bringing it in the error limit of the calculation. Again, no information about the $[3d_{5/2}]^3$ and $[3d_{3/2}]^3$ subgroups was obtained as their influence was below the error limit. The calculation for $J = 7/2$ was off the error limit. Ignoring $[3d_{3/2}][3d_{5/2}]^2$ underestimated A by 21 MHz and ignoring $[3d_{3/2}]^2[3d_{5/2}]$ overestimated A by 21 MHz. Good agreement was achieved for $J = 9/2$ if, again, the $[3d_{3/2}][3d_{5/2}]^2$ subgroup was ignored. The final results of the A factor for the hyperfine structure splitting of the ground state of Vanadium were then calculated as given in Table 18. Compared with the experimental values, the estimated error of the calculation was verified except for the $J = 7/2$, where the deviation from the experimental value was 8%. This deviation might be due to condensing.

4.4 The script for the applied method

The calculations on Vanadium led to the development of a script file that performs the calculations. The script RUNNER handles the in- and output of the ATSP or GRASP utilities. It is based on the BASH SHELL and GAWK

The specific information about the case (i.e. reference configuration state function, state, nuclear data) and the data for the the calculation (i.e. limit for including a group, truncation limit for condensing (TL), acceptable difference for condensed and uncondensed calculation of the A factor (Con.limit) and convergence limit in the multiconfiguration approach) are stored in a file CASEDATA.

The complete configuration state function space is obtained by LSGEN [6] in the multiconfiguration Hartree-Fock or CSL [7] for the Dirac-Fock case. The program CLISTID reads this configuration state function file and with the information from the CASEDATA file it creates the groups. In the output file GROUPS the orbitals that are allowed to vary have to be defined. This program was written in the C programming language to handle a large number of configuration state functions.

The script RUNNER is based on these three files as indicated on top of Fig. 20. It starts from an initial configuration state function list and an initial A factor A_{start} and adds the first group of the GROUPS file. It calls the procedures to perform the self-consistent calculation until convergence is achieved or an error occurred. If successful the program to calculate the hyperfine structure is called and the new A factor is compared with the starting one. If the difference is below the limit, the group is erased from the configuration state function list and RUNNER starts over with the next group.

If the difference between the old and the new A factor is above the limit, the configuration state function space is checked. If it comprises more configuration state functions than a maximal number MAX.NR., the configuration state function space is condensed at all weights below the truncation limit TL. The A factor A_{con} is determined in multiconfiguration approximation and the factor is checked if it does not differ from the uncondensed result by more than the value CON.LIMIT.

If it does differ more, the wave functions from the condensed calculation are taken and the uncondensed configuration state function space is used in configuration interaction calculation to obtain the A factor A_{ci}. If the difference between A and A_{ci} is larger than the limit CON.LIMIT, the truncation value TL is divided by 10 and the uncondensed configuration state function space is condensed using the less severe truncation value.

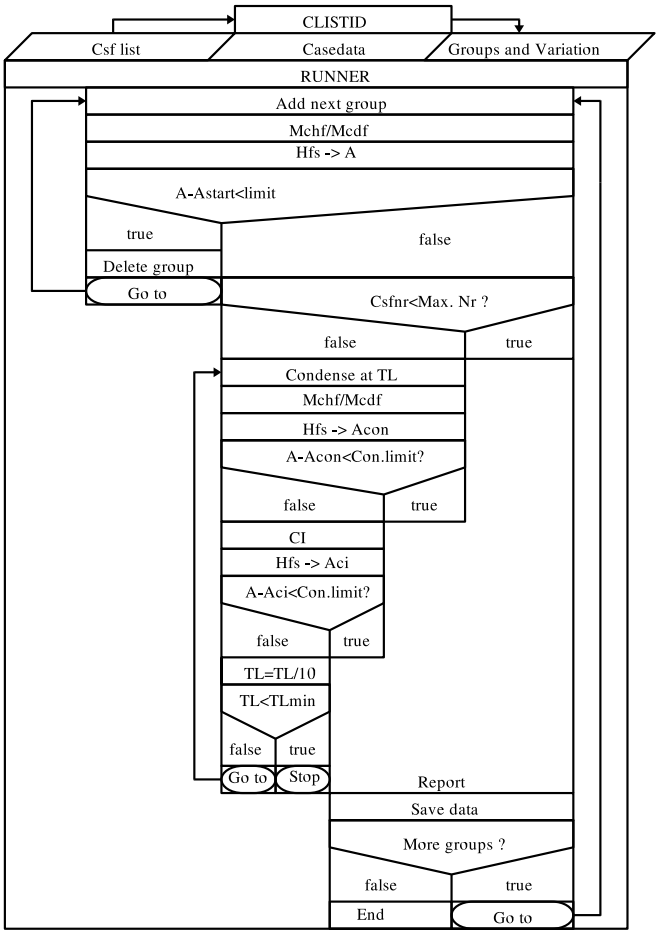

Fig 20. The flowchart for the method of large scale ab initio hyperfine structure calculations.

This procedure is repeated until the change of the A factor due to condensing is below the limit CON.LIMIT. The script stops if TL is below a certain value TLMIN. RUNNER creates a report file that summarizes the calculation and saves all new data into a directory. If more groups have to be calculated, it starts over adding the next group.

For Vanadium, the group limit was set to 0.2% on the experimental value. The configuration state function space had to be condensed in the multiconfiguration Dirac-Fock case. The initial truncation value was 0.0001 with an allowed minimal value of 0.000001. The truncation limit was set to 1%. The script can be used to perform similar calculations by adjusting the input files CASEDATA, CSF LIST and the file GROUPS .

Conclusion

1. The approach based on the combination of the angular momentum theory, on a generalized graphical approach, on the second quantization in coupled tensorial form, on the quasispin space and on the use of fully reduced coefficients of fractional parentage allows one to find the general irreducible tensorial form of the hyperfine interaction operator as well as the matrix elements of the above-mentioned operator, diagonal and off-diagonal with respect to electronic configurations included, thus accounting for the correlation effects in a general case.

2. The atomic application development systems RACAH and JUCYS are now sufficiently developed to create specialized packages for atomic structure calculations (in this thesis the hyperfine structure) based on symbolic programming.

3. The developed method to calculate the hyperfine structure from the multiconfiguration atomic state function make a detailed hyperfine structure calculation for complex many-electron atoms possible. The proposed approach allows one to detect the convergence, the influence of defined correlation groups and thus to make well defined approximations for the configuration state function space.

4. The dependency of the A factor on the correlation groups is similar in the multiconfiguration Hartree-Fock and Dirac-Fock approximation in the calculations for Vanadium. The $3s$ and $4s$ correlation groups strongly polarize these orbitals, their net effect, however, compensates. The valence correlations are captured after the third layer. Core-valence correlations and core-core correlations with two different layers are unimportant.

5. For Vanadium, both the multiconfiguration Hartree-Fock approximation and the Dirac-Fock approximation lead to good agreement with the experimental results only if the correlations leading to the contact contribution of the core electrons are included after sufficient other correlations have been accounted for.

6. The script created that handles the in- and output between the ATSP or GRASP modules. The calculations as described for Vanadium are thereby automated. The script can be used for any other atom or ion.

Outlook

The thesis shows that with the multiconfiguration approach calculation of the hyperfine structure for complex atoms and ions can be carried out with an accuracy that is comparable to the semiempirical approach. The influence of core correlation groups has to be studied further. It would be interesting to study if maybe this can be done in combination with the perturbational approach. Parts of the underlying techniques are made available in the form of the symbolic programming environment of HFS and might contribute to further developments of the theory of complex many-electron atoms, the theory of hyperfine structure included.

About the author

Oliver Scharf was born 1974 in Berlin, Germany. He studied physics from 1995 to 2002 at the Technische Universität Berlin and graduated in 2002 as diplom physicist. From 2002 to 2006 he did his doctorate studies at the Vilnius University Institute of Theoretical Physics and Astronomy, Lithuania.

The author thanks Prof. G. Gaigalas for his scientific advises, his help, friendship and patience, Prof. Z. Rudzikas for his help in making this project possible, and my family for their love and support. Thanks also to the staff of the institute for their help, to Susan Aurich for polishing my English and to Frédérique for being there all this time.

Bibliography

[1] H. B. G. Casimir. *On the interaction between atomic nuclei and electrons.* San Francisco, W.H. Freeman, 1963.

[2] Bureau International des Poids et Measures. *The international System of Units.* Organisation Intergouvernementale de la Convention du Métre, 7th edition, 1998.

[3] R. L. Kurucz. Atomic data for interpreting stellar spectra: isotopic and hyperfine data. *Physica scripta*, T47:110 – 117, 1993.

[4] D. S. Leckrone, S. Johansson, G. M. Wahlgren, and S. J. Adelman. High resolution UV stellar spectroscopy with the HST/GHRS, challenges and opportunities for atomic physics. *Physica scripta*, T47:149 – 156, 1993.

[5] S. Kröger, O. Scharf, and G. Guthöhrlein. New and revised energy levels of atomic Niobium. *Europhysics Letter*, 66(3):344 – 349, 2004.

[6] C. Froese Fischer. The MCHF atomic structure package. *Computer Physics Communications*, 64:369 – 398, 1991.

[7] F. A. Parpia, C. Froese-Fischer, and I. P. Grant. GRASP92: A package for large-scale relativistic atomic structure calculations. *Computer Physics Communications*, 94:249 – 271, 1996.

[8] Z. Cai, V. M. Umar, and C. F. Fischer. Large-scale relativistic correlation calculations: Levels of Pr^{+3}. *Physical Review Letters*, 68:297 – 300, 1992.

[9] S. Fritzsche and I. P. Grant. Ab initio calculation of the $2s^2\ ^1s_0 - 2s3p\ ^3p_1$ intercombination transition in beryllium like ions. *Physica scripta*, 50:473 – 480, 1994.

[10] P. Jönsson. Multi-configuration Hartree- and Dirac-Fock calculations of atomic hyperfine structures. *Physica scripta*, 48:678, 1993.

[11] J. Carlsson, P. Jönsson, M. Godefroid, and C. F. Fischer. Accurate multiconfiguration Hartree-Fock calculations of isotope shifts in C I and C IV. *Journal of Physics B*, 28:3729 – 3740, 1995.

[12] T. Brage and C. F. Fischer. Systematic studies of correlation in complex ions. *Physica Scripta*, T47:18 – 28, 1993.

[13] J. Bieroń, F. A. Parpia, C. Froese Fischer, and P. Jönsson. Large-scale multiconfiguration Dirac-Fock calculation of hyperfine interaction constants for nd^2 levels of Sc^+ and Y^+. *Physical Review A*, 51(6):4603 – 4610, 1995.

[14] W. J. Childs and U. Nielsen. Hyperfine structure of the $(5d + 6s)^3$ configuration of ^{139}La I: New measurements and *ab initio* multiconfiguration Dirac-Fock calculations. *Physical Review A*, 37(1):6 – 15, 1988.

[15] L. Young, W. J. Childs, T. Dinneen, C. Kurtz, H. G. Berry, and L. Engström. Hyperfine structure of Sc II: Experiment and theory. *Physical Review A*, 37(11):4213 – 4219, 1988.

[16] J. Bieroń. Multiconfiguration Dirac-Hartree-Fock calculations of the hyperfine structures of Radium. *Journal of Physics B*, 38:2221 – 2228, 2005.

[17] Maple is a registered trademark of Waterloo Maple Inc.

[18] R. D. Cowan. *The Theory of atomic structure and spectra.* University of California Press, first edition, 1981.

[19] J. Vizbaraitė, J. Kaniauskas, and Z. Rudzikas. On the theory of the hyperfine structure of many-electron atoms. *Lietuvos Fizikos Rinkinys*, 16:37 – 48, 1975.

[20] P. Raghavan. Table of nuclear moments. *Atomic Data and Nuclear Data Tables*, 42:189, 1989.

[21] P. G. H. Sandars and J. Beck. Relativistic effects in many-electron hyperfine structure. I. Theory. *Proceedings of the Royal Society of London*, 289:97 – 113, 1965.

[22] I. Lindgren and A. Rosén. Relativistic self-consistent-field calculations with application to atomic hyperfine interaction. Part III: Comparison between theoretical and experimental hyperfine-structure results. *Case Studies in Atomic Physics*, 4:197 – 298, 1974.

[23] D. Messnarz. *Laserspektroskopische und parametrische Analyse der Fein- und Hyperfinestruktur des Tantal-Atoms und Tantal-Ions.* Wissenschaft und Technik Verlag Berlin, 1 edition, 2001.

[24] J. Dembczyński, W. Ertmer, U. Johann, and P. Unkel. A new parametrization method for hyperfine interactions. Determination of nuclear quadrupole moments almost free of Sternheimer corrections. *Zeitschrift für Physik A*, 321:1 – 13, 1984.

[25] I. Lindgren and J. Morrison. *Atomic many-body theory.* Springer–Verlag, Berlin, Heidelberg, New York, 1 edition, 1982.

[26] A. Jucys. Fock equations in a multiconfiguration approach. *Journal of Experimental and Theoretical Physics*, 23(2(8)):129 – 139, 1952.

[27] G. Racah. Theory of Complex Spectra. I. *Physical Review*, 61:186 – 196, 1941.

[28] G. Racah. Theory of Complex Spectra. II. *Physical Review*, 62:438 – 448, 1942.

[29] G. Racah. Theory of Complex Spectra. III. *Physical Review*, 63:367 – 378, 1943.

[30] G. Racah. Theory of Complex Spectra. IV. *Physical Review*, 76(9):1352 – 1362, 1949.

[31] A. P. Jucys, I. B. Levinson, and V. V. Vanagas. Mathematical apparatus of the theory of angular momentum. 1962.

[32] A. P. Jucys and A. A. Bandzaitis. *Theory of angular momentum in quantum mechanics.* Mokslas, Vilnius, 2 edition, 1977.

[33] P. G. Burke. A program to calculate a general recoupling coefficient. *Computer Physics Communications*, 1(4):241 – 250, 1970.

[34] A. Bar-Shalom and M. Klapisch. NJGRAF: An efficient program for calculation of general recoupling coefficients by graphical analysis, compatible with NJSYM. *Computer Physics Communications*, 50:375 – 393, 1988.

[35] M. Klapisch. A tribute to professor Jucys: On the influence of his theories on the modern atomic physics computing programs. *Lithuanian Journal of Physics*, 44(2):85 – 89, 2004.

[36] G. Gaigalas, J. Kaniauskas, and Z. Rudzikas. A diagrammatic technique in the angular momentum theory and second quantization. *Lietuvos Fizikos Rinkinys*, 25(6):3 – 13, 1985.

[37] G. Gaigalas, Z. Rudzikas, and C. Froese Fischer. An efficient approach for spin-angular integrations in atomic structure calculations. *Journal of Physics B*, 30:3747 – 3771, 1997.

[38] G. Gaigalas and Z. Rudzikas. Reduced coefficients (subcoefficients) of fractional parentage for p-, d-, and f-shells. *Atomic Data and Nuclear Data Tables*, 70:1 – 39, 1998.

[39] H. Friedrich. *Theoretische Atomphysik*. Springer-Verlag Berlin, 1990.

[40] C. Froese Fischer. *Computational atomic structure. An MCHF approach*. Institute of Physics Publishing, Bristol and Philadelphia, 1997.

[41] Z. Rudzikas. *Theoretical Atomic Spectroscopy*. Cambridge University Press, Cambridge, 1997.

[42] H. A. Bethe and E. E. Salpeter. *Quantum mechanics of one- and two-electron atoms*. Springer Verlag, Berlinans New York, 1957.

[43] F. A. Parpia and A. K. Mohanty. Relativistic basis-set calculations for atoms with Fermi nuclei. *Physical Review A*, 46:3735 – 3745, 1992.

[44] G. Gaigalas, S. Fritzsche, and B. Fricke. Maple procedures for the coupling of angular momenta. III. Standard quantities for evaluating many-particle matrix elements. *Computer Physics Communications*, 135:219 – 237, 2001.

[45] I. Lindgren and A. Rosén. Relativistic self-consistent-field calculations with application to atomic hyperfine interaction. Part II: Relativistic theory of atomic hyperfine interaction. *Case Studies in Atomic Physics*, 4:150 – 196, 1974.

[46] A. Bohr and V. F. Weisskopf. The influence of nuclear structure on the hyperfine structure of heavy elements. *Physical Review*, 77(1):94 – 98, 1950.

[47] P. Jönsson and C.-G. Wahlström. A program for computing magnetic dipole and electric quadrupole hyperfine constants from MCHF wave functions. *Computer Physics Communications*, 74:399 – 414, 1993.

[48] S. Fritzsche. Maple procedures for the coupling of angular momenta I. Data structures and numerical computations. *Computer Physics Communications*, 103:51 – 73, 1997.

[49] S. Fritzsche, S. Varga, D. Geschke, and B. Fricke. Maple procedures for the coupling of angular momenta II. Sum rule evaluation. *Computer Physics Communications*, 111:167 – 184, 1998.

[50] S. Fritzsche, G. Gaigalas, and B. Fricke. Maple procedures for the coupling of angular momenta III. Standard quantities for evaluating many-particle matrix elements. *Computer Physics Communications*, 135:219 – 237, 2001.

[51] T. Inghoff, S. Fritzsche, and B. Fricke. Maple procedures for the coupling of angular momenta IV. Spherical harmonics. *Computer Physics Communications*, 139:297 – 313, 2001.

[52] S. Fritzsche, T. Inghoff, T. Bastug, and M. Tomaselli. Maple procedures for the coupling of angular momenta V. Recoupling coefficients. *Computer Physics Communications*, 139:314 – 326, 2001.

[53] G. Gaigalas and S. Fritzsche. Maple procedures for the coupling of angular momenta VI. LS-jj transformations. *Computer Physics Communications*, 149:39 – 69, 2002.

[54] G. Gaigalas, O. Scharf, and S. Fritzsche. Maple procedures for the coupling of angular momenta. VIII. Spin-angular coefficients for single-shell configurations. *Computer Physics Communications*, 166:141 – 169, 2005.

[55] O. Scharf, G. Gaigalas, S. Fritzsche, M. Gedvilas, E. Gaidamauskas, and G. Kirsanskas. Application of the Racah package for dealing with the expressions from the atomic shell model. *Nuclear Instruments and Methods in Physics Research B*, 235:135 – 139, 2005.

[56] O. Scharf, S. Fritzsche, and G. Gaigalas. Hyperfine structure parametrization in Maple. *Computer Physics Communications*, in press, 2006.

[57] M. Gedvilas. Master's thesis, Vilniaus Universitetas Fizikos Fakultetas Teorinės Fizikos Katedra, 2004.

[58] S. Büttgenbach and R. Dicke. Hyperfine structure of nine levels in two configurations of ^{93}Nb. *Zeitschrift für Physik A*, 275:197 – 202, 1975.

[59] A. Hibbert and C. Froese Fischer. A general program for computing angular integrals of the non-relativistic Hamiltonian with non-orthogonal orbitals. *Computer Physics Communications*, 64:417 – 430, 1991.

[60] G. Gaigalas. The library of subroutines for calculating standard quantities in atomic structure theory. *Lithuanian Journal of Physics*, 41(1):39 – 54, 2001.

[61] C. Froese Fischer, G. Tachiev, G. Gaigalas, and M. Godefroid. An MCHF atomic-structure package for large-scale calculations. Unpublished documentation of the new version based on dynamic memory allocation, sparse matrix methods, and a recently developed angular library, 2003.

[62] M. Tong, P. Jönsson, and C. Froese Fischer. Convergence studies of atomic properties from variational methods: Total energy, ionization energy, specific mass shift, and hyperfine parameter for Li. *Physica Scripta*, 48:446 – 453, 1993.

[63] P. Jönsson and C. Froese Fischer. Large-scale multiconfiguration Hartree-Fock calculations of hyperfine-interaction constants for low-lying states in Beryllium, Boron, and Carbon. *Physical Review A*, 48(6):4113 – 4123, 1993.

[64] M. G. Edmunds. Calculation of hyperfine structure of Scandium and Vanadium for stellar spectral analysis. *Astronomy and Astrophysics*, 23(2):311 – 316, 1973.

[65] W. J. Childs and L. S. Goodman. Hyperfine structure of nine levels in two configurations of V^{51}. I. Experimental. *Physical Review*, 156(1):64 – 70, 1967.

[66] P. Unkel, P. Buch, J. Dembcyński, W. Ertmer, and U. Johann. Sternheimer free determination of the ^{51}V nuclear quadrupole moment from hyperfine structure measurements. *Zeitschrift für Physik D: Atoms, Molecules and Cluster*, 11:259 – 271, 1989.

[67] W. J. Childs. Hyperfine structure of nine levels in two configurations of V^{51}. II. Theoretical. *Physical Review*, 156(1):71 – 81, 1967.

[68] A. Hibbert, R. Glass, and C. F. Fischer. A general program for computing angular integrals of the Breit-Pauli Hamiltonian. *Computer Physics Communications*, 64:455–472, 1991.

[69] G. Gaigalas, T. Zalandauskas, and S. Fritzsche. Spectroscopic LSJ notation for atomic levels obtained from relativistic calculations. *Computer Physics Communications*, 157:239 – 253, 2004.

Santrauka

Atomų ir spektrinių linijų hipersmulkioji struktūra (hss) yra sąlygojama sąveikos energijos tarp branduolio statinių magnetinio ir elektrinio laukų ir elektrono apvalkalo magnetinių ir elektrinių laukų. To suskilimo dydis yra proporcingas vadinamajam A daugikliui, jį šiek tiek patikslinant atsižvelgus į B parametrą. Tolimesni patikslinimai, išskyrus specialius atvejus, yra dar mažesni ir į juos retai atsižvelgiama.

Šiuolaikiniai eksperimentiniai metodai įgalina matuoti praktiškai bet kurio atomo ir jono spektrinių linijų suskilimą, įskaitant ekstremalius jonizacijos laipsnius. Detalios spektrinių linijų sandaros žinojimas esminiai padeda interpretuoti ir analizuoti aukštos skiriamosios gebos spektrus. Turint tikslines A ir B parametrų vertes, galima efektyviai interpretuoti linijų formas, identifikuoti šuolius tarp smulkiosios struktūros linijų sudėtinguose spektruose, kontroliuoti spektro linijų identifikavimą.

Disertacija sudaryta iš penkių skyrių. Pirmajame pateikta trumpa hipersmulkiosios struktūros tyrimų istorinė apžvalga. Remiantis egzistuojančiomis teorijomis antrajame skyriuje išvestos hipersmulkiosios struktūros operatorių matricinių elementų išraiškos. Trečiajame skyriuje aprašytos kompiuterinės programos, įgalinančios teoriškai tirti šias sąveikas remiantis ankstesniajame skyriuje gautomis bendromis formulėmis. Ketvirtajame skyriuje naujasis algoritmas pritaikytas vanadžio atomo pagrindinės būsenos hipersmulkiajai struktūrai tirti naudojant tiek daugiakonfigūracinius Hartrio ir Foko, tiek ir Dirako-Foko artutinumus. Paskutiniajame skyriuje pateikiamos išvados bei trumpai formuluojamos tyrimų perspektyvos.

Disertacijoje pateikta hipersmulkiųjų sąveikų teorinio tyrimo metodika, atsižvelgiant į naujus pasiekimus integravimo sukininių ir kampinių atžvilgiu srityje, yra gautos bendrosios A ir B parametrų išraiškos, tinkančios bet kuriam atomui, turinčiam bet kurį atvirų elektronų sluoksnių skaičių. Metodika remiasi judesio kiekio momento teorijos, universalaus grafinio vaizdavimo, antrinio kvantavimo surištame tenzoriniame pavidale, kvazisukinio bei pilnai redukuotų kilminių koeficientų deriniu. Ji įgalino vesti universalias neredukuotinio hipersmulkiosios struktūros sąveikos operatoriaus ir jo matricinių elementų išraiškas. Pastarieji aprašo tiek diagonalinius, tiek ir nediagonalinius konfigūracijų atžvilgiu matricinius elementus, tuo atveriant galimybę atsižvelgti į koreliacinius efektus (žiūr. formules (2.22), (2.23), (2.24) ir (2.50)).

Remiantis išvestomis formulėmis parašytos universalios kompiuterinės programos hipersmulkiajai struktūrai skaičiuoti tiek naudojant daugiakonfigūracinį Hartrio ir Foko

artutinumą, tiek ir pusiauempiriškai. Buvo naudojama simbolinio programavimo MAPLE kalba, įgalinant lengvai pritaikyti šią metodiką analogiškoms fizikinėms problemoms. Esančios RACAH ir JUCYS atomo struktūros elektroninės duomenų bazės buvo išplėstos į viendalelių operatorių matricinių elementų integravimą sukinių ir judesio kiekio momentu erdvėse. Šios išplėtotos elektroninės duomenų bazės buvo panaudotos programuoti paketą HFS, kuris įgalina operuoti su hipersmulkiųjų sąveikų išraiškomis bei rasti jų skaitines vertes. Programa buvo išbandyta pusiauempiriškai analizuojant pirmųjų devynių niobio lygmenų hipersmulkiąją struktūrą. Ji taip pat buvo instaliuota Kaselio universiteto Fizikos skyriuje (Vokietija) [†].

Nauja integravimo sukinių ir judesio kiekio momentų erdvėse metodika buvo įdiegta Daugiakonfigūracinio Hartrio ir Foko atominių struktūrų pakete ATSP hipersmulkiosioms sąveikoms nagrinėti. Nauja nepublikuoto MCHF atomų struktūros paketo versija, kuri remiasi dinaminiu atminties išdėstymu, išsklaidytų matricų metodais ir nauja kampų biblioteka, buvo įdiegta Vilniaus pedagoginio universiteto BENDROSIOS FIZIKOS KATEDROS spiečiuje glaudžiai bendradarbiaujant su C. F. Fischer (NIST, JAV). Taip pat ten buvo instaliuotas daugiakonfigūracinių Dirako ir Foko skaičiavimų paketas GRASP.

Programos ir esantieji kompiuterių pajėgumai įgalina atlikti teorinius tyrimus atsižvelgiant į priemaišinių konfigūracijų suformuotas įvairių koreliacinių efektų grupes bei jų kompensavimąsi. Naudojant šią programinę įrangą galima įvertinti tų grupių konvergavimą ir jų įtaką hipersmulkiajai struktūrai. Tuo būdu galima suformuluoti pataisinių konfigūracijų parinkimo rekomendacijas, įvertinti skaičiavimų paklaidas bei gauti detalią informaciją apie koreliacinius efektus.

Keturių pagrindinės vanadžio būsenos lygmenų hipersmulkiosios struktūros ($3d^3\ {}^4_3F$ $4s^2\ {}^2S\ \ {}^4F_J$, $J = 3/2, 5/2, 7/2$ ir $J = 9/2$) tyrimai naudojant daugiakonfigūracinių Hartrio ir Foko bei Dirako ir Foko artutinumus iliustruoja išplėtotos metodikos ir parašytų programų tinkamumą ir efektyvumą.

Vanadžiui abu minėtieji artutinumai įgalina pasiekti gerą atitikimą eksperimentiniams rezultatams tik tuomet, kai atsižvelgiama ne tik į pakankamai daug priemaišinių konfigūracijų, bet taip pat ir priimamos dėmesin koreliacijos, sąlygojančios nenulinį kontaktinių sąveikų indėlį.

Disertacijos rezultatai buvo publikuoti šešiuose moksliniuose straipsniuose bei aprobuoti penkiose nacionalinėse ir tarptautinėse konferencijose.

[†] http://www.physik.uni-kassel.de/fritzsche/programs.html